LLC Resonant Current Doubler Converter

Haoning (William) Chen

A thesis submitted in partial fulfillment
of the requirements for the degree of
Master of Engineering
in
Electrical and Electronic Engineering
at the
University of Canterbury,
Christchurch, New Zealand.
Dec 2012

ABSTRACT

The telecommunications market is one of the large rapidly growing fields in today's power supply industry due to the increasing demand for telecom distributed power supply (DPS) systems. The half-bridge LLC (Inductor-Inductor-Capacitor) resonant converter is currently the most attractive topology for the design and implementation of 24V/48V DC telecom power converters.

The current doubler rectifier (CDR) converter topology was invented and described in the early 1950s which can offer the unique characteristic of halving the output voltage while doubling the output current compared to a standard rectifier.

In this thesis, the current doubler converter topology with its unique characteristic is evaluated as a complementary solution to improve the LLC resonant converter performance, especially for the low output voltage and high output current telecommunication applications.

A novel half-bridge LLC resonant current doubler converter (LLC-CDR) is proposed in this thesis which can offer several performance benefits compared to conventional LLC-standard rectifier design . The unique characteristics of the LLC-CDR topology can offer significant improvements by transformation of a 48V converter into a 24Vconverter with the same power density.

This thesis introduces a new SPICE-based simulation model to analyse the operation of this novel LLC-CDR converter circuit design. This model can be used to define the critical component parameters for the LLC-CDR circuit output inductor values. It can also be used to predict the circuit overall performance under different load conditions. Both time-domain based transient simulation analysis and frequency-domain based AC analysis provided by this simulation model showed favourable results in comparison to bench measurement results on a prototype. The model provides a valuable insight to reveal some of the unique characteristics of this LLC-CDR topology. It demonstrates a proof of concept that the conventional LLC resonant

converter can be easily redesigned for low voltage, high current applications by using the LLC-CDR topology without requiring a new design for the LLC resonant stage components and the power transformer.

A new magnetic integration solution was proposed to significantly improve the overall performance in the LLC-CDR topology that had not been published before. The LLC-CDR converter hardware prototypes with two output inductors coupled and uncoupled configurations were extensively modelled, constructed and bench tested. Test results demonstrated the suitability of an integrated coupled inductors design for the novel LLC-CDR converter application. The integrated coupled inductors design can significantly improve the LLC-CDR converter frequency-domain based AC simulation analysis results. In addition, these results also illustrate the potential benefit of how the magnetic integration design in general could reduce the magnetic component size, cost, and weight compared to the uncoupled inductors design.

Finally, a hardware prototype circuit was constructed based on a commercial 1800W single phase telecom power converter to verify the operation of this novel half bridge LLC-CDR topology. The converter prototype successfully operated at both no load and full load conditions with the nominal output voltage halved from 48VDC to 24VDC, and doubled the output current to match the same output power density. It also demonstrates that the efficiency of this novel half bridge LLC –CDR is 92% compares to 90% of EATON's commercial 24VDC LLC resonant converter, which can fulfill the research goals.

ACKNOWLEDGEMENTS

I would like to take this opportunity to express my deeply gratitude to a number of people, this thesis would not have been done without your support and my dream would not come true. I would like to give the most sincerely appreciation to my academic supervisor Paul Gaynor. Thank you so much for taking me as one of your postgraduate students and always guiding me through to fulfill the academic interests to get my Master degree.

I would like to thank my industry mentor Michael Harrison for sharing his broad knowledge and his technical advice on this project. I also would like to specially thank to my industry supervisor Phil Hunter. Thank you very much for the valuable guidance and input you have given me while undertaking this project. Thank you very much for overseeing my project research and sharing your technical expertise on the hardware prototype. I would also like to thank Charles Dunn as my industry co-supervisor. Thanks for taking over the supervisor duties while Phil is away. Thanks to the Power Conversion Group Manager Craig Jackson at Eaton, for your continuous support and assistance in many occasions. Thanks to all the other engineers, Graeme, James, Dave, Ravi, John, Tomasz, Singa.

I gratefully thank to the financial support that I received from the Foundation for Research Science and Technology under TP081019, without your support this project would not have been possible to finish.

Finally I would like to thank to my wife Rui Chen and my parents YanYunHao, Hui Chen and my daughter Stephanie Chen. Thanks for your love, long term support and encouragement.

Table of Contents

Chapter 1

Introduction

1.1 Motivation and Research Objectives

Every year a huge amount of energy is used to power fixed telecommunications, mobile communications, and data server centers. As network equipment is becoming more Internet Protocol-based, the power consumption for telecom and data server centers is continuously increasing. Growth in the telecommunications market is always associated with growth in supporting equipment. However, the environmental and economic impacts of substantial electrical energy use are serious problems for the modern world [1].

Telecommunication operators are striving to cut energy costs across the network through better operating efficiency and carbon footprint reduction. In the recent telecommunication industry, there is a strong market trend for new technology based telecom power supplies (usually called power rectifiers) which can achieve a high efficiency of around 96%. In contrast, the previous generation of telecom power rectifiers could only achieve around 92% efficiency. This new increase in efficiency means a 50% cost saving for the telecommunication operators [2]. EATON has recently developed as one of its main products the APR48-ES, which is a 48VDC energy saver power rectifier with a peak efficiency of 96%.This product was developed following the strong market demand for low loss energy systems. The current EATON 48VDC and 24VDC power rectifiers, that were designed and manufactured a few years ago in 2007, both have an efficiency of 92% and 90%. It is very important for EATON to complete their high efficiency product portfolio with a new 24VDC high efficiency product to meet the potential increased market demand in the future.

The objective of this project is to investigate, design and present a novel design solution for a new 24VDC telecom converter which is based on the platform of EATON's current 48VDC half-bridge LLC resonant converter topology. In order to achieve this goal, a novel half-bridge LLC resonant current doubler DC-DC converter topology has been designed, simulated, and evaluated in this project. The main challenge in the technical side of this project is to focus on the benefits of using the current doubler converter topology on the secondary- side of a half-bridge LLC resonant converter for high output current applications. This focus has been made due to the unique characteristic of the current doubler converter, which can ultimately halve the output voltage and double the output current of a standard LLC resonant converter with no significant magnetic component design changes inside the half-bridge LLC resonant circuit.

As a result, the successful outcomes of this novel topology can be potentially of benefit to EATON for their new 24VDC high efficiency product development which can be based on the new 48VDC 96% high efficiency product. Use of a current doubler output stage could help EATON to deliver a new high efficiency and high output current product successfully with a reduced project development time. In particular, it could also achieve business cost saving and reduces any technical risk impact to the business.

1.2 Telecommunications Power Converters

With the development of information technology, the telecommunications market is one of the large rapidly growing fields in today's power supply industry. In this fast growing of telecommunications market, the DC power supply plays an important role in supplying the telecom equipment. Telecommunications power converters are designed to provide quality DC power from an AC mains input for a wide range of telecom /data center applications [3]. Telecommunication power converters are also referred to as front–end AC/DC converters /rectifiers in many telecom distributed power supply (DPS) systems.

As computers and telecom equipment keep increasing their power density and functionality, power converters require more power transfer and less size. To meet this

requirement, DPS systems have been widely adopted to distribute the power among many power processing converters instead of using one single bulky power supply [4].

The DPS system as shown in Figure 1- 1 is named as an intermediate bus structure. This is the typical system used for telecom equipment and has many advantages. In this system, the intermediate bus voltage is normally 48V. This bus voltage is needed for different loads which are generated through two stage approaches. In the first stage, many distributed front-end AC/DC converters /rectifiers are paralleled to draw a high power factor current waveform from a single AC source and converts to a 48VDC or 24V DC intermediate bus voltage with low noise. The next stage converter transfers the intermediate bus voltage into different voltage loads such as: on-board converters and voltage regulator modules (VRM).

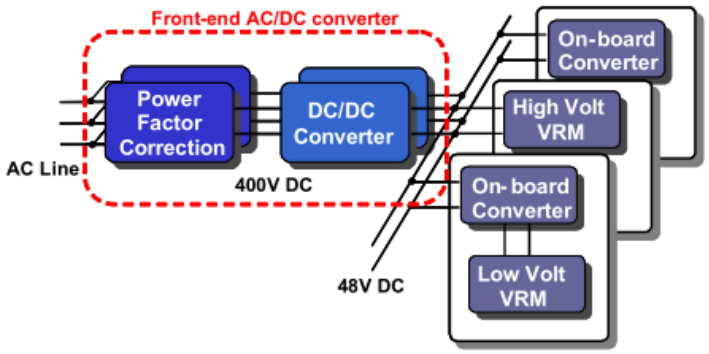

Figure 1-1 : DPS Front-end AC/DC converter [3].

The DPS system has been used exclusively in today's telecommunications and data server systems because it has many advantages compared to a centralized power system. Firstly, it provides highly reliable power to the telecom customer due to its modular design. Each front–end converter module can share part of the total load power, thus both the electrical and thermal stress on the components are greatly reduced. Secondly, because in the DPS system all front–end converter modules are connected in parallel. This approach makes the system easy to reconfigure and extend by using N+1 redundancy. By adding one additional module to the system, in this way the system can still maintain reliable power even if one module fails. Thirdly, hot- swap becomes a

popular feature of the DPS system for the customer to replace the failed module unit without interruption of system operation. This makes system maintenance very easy for the telecom provider. Avoidance of shutting down the whole system is a desirable approach for highly reliable telecom or data center power systems. Therefore, the DPS system front-end AC/DC converter with LLC resonant converter topology inside becomes a popular approach in today's telecommunications power converter market.

The half-bridge LLC (Inductor -Inductor-Capacitor) resonant DC-DC converter is a popular topology, which has been widely used in EATON telecommunication products like the new APR48-ES (48VDC high efficiency power rectifier) and the current 48VDC and 24VDC power rectifiers. The name describes a series connection of two inductors (LL) and one capacitor (C) with a centre-tapped transformer. The LLC resonant half-bridge converter performs power conversion with frequency modulation instead of pulse-width modulation (PWM) [5].

The current doubler rectifier (CDR) converter is a traditional topology that has been recently rediscovered, which is used for high output current DC-DC converters. This circuit can be used with many primary topologies, such as push-pull, half bridge, and full bridge circuits. Both LLC resonant half-bridge converters and CDR converters have been widely used in many high power density power-supply designs and their applications [6].

The traditional methods used to build any new LLC DC-DC converter requires a re-design of all the magnetic components, including the two resonant inductors, resonant capacitor and transformer. However, designing such new converters presents many technical challenges and business risks to meet the telecommunication industry requirements. Therefore, this thesis is mainly focused on the development of a novel half-bridge LLC resonant current doubler converter which provides a low-cost and quick approach to transforming a EATON 48VDC power converter /rectifier into a 24VDC power rectifier with the same power rating and density.

1.3 Thesis Outline

One of the biggest challenges in the technical side of this project was to investigate the combination of the well-known LLC resonant converter topology with the traditional CDR topology. In this thesis, hardware prototypes have been designed and constructed. Their experimental performances have been compared with correspondingly developed SPICE-based models and simulations.

In Chapter 2, an overview of the popular LLC resonant converter topology operation for the telecom DC/DC converter application is provided. Firstly, three traditional resonant topologies are investigated. These are the series resonant converter (SRC), parallel resonant converter (PRC), and series-parallel resonant converter (SPRC). The characteristics and disadvantages of these conventional converters are explored in detail. Secondly, The LLC resonant converter is detailed and shown to be the premier solution for the telecom DC/DC converter, because it operates well over a wide range input voltage and reduces switching losses at high switching frequencies. Thirdly, with DC characteristic curve analysis, the LLC operating principle and design of an LLC resonant converter is presented. Finally, the EATON 48V rectifier LLC resonant converter performance is investigated and simulated with SPICE model based circuits.

Chapter 3 introduces and explores the traditional current doubler rectifier topology and its operation. The CDR is widely used as an alternative solution for low voltage and high current applications because of reduced transformer winding losses. It has the unique feature of halving the output voltage of a standard LLC resonant converter, but doubling the output current. Therefore, a novel half-bridge LLC resonant current doubler topology is identified for this project.

In Chapter 4, a novel half-bridge LLC resonant current doubler topology with two un-coupled output inductors is presented. Several SPICE model-based simulation circuits are designed and analyzed in order to understand the unique switching characteristic both described in the time domain (transient analysis) and in the frequency domain (steady-

state AC analysis). The simulation results are analyzed in comparison with the LLC resonant converter. Some disadvantages about the un-coupled output inductor arrangement are explored and discussed in detail. Results from a hardware prototype are provided. The hardware is used to examine the novel half-bridge LLC resonant current doubler topology performance. Finally, some key components of the design and the experimental results are discussed.

In Chapter 5, after investigating the novel half-bridge LLC resonant current doubler topology performance in Chapter 4, some unique features are identified which have not previously been reported in the literature. The novel findings provide valuable insight into this new topology which could be potential beneficial to the industry product development. Therefore, the novel half-bridge LLC resonant current doubler with two magnetically coupled output inductors are presented for this project. Furthermore, several SPICE model-based simulation circuits are designed and analyzed in comparison to the topology stated in Chapter 4. Finally, to demonstrate the apparent benefits, a hardware prototype is constructed and implemented with coupled output inductors. Experimental results are presented to show that both the converter performance and efficiency have been improved compared to the uncoupled inductor form. It also shows in detail that the experimental measured results have a good match with SPICE model based simulations.

Chapter 6 summarizes the unique characteristics of the novel half-bridge LLC resonant current doubler and draws conclusions about this novel topology most likely to benefit EATON for new product development. Finally, future research work is discussed.

Chapter 2

LLC Resonant Converter

Resonant converter topologies have been widely used in telecom DC/DC converters / rectifiers since, as it will be shown, they can achieve low switching losses ensuring the resonant converter can operate at high switching frequency. As such, the converter can achieve high efficiency with minimal physical volume and weight. This chapter provides background information about four resonant topologies. The DC characteristic plot is an important tool used to analyze resonant topology performance. The major goal of this chapter is to detail the LLC resonant converter design and operation.

2.1 Zero Voltage and Zero Current Switching.

In some switch mode converter topologies, increasing the switching frequency is a desirable solution to reduce the size of the circuit magnetic components and capacitors. However, increasing the switching frequency also increases the converter switching losses and hence reduces the system efficiency. One approach is to utilize LC circuit resonance to shape either the current or the voltage across the power switching element to provide zero-voltage switching (ZVS) and/or zero-current switching (ZCS) [7]. Therefore, when switching takes place, the capacitor and inductor resonances shape the waveform so that there is no current through and/or voltage across the switch, and as such there are minimal power losses as shown in Figure 2-1.

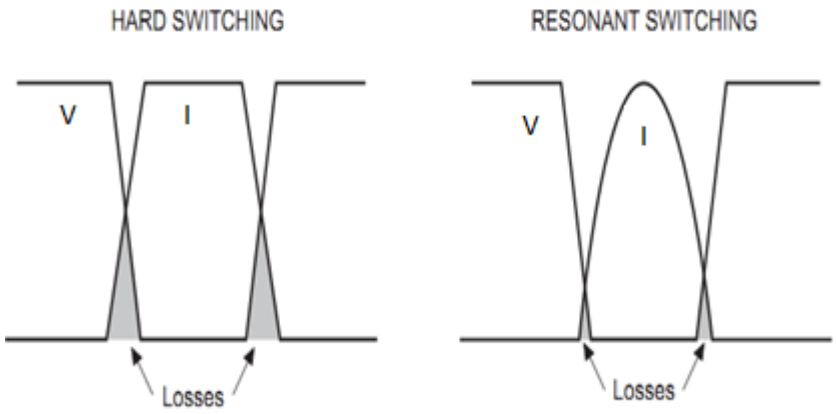

Figure 2-1 : Waveforms (of voltage, V and current, I) of hard switching and resonant switching [7].

A typical ZVS circuit consists of a switch in parallel with a diode. In this configuration, the resonant capacitor is connected in parallel with the switch, and the resonant inductor is connected in series. A voltage source is connected to provide the power to the circuit. The ZVS circuit and waveforms are shown in Figure 2-2.

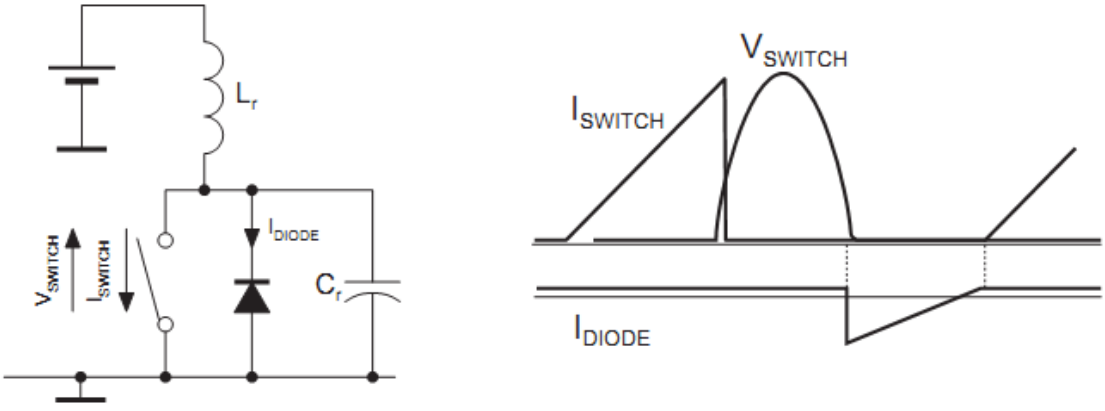

Figure 2- 2 : ZVS circuit topology and switching waveforms [7].

Figure 2-2 shows that when the switch turns on, a linear current flows through the inductor. When the switch turns off, the energy that is stored in the inductor flows into the resonant capacitor. This results in a sinusoidal voltage across the capacitor and the switch. The negative half-cycle of the voltage is blocked by the diode. During this

negative half-cycle, both the current and voltage in the switch are close to zero, therefore it can be turned on without power losses [8].

A typical ZCS circuit consists of a switch in series with the resonant inductor, and in parallel with a diode, and this entire branch is in parallel with the resonant capacitor. In this configuration, a current source is used to supply energy to the circuit. The ZCS circuit and waveforms are shown in Figure 2-3.

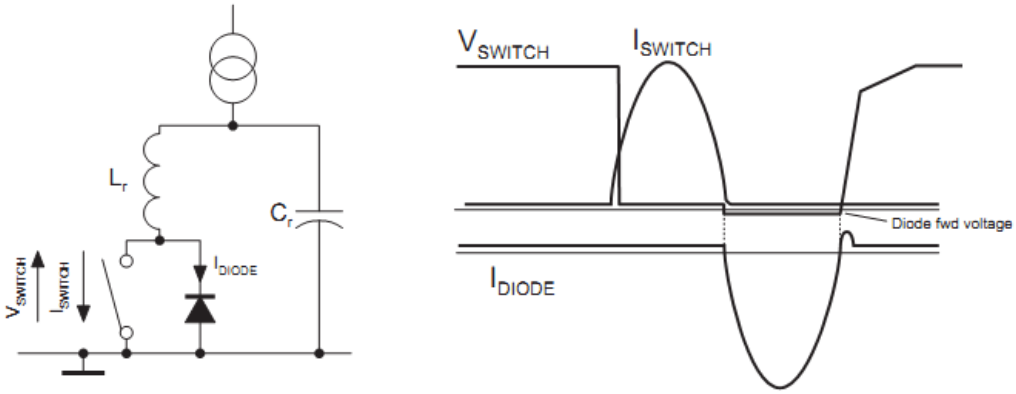

Figure 2- 3 : ZCS circuit topology and switching waveforms [7].

When the switch turns off, the resonant capacitor is charged up with a constant current, hence the energy is stored in the capacitor and the voltage across it increases linearly. When the switch turns on, the energy stored in the capacitor is now transferred to the inductor, resulting in a sinusoidal current flowing into the switch during the positive half cycle [13]. During the negative half cycle, the current flows through the anti-parallel diode, and there is close to zero current through or voltage across the switch, therefore it can be turned off with minimal power losses.

In a resonant circuit a ZCS circuit shapes the current waveform, while a ZVS circuit shapes the voltage waveform. If power MOSFETs are to be utilized for switching, in ZVS, the MOSFET turns on without any voltage between the drain and source, and so there are almost no switching losses. When the MOSFET turns off a current, since the switching times of MOSFETs are usually small, the turn off losses will not be excessive so long as the current is not very large, and the switching frequency is not too high [7].

2.2 Three Traditional Resonant Topologies

The series resonant converter, parallel resonant converter, and series parallel resonant converter are the three most popular resonant converter topologies in the power range of interest. They normally consist of a resonance inductor L_r and a capacitor C_r, which is also called the resonant tank circuit. Oscillating voltage and current, due to L_rC_r resonance in the tank are applied to the load [9]. In these resonant converter topologies, the power flow to the load is controlled by the resonant tank impedance. In other terms, the power flow is controlled by the switching frequency f_s in comparison to the resonant frequency f_o of the resonant tank [10]. The resonant converter switches can be switched at zero voltage and /or zero current.

2.2.1 Series resonant converter

It is important to obtain the frequency characteristics from the simplified L_rC_r series resonant circuit as shown in Figure 2-4.

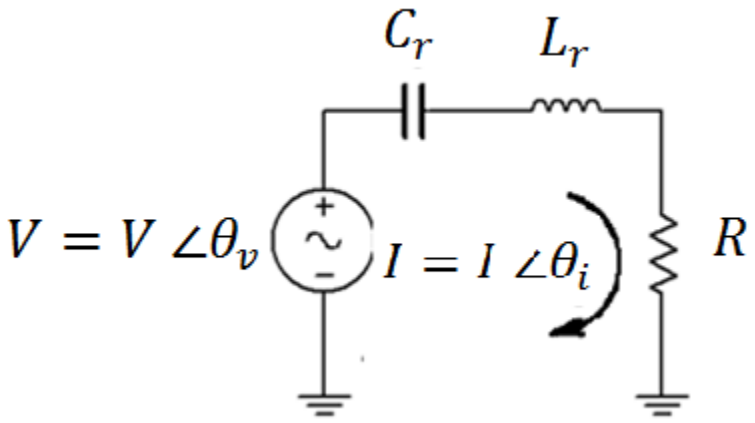

Figure 2-4: Simplified LC series resonant circuit.

A series resonant circuit consists of a resistor, a capacitor, and an inductor connected in series. The inductive reactance magnitude (X_L) increases as the frequency increases while the capacitive reactance magnitude (X_C) decreases as the frequency increases. The resonance effect occurs when the inductive reactance and capacitive reactance are equal in magnitude (they are 180^0 in opposition). As a result the two impedances cancel each

other out and the total impedance drops to a minimum of R [10]. The resonant frequency ω_0 and the characteristic impedance Z_o of the L_rC_r circuit are defined by Eqn 2-1 and Eqn 2-2.

$$\omega_0 = 2\pi f_0 = \frac{1}{\sqrt{L_r C_r}} \qquad \text{Eqn 2-1}$$

$$Z_0 = \sqrt{\frac{L_r}{C_r}} \qquad \text{Eqn 2-2}$$

In the presence of a load resistance R, the quality factor Q of the circuit can be defined as the ratio of the reactance (of either the resonant capacitor or resonant inductor at the resonant frequency) to the circuit resistance, $Q=X/R$ as shown in Eqn 2-3.

$$Q = \frac{\omega_0 L_r}{R} = \frac{1}{\omega_0 C_r R} = \frac{Z_o}{R} = \frac{\sqrt{\frac{L_r}{C_r}}}{R} \qquad \text{Eqn 2-3}$$

The total impedance is given by the sum of the inductive and capacitive impedances:

$$Z = Z_L + Z_c \qquad \text{Eqn 2-4}$$

By writing the inductive impedance as $Z_L = j\omega L$ and the capacitive impedance as $Z_C = (j\omega C)^{-1}$ in Eqn 2-4 we have:

$$Z_\omega = j\omega L + \frac{1}{j\omega C} \qquad \text{Eqn 2-5}$$

Writing this expression under a common denominator gives

$$Z_\omega = j\frac{(\omega^2 LC - 1)}{\omega C} \qquad \text{Eqn 2-6}$$

Finally, as defined the resonant frequency in Eqn 2-1 the impedance becomes

$$Z_\omega = jL\left(\frac{\omega^2 - \omega_0^2}{\omega}\right) \qquad \text{Eqn 2-7}$$

This implies that in the limit as $\omega \rightarrow \pm \omega_0$ the total impedance Z will be zero. Therefore when the series L_rC_r circuit is connected in series with a load, it will act as a band-pass filter having minimum impedance at the resonant frequency [10].

The frequency characteristic of an LC series resonant circuit is shown in Figure 2-5.

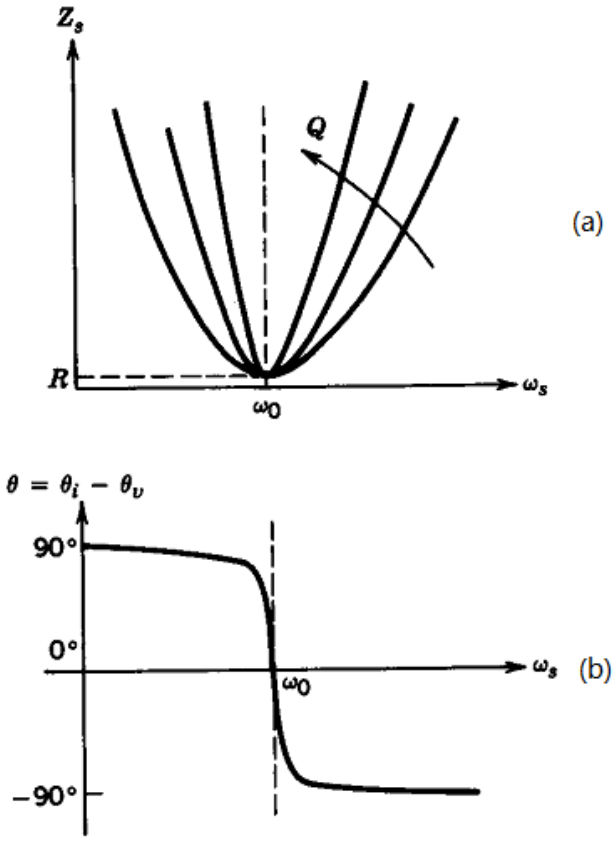

(a): Impedance Z_s and quality factor Q as a function of frequency.

(b): Phase angle as a function of frequency.

Figure 2-5 : Frequency characteristics of a series resonant circuit [9].

Figure 2-5(a) shows the magnitude Z_s of the circuit impedance as a function of frequency with Q as a parameter (noting that R decreases as Q increases as shown in Eqn 2-3) [9]. It also shows that when the switching frequency ω_s is equal to ω_0, Z_s becomes purely resistive.

Figure 2-5(b) shows the phase angle θ (= $\theta_i - \theta_v$) as a function of frequency. It also shows that the capacitor impedance dominates over inductor impedance at frequencies below ω_0 (ω_s<ω_0), therefore the current leads voltage. At frequencies above ω_0(ω_s>ω_0), the inductor impedance dominates and the current lags voltage [9]. At the resonant frequency ω_0, the phase angle θ approaches to 0^0, which corresponds to the resonant tank impedance being purely resistive.

The series resonant converter (SRC) implies a series connection of one inductor *Lr* and one capacitor *Cr* in the primary side of the main transformer. The circuit diagram is shown in Figure 2-6.

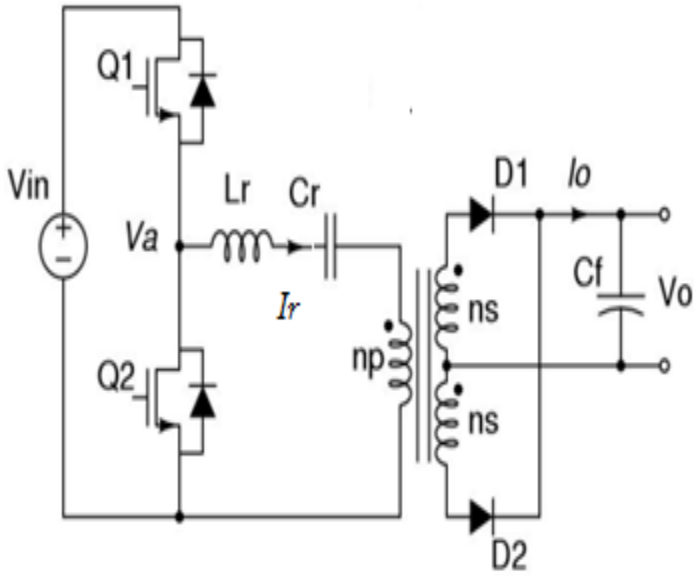

Figure 2-6: Series resonant converter (SRC).

As can see from Figure 2-6, the series inductor *Lr* and capacitor *Cr* form an LC resonant tank which is in series with the load. As a result, the resonant tank and the load form a voltage divider, and the DC gain is always below 1 V/V [5]. Examples of the switching waveforms are shown in Figure 2-7 [5].

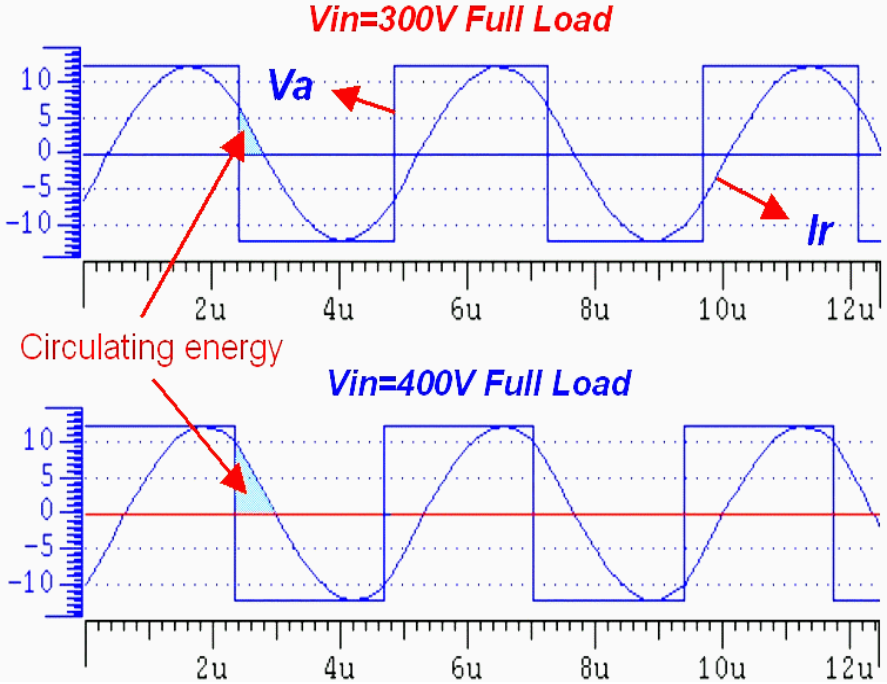

Va: Half bridge switching voltage ;Ir: Resonant current.

Figure 2- 7 : LC resonant tank switching waveforms of a series resonant converter [5].

Figure 2-7 shows the SRC resonant tank switching waveforms with two different input voltages operating under full load condition. From the waveforms, as the input voltage increases from 300V to 400V with the same output power, the circulating energy increases substantially (the circulating energy is shown in the shaded area). As the input voltage increases, the SRC switching frequency increases away from the resonant frequency to keep the output power constant. As a result, the impedance of the resonant tank increases which means more and more energy is circulating in the resonant tank.

The DC characteristic plot of this SRC is shown in Figure 2-8, where f_0 is the resonant frequency of the tank, f_s is the switching frequency, and Q is the quality factor (which describes the load condition changes).

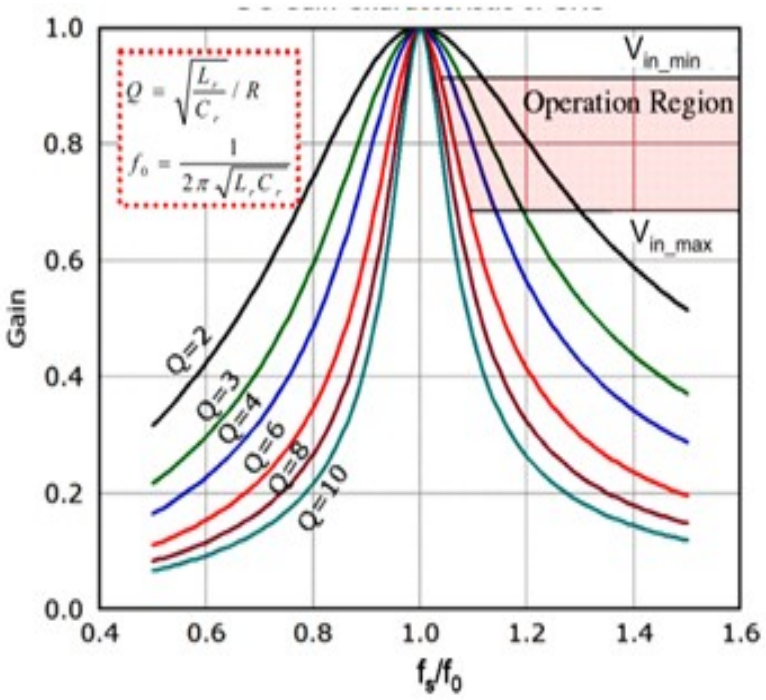

Figure 2-8: DC characteristic plot of the SRC [4].

Referring to Figure 2-8, on the left hand side of the resonant frequency, the SRC operates under Zero-Current-Switching (ZCS); on the right hand side of the resonant frequency, the SRC operates under Zero-Voltage-Switching (ZVS).The resonant tank impedance changes as the frequency of the input voltage changes. At the resonant frequency, the resonant tank impedance is a minimum and the DC gain is at the maximum. Therefore, essentially all the energy inside the resonant tank transfers to the load. The preferred operating region is marked on Figure 2-8, where the switching frequency is higher than the resonant frequency. This indicates that ZVS is in effect which offers low switching losses.

It can be seen that the switching frequency needs to be increased quite high to regulate the output voltage at light load (low required gain). This means the SRC will not have sufficient capability to regulate the output voltage at close to no load conditions. This is a major disadvantage for telecom DC/DC converters / rectifiers because the SRC will lose voltage regulation at no load [11]. Another problem for this topology is that when the

input voltage increases such that a lower gain is required, the switching frequency is higher and away from the resonant frequency. Therefore, instead of transferring essentially all the energy to the load (at resonance), more and more energy is circulating inside the resonant tank. As a result, the turn off current for the power switch is very high, and the switching losses are then also higher. From the above analysis, the SRC is not a good option for a telecom front–end converter /rectifier.

2.2.2 Parallel resonant converter

It is important to obtain the frequency characteristics from the simplified L_rC_r parallel resonant circuit as shown in Figure 2-9.

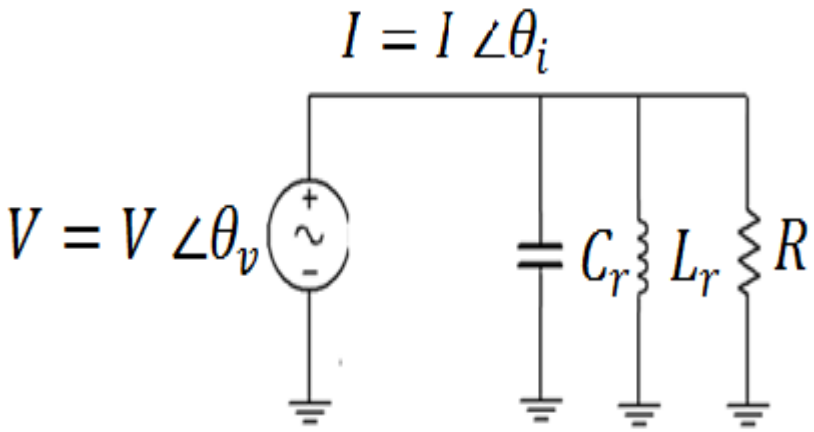

Figure 2- 9 : Simplified L_rC_r parallel resonant circuit.

A parallel resonant circuit consists of a resistor, a capacitor, and an inductor in parallel. The resonance effect occurs when the inductive reactance and capacitive reactance are equal in magnitude (they are 180^0 in opposition), therefore the two impedances cancel each other out and the total impedance is maximized to R [10]. The resonant frequency ω_0 and the characteristic impedance Z_o of the L_rC_r parallel circuit are defined by Eqn 2-1 and Eqn 2-2.

In the presence of a load resistance R, the quality factor Q of the circuit can be defined as the ratio of the circuit resistance to the reactance (of either the resonant capacitor or resonant inductor at the resonant frequency), Q=*R*/*X* as shown in Eqn 2-8.

$$Q=\omega_0 C_r R=\frac{R}{\omega_0 L_r}=\frac{R}{Z_o}=\frac{R}{\sqrt{\frac{L_r}{C_r}}} \qquad \text{Eqn 2-8}$$

The total impedance is then given by:

$$Z=\frac{Z_L Z_c}{Z_L+Z_c} \qquad \text{Eqn 2-9}$$

and after substitution of Z_L and Z_c and simplification, gives

$$Z_\omega = -j\frac{\omega L}{\omega^2 LC-1} \qquad \text{Eqn 2-10}$$

which further simplifies to

$$Z_\omega=-j\left(\frac{1}{C}\right)\left(\frac{\omega}{\omega^2-\omega_0^2}\right) \qquad \text{Eqn 2-11}$$

Where resonant frequency is defined by Eqn 2-1. Thus

$$\lim_{\omega\to\pm\omega_0} Z_\omega=\infty \qquad \text{Eqn 2-12}$$

The parallel LC circuit connected in parallel with a load will act as band-stop filter which has maximum impedance at the resonant frequency [12]. The frequency characteristic of a LC parallel resonant circuit is shown in Figure 2-10.

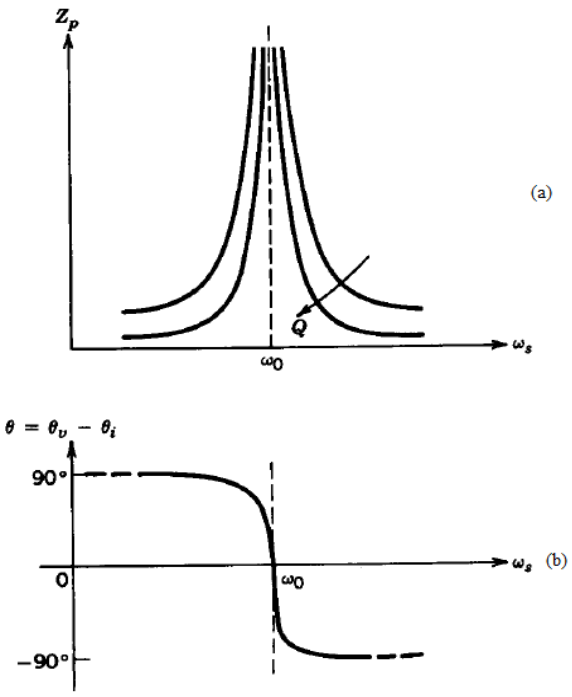

Figure 2- 10 : Frequency characteristics of a parallel resonant circuit [9]. (a): Impedance Z_p and quality factor Q as a function of frequency. (b): Phase angle as a function of frequency.

Figure 2-10 (a) shows that the magnitude Z_p of the circuit impedance as a function of frequency with Q as a parameter, (note that Q now increases with increasing *R* as identified in Eqn 2-8) [9]. It also shows that when the switching frequency ω_s is equal to ω_0, Z_p is infinite.

Figure 2-10 (b) shows the phase angle θ (= $\theta_i - \theta_v$) as a function of frequency. It also shows that the inductor impedance is lower than the capacitor impedance at frequencies below ω_0 ($\omega_s < \omega_0$), therefore the voltage leads the current. When the frequencies above ω_0 ($\omega_s > \omega_0$), the capacitor impedance is lower than the inductor impedance and the voltage lags the current [13]. At the resonant frequency ω_0, the phase angle θ approaches to 0^0, the result is a maximum impedance magnitude at resonance.

The parallel resonant converter (PRC) implies a connection of one inductor Lr and one capacitor Cr in parallel with the output load on the primary side of the main transformer. The circuit diagram is shown in Figure 2-11.

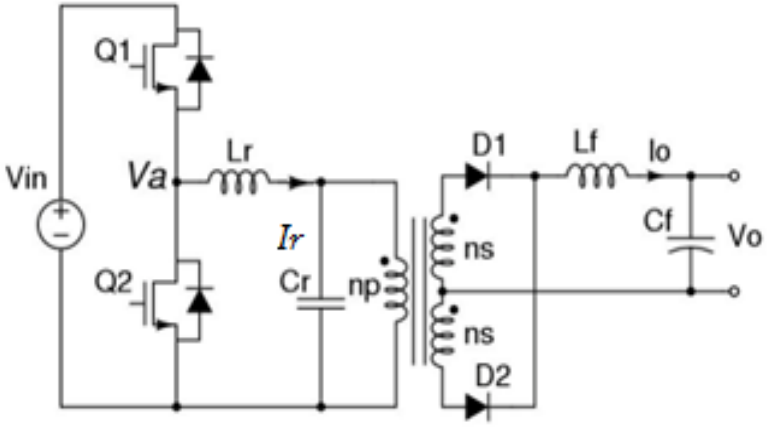

Figure 2-11: Parallel Resonant Converter (PRC).

The PRC resonant tank switching waveforms are shown in Figure 2-12.

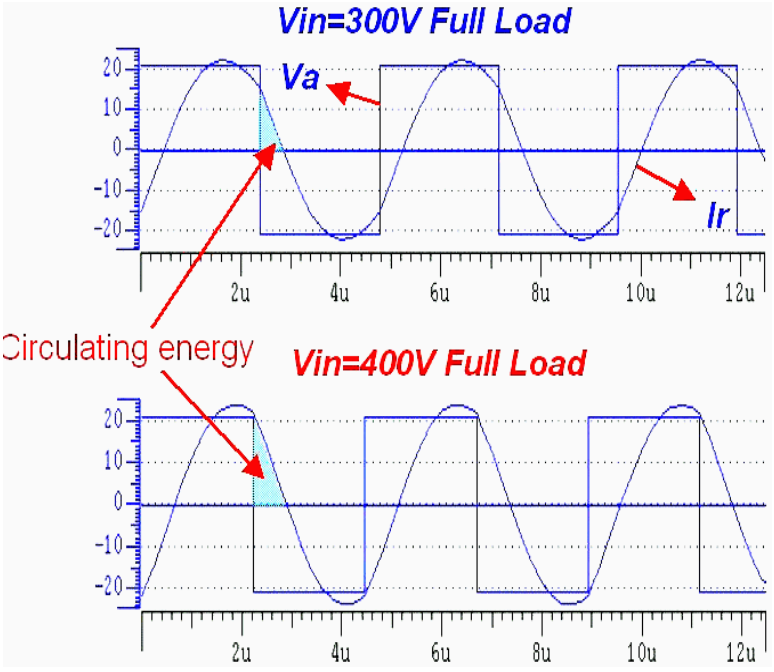

Va: Half bridge switching voltage ;Ir: Resonant current.

Figure 2- 12 : LC resonant tank switching waveforms of a PRC [5].

Figure 2-12 shows the PRC resonant tank switching waveforms with two different input voltages operating under full load condition. From the waveforms, as the input voltage increases from 300V to 400V the circulating energy increases substantially (the circulating energy is shown in the shaded area). As the input voltage increases, the PRC switching frequency increases away from the resonant frequency in order to keep the output power constant. As a result more and more energy is circulating in the resonant tank.

The DC characteristic plot of PRC is shown in Figure 2-13, where f_0 is the resonant frequency, f_s is the switching frequency, and Q is the quality factor.

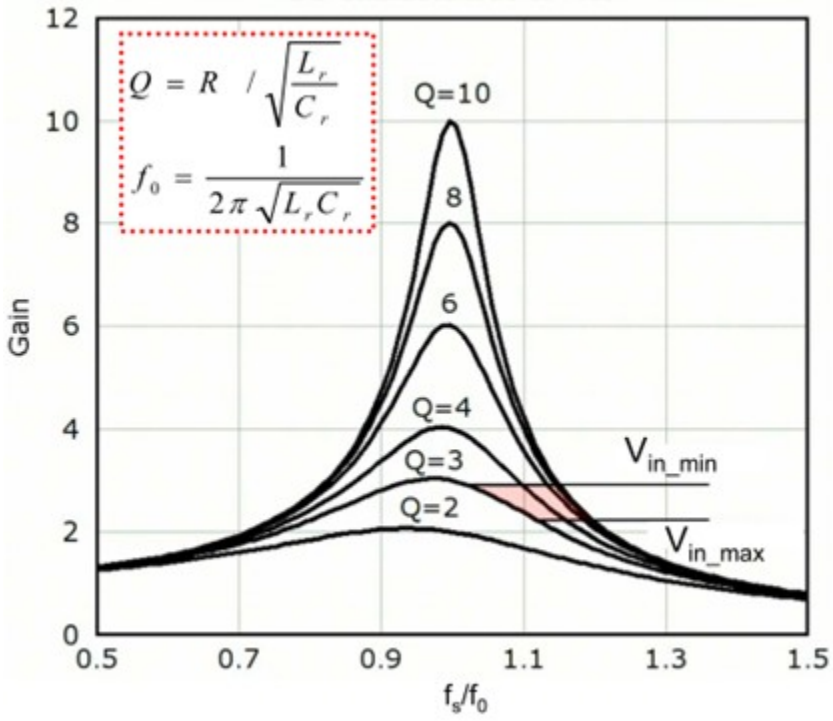

Figure 2-13: DC characteristic plot of PRC [5].

The preferred operating area for the PRC is to the right side of the resonant frequency (where $f_s > f_0$) as shown in the shaded area in Figure 2-12. In this area the PRC operates with ZVS for turn on, but has non-zero current for turn off (similar to the SRC operation). At the resonant frequency, the resonant tank impedance is maximum and the DC gain is at the maximum for the PRC. However, compared to the SRC, the operating area of the PRC is much smaller, hence the output voltage regulation is better as the switching

frequency change is small at close to no load, but the circulating energy is still very high for the PRC.

Similar to the SRC, a problem for this topology is that when the input voltage increases such that a lower gain is required, the switching frequency is higher and away from the resonant frequency. The circulating energy in the PRC is larger than an equivalent SRC. As a result, the turn off current for the power switch is relatively high, and the switching losses are also higher. From the above analysis, the PRC is also not a good option for telecom front–end converters /rectifiers.

2.2.3 Series parallel resonant converter SPRC or LCC

The series parallel resonant converter (SPRC or LCC) implies a series connection of one inductor Lr and capacitor Csr, in parallel with another capacitor Cpr. The circuit diagram is shown in Figure 2-14.

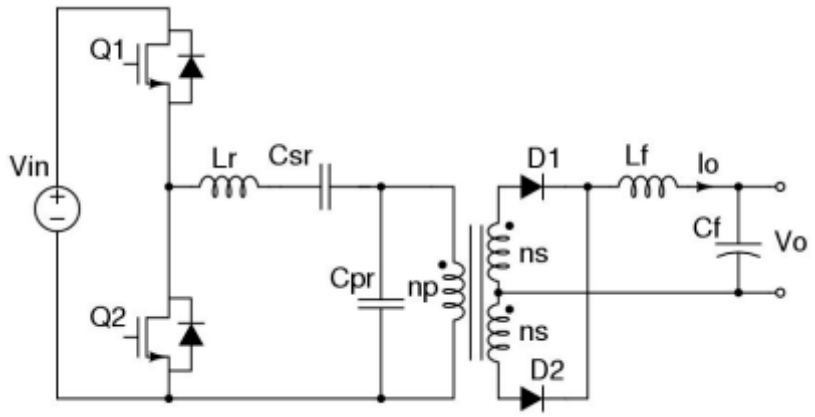

Figure 2-14: Series parallel resonant converter (SPRC or LCC).

This LCC resonant converter can be considered as a combination of an SRC and a PRC, therefore it combines characteristics of both the SPC and PRC. With the load in series with the series tank Lr and Csr, the circulating energy is smaller compared to the PRC. With the parallel capacitor Cpr, the LCC converter can regulate the output voltage at no load.

In order to analyse the LCC converter, its AC equivalent circuit is derived based on AC analysis techniques, as shown in Figure 2-15. The resonant network has the effect of filtering the higher harmonic currents, so that essentially only sinusoidal current appears at the input to the resonant circuit [14].

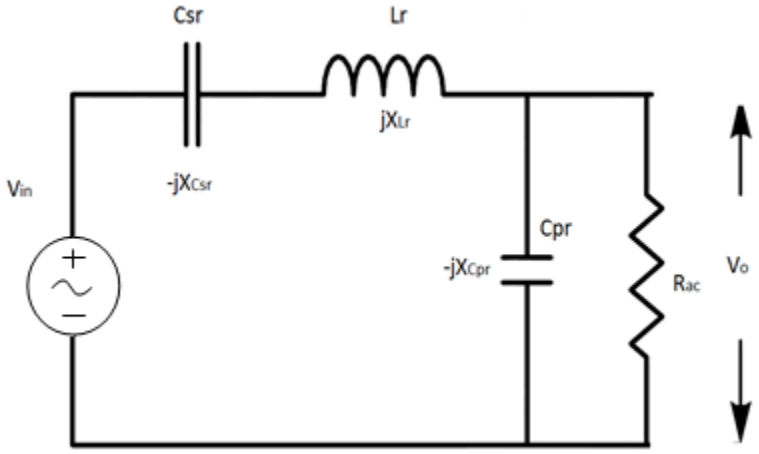

Figure 2-15: LCC AC Equivalent Circuit [15].

This fact allows classical AC analysis techniques to be used. In the AC analysis, the output rectifier (D1, D2 as identified in Figure 2-14) and the filter (Lf, Cf) are replaced by the equivalent ac resistance Rac and the square-wave input voltage source is replaced by its fundamental sinusoidal equivalent voltage waveform, as shown in Figure 2-15. This is the also called the first harmonic approximation (FHA) method. The power transfer from input to output is assumed to be only through the fundamental component and all the harmonics are neglected [14].

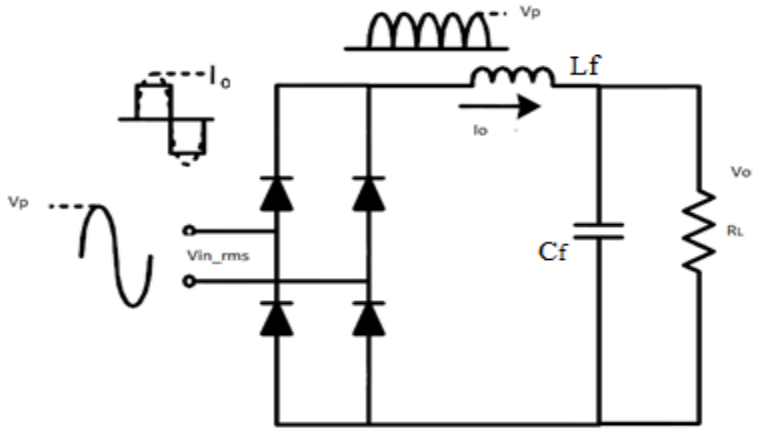

Figure 2- 16 : LCC Equivalent ac resistor as present by rectifier loads [15].

In Figure 2- 16, four diodes are used to ensure full-wave rectification is maintained to replace the centre-tapped transformer. Because R_L represents a pure resistive load and the controller IC is used to drive the LLC resonant circuit work in the vicinity of its resonant frequency, based on FHA analysis, the circuit operates as a tuned LC filter. Therefore when studying with the resonant converter, Rac can be seen as an equivalent purely resistive load.

The equivalent AC resistance for the rectifier and the RMS value of the fundamental component of input square-wave voltage are calculated by:

$$V_{in\_rms}=\frac{\pi}{2\sqrt{2}}V_o \qquad \text{Eqn 2-13}$$

$$I_{in\_rms}=\frac{2\sqrt{2}}{\pi}I_o \qquad \text{Eqn 2-14}$$

$$R_{ac}=\frac{V_{in\_rms}}{I_{in\_rms}}=\frac{\pi^2 V_o}{8\,I_o}=\frac{\pi^2}{8}R_L \qquad \text{Eqn 2-15}$$

$$f_o=\frac{1}{2\pi\sqrt{\frac{L_r C_{pr} C_{sr}}{C_{pr}+C_{sr}}}} \qquad \text{Eqn 2-16}$$

Where f_o is the LCC resonant frequency. The series resonant frequency ω_0 and the series quality factor Q are defined by Eqn 2-1 and Eqn 2-3. By using the AC analysis technique and equivalent load resistor Rac, the voltage gain of the LCC circuit in Figure 2-16 an be expressed as Eqn 2-17 [16].

$$\frac{V_{o\_rms}}{V_{in\_rms}}=\frac{1}{1+\frac{X_{Csr}}{X_{Cpr}}-\frac{X_{Lr}}{X_{Cpr}}+j[\frac{X_{Lr}}{R_{ac}}-\frac{X_{Csr}}{R_{ac}}]} \qquad \text{Eqn 2-17}$$

The equivalent impedance Z_{eq} is defined by:

$$Z_{eq}=j(X_L-X_{cs})+\frac{1}{\frac{1}{R_{ac}}-\frac{1}{jX_{Cp}}} \qquad \text{Eqn 2-18}$$

With R_{ac} defined in Eqn 2-15, given by $X_{Lr}=\omega Lr$, $X_{Csr}=\frac{1}{\omega C_{sr}}$, $X_{Cpr}=1/\omega C_{pr,}$ Z_{eq} can be rewritten by:

$$Z_{eq}=[j(\frac{\omega L}{R_L}-\frac{1}{\omega C_s R_L})+\frac{1}{\frac{8}{\pi^2}+j\omega C_p R_L}] \qquad \text{Eqn 2-19}$$

The LCC resonant tank switching waveforms are shown in Figure 2-17.

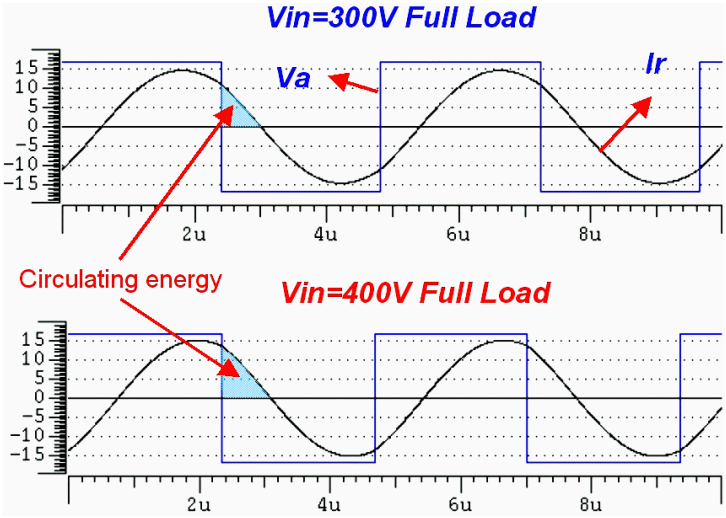

Va: Half bridge switching voltage; Ir: Resonant current.

Figure 2-17: LCC resonant converter switching waveforms [5].

Figure 2-17 shows the LLC resonant tank switching waveforms with two different input voltages operating under full load condition. From the waveforms, as the input voltage increases from 300V to 400V, the circulating energy increases. The resonant current Ir in the LCC circuit is reduced compared to the equivalent Ir in the PRC circuit, but increased compared to the SRC circuit.

Therefore, the circulating energy in the LCC converter is smaller than the PRC circuit, but bigger than the SRC circuit. The DC characteristic plot of the LCC converter is shown in Figure 2-18, where f_0 is the LCC resonant frequency, f_s is the switching frequency, and Q is shown the quality factor.

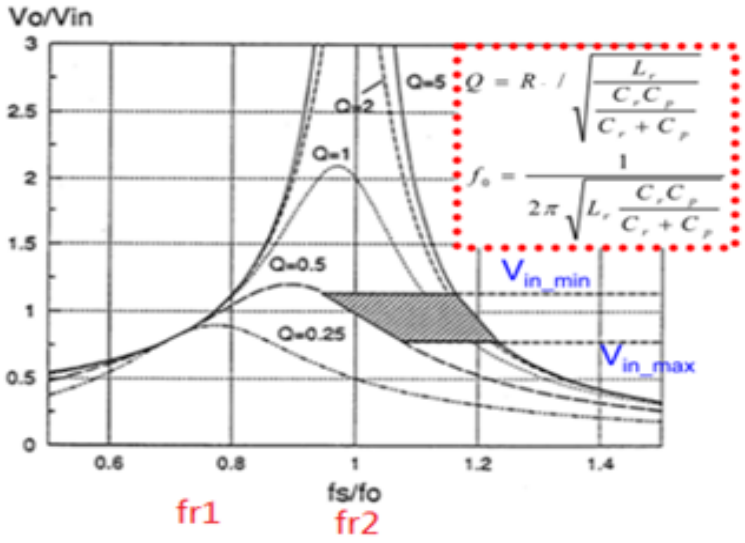

Figure 2-18: DC characteristic plot of SPRC or LCC [5].

Figure 2-18 shows the more complex characteristic of the LCC in that it consists of two resonant frequencies. They are the series resonant frequency, fr1, consistent with the series resonant tank Lr and Csr and the LCC resonant frequency fr2 (previously identified as f_0) consistent with Lr, Csr and Cpr. In Figure 2-18, each curve is represented by a different value of Q. It shows that when Q decreases, the peak of the resonant curves move towards the frequency fr1. As such, if the load resistance is low enough to effectively short out the parallel capacitor Cpr, then the curve peak will be at fr1[16]. As a result, at low Q, the LCC resonant tank is operating in the SRC mode. When Q increases, the peak of the resonant curves move towards fr2 (f_0), where the parallel capacitor Cpr is now part of the LCC resonant tank. At high Q, the LCC is operating at light load or no load and in PRC mode.

The output voltage regulation for the LCC converter is better than either the SRC or PRC converters at no load condition. This is because the LCC converter can achieve a switching frequency change within a narrow range for load changes close to no load [4]. Like the SRC and PRC converters, the preferred operating region is to the right-hand side of fr2 to achieve ZVS at turn on for all load conditions. But at high frequency, it is still desirable to operate at the series resonant frequency fr1 to achieve best load regulation

and high efficiency. Although the LCC converter combines the advantages of the SRC and the PRC converters, unfortunately, the circulating energy and turn-off current of the power switch devices still increases as the input voltage increases. In practice, the operating frequency range is in the right hand side of fr2.

Overall, in order to achieve a wide input voltage range telecom converter design, all these traditional resonant converters encounter the same problems with higher than desired switching losses. To achieve high switching frequency and high efficiency with small switching losses for a wide range of input voltages, a different topology is required. The LLC resonant converter topology is introduced as a solution and analyzed in the following sections.

2.3 The LLC Resonant Converter

As can see from the previous sections in this Chapter, the three traditional resonant converter topologies are not particularly suitable for telecom DC/DC converters. Thus, a possible LLC resonant converter topology is introduced to overcome the observed limitations. The LLC resonant topology can be seen as a modified version of an SRC converter. An LLC converter comprises of a series connection of an inductor Lr, a capacitor Cr, and a second inductor Lm (that is connected in parallel with the transformer primary winding).The circuit diagram is shown in Figure 2-19.

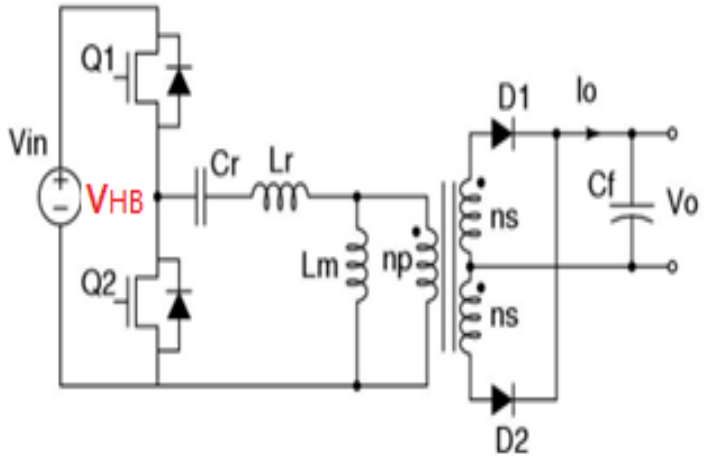

Figure 2-19: LLC Resonant Converter [3].

The LLC resonant converter looks very similar to the LC series resonant converter (SRC) apart from the addition of the inductor Lm. The value of Lm is normally around 3 ~8 times larger than the resonant inductor Lr, in most practical designs [5]. Lm can be practically realized by using the magnetizing inductance of the transformer [5], hence the symbol notation of Lm. In order to analyse the LLC converter, its AC equivalent circuit is derived based on AC analysis techniques, as shown in Figure 2-20.

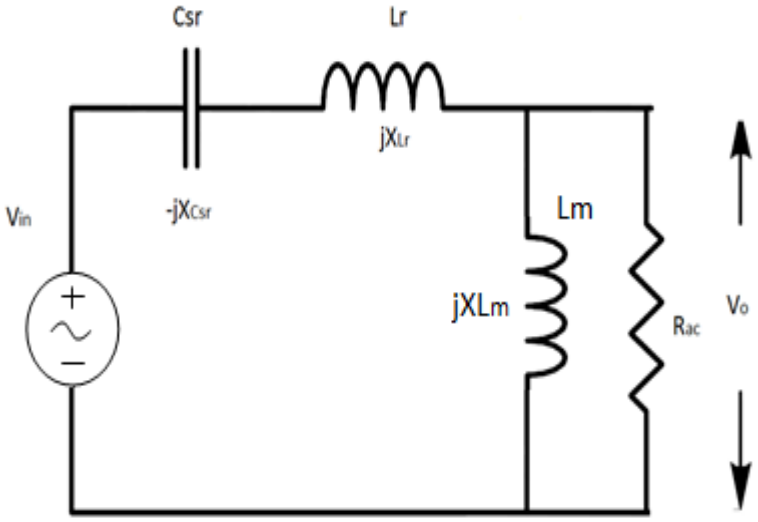

Figure 2-20: The LLC converter ac equivalent circuit [17].

The LLC converter equivalent AC resistor as present by rectifier loads is shown in Figure 2-21.

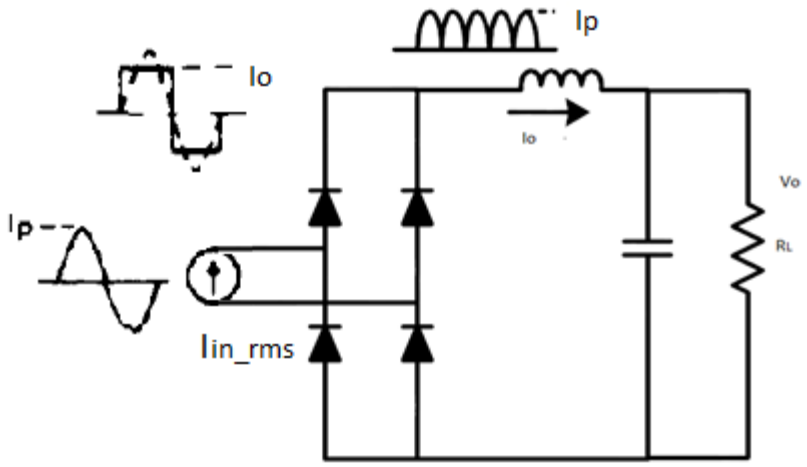

Figure 2-21: LLC Equivalent AC resistor as present by rectifier loads [17].

In Figure 2-21, four diodes are used to ensure full-wave rectification is maintained to replace the centre-tapped transformer. AC analysis of the LLC resonant circuit is made in a similar manner to the earlier analysis of the LCC resonant circuit. The equivalent AC resistance for the rectifier and the RMS value of the fundamental component of input square-wave voltage are calculated by:

$$V_{in\_rms}=\frac{2\sqrt{2}}{\pi}V_o \qquad \text{Eqn 2-20}$$

$$I_{in\_rms}=\frac{\pi}{2\sqrt{2}}I_o \qquad \text{Eqn 2-21}$$

$$R_{ac}=\frac{V_{in\_rms}}{I_{in\_rms}}=\frac{8V_o}{\pi^2 I_o}=\frac{8}{\pi^2}R_L \qquad \text{Eqn 2-22}$$

$$f_o=\frac{1}{2\pi\sqrt{L_r C_r}} \qquad \text{Eqn 2-23}$$

The DC characteristic plot of the LLC converter is shown in Figure 2-22, where fr1 is the upper resonant frequency (equivalent to fo), f_s is the switching frequency, and Q is the quality factor.

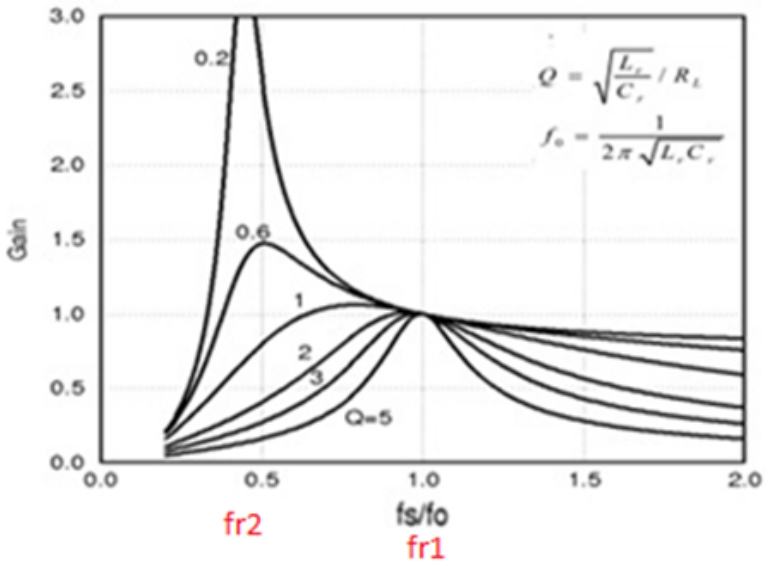

Figure 2-22: DC characteristic plot of the LLC resonant converter [5].

Observing the LLC DC characteristic plot shown in Figure 2-22, it can be seen that there are two resonant frequencies. Because the LLC resonant converter is derived from the SRC, the higher resonant frequency (fr1) is equivalent to the SRC resonant frequency fo. This higher resonant frequency is determined by the resonant network of inductor Lr and capacitor Cr; the lower resonant frequency, fr2, is determined by the series combination of Lm, Lr and Cr. As the load increases, the switching frequency increases.

At normal operating conditions, the LLC resonant converter operates higher than, but very close to the resonant frequency fr1, which is the best operation point to obtain high efficiency [5]. Although the LLC resonant converter also has two resonant frequencies, both the lower and higher resonant frequencies operate with ZVS for turn on. This is a great benefit for telecom front– end AC/DC converter designs, whereby the output voltage can be regulated within a narrow frequency range. The LLC resonant converter can be optimized to achieve high efficiency with a wide input voltage range because its resonant frequency fr1 is located in the inductive region as shown in Figure 2-22.

From above analysis, the LLC resonant converter has some significant advantages compared to the other three identified resonant converters. Namely, LLC converters can

regulate the output voltage with a wide range of input voltage and output load over a relatively small switching frequency change, it can achieve ZVS (for turn on) from virtually no load to full load, it has low turn-off current for the primary side power switches (helping to reduce switching losses), it can achieve ZCS for the secondary side rectifiers, and reduces voltage stress. Therefore, LLC resonant converters provide a near perfect solution for the telecom front –end converter application.

2.4 Detailed Operation Of The LLC Resonant Converter

The operating region of the LLC resonant converter is shown in Figure 2-23. As introduced in Section 2.3, to best illustrate and differentiate between the two resonant frequencies, we use fr1 to show the higher resonant frequency (fr1 is equivalent to fo), and fr2 to show the lower resonant frequency. As can be seen from Figure 2-23, the operating region of the LLC resonant converter is divided into two primary switching type regions: the ZCS region and the ZVS region. When the converter is switching at frequencies higher than resonant frequency fr1, it is always running in ZVS mode (for turn on). When the converter is switching at frequencies lower than resonant frequency fr2, it is always running in ZCS mode. When the converter is switching at frequencies between the resonant frequencies fr1 and fr2, the load condition determines whether the converter is operating in ZVS or ZCS mode.

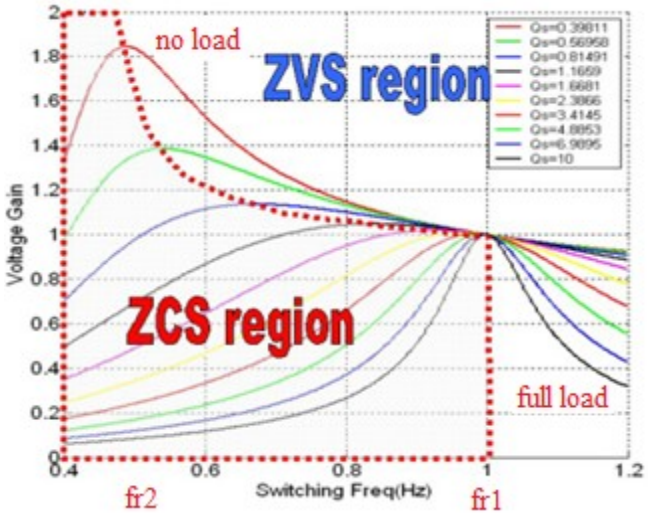

Figure 2-23: DC characteristic plot of LLC with ZVS and ZCS region [3].

Because power MOSFETs are widely used as the primary power switches in LLC resonant converter applications, their operating characteristics make ZVS the preferential mode. This is because a MOSFET, which can be modeled as a parallel connected parasitic capacitor with the series Rds_on resistor, that has a high drain-source voltage when off, can experience significant switching losses every time it is turned on [9]. In principle, to ensure that an LLC resonant converter is operating in the ZVS region, it is important to choose the right value for Lr, Lm and Cr, so that the converter is always running above resonant frequency fr2.

The two resonant frequencies are calculated as shown by Eqn 2-24 and Eqn 2-25:

$$f_{r1}=\frac{1}{2\pi\sqrt{L_rC_r}} \qquad \text{Eqn 2-24}$$

$$f_{r2}=\frac{1}{2\pi\sqrt{(L_{m+}L_r)C_r}} \qquad \text{Eqn 2-25}$$

The magnetizing inductor can be utilized to achieve soft switching for the primary side MOSFET switches. It also can be part of the resonant tank switching to modify the voltage gain characteristic. Furthermore, according to the resonant switching frequency, the LLC converter can operate in three different regions as shown in Figure 2-24. These three regions are: Region 1, where the switching frequency is above resonant frequency fr1; Region 2, where the switching frequency is between the two resonant frequencies fr1 and fr2 (for a given Q); Region 3, where the switching frequency is below resonant frequency fr2 (for a given Q). The best practice for LLC converter design is to make sure it always operates in either region 1 or region 2.The converter should be prevented from entering region 3.

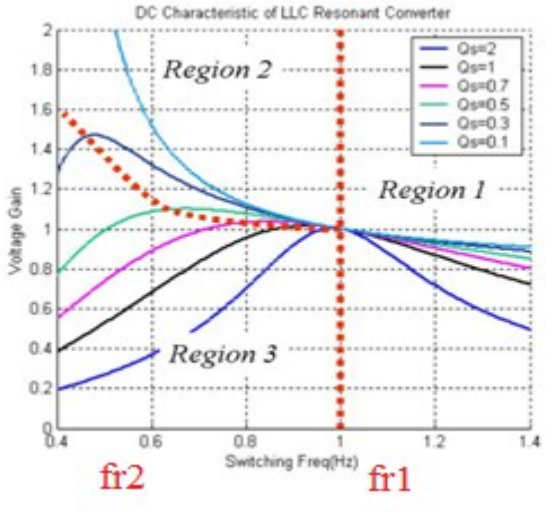

Figure 2-24: Three operating regions of LLC resonant converter [3].

2.4.1 Operation above the resonant frequency fr1.

In region 1, when the LLC resonant converter switching frequency fs is higher than fr1, the circuit operates very similarly to the SRC as the magnetizing inductance Lm never resonates with capacitor Cr. This is because Lm is clamped by the output voltage and the resonant tank treats it as an inductive load [18]. With this inductive load, the LLC resonant converter can achieve ZVS for turn on (especially at no load condition) without having a very high switching frequency. As this region is the inductive load region, the LLC converter is always under ZVS operation regardless of the load condition. Figure 2-25 shows the region 1 ZVS operation waveforms (where fs is above fr1). Figure 2-26 shows the equivalent circuit operation for fs>fr1.

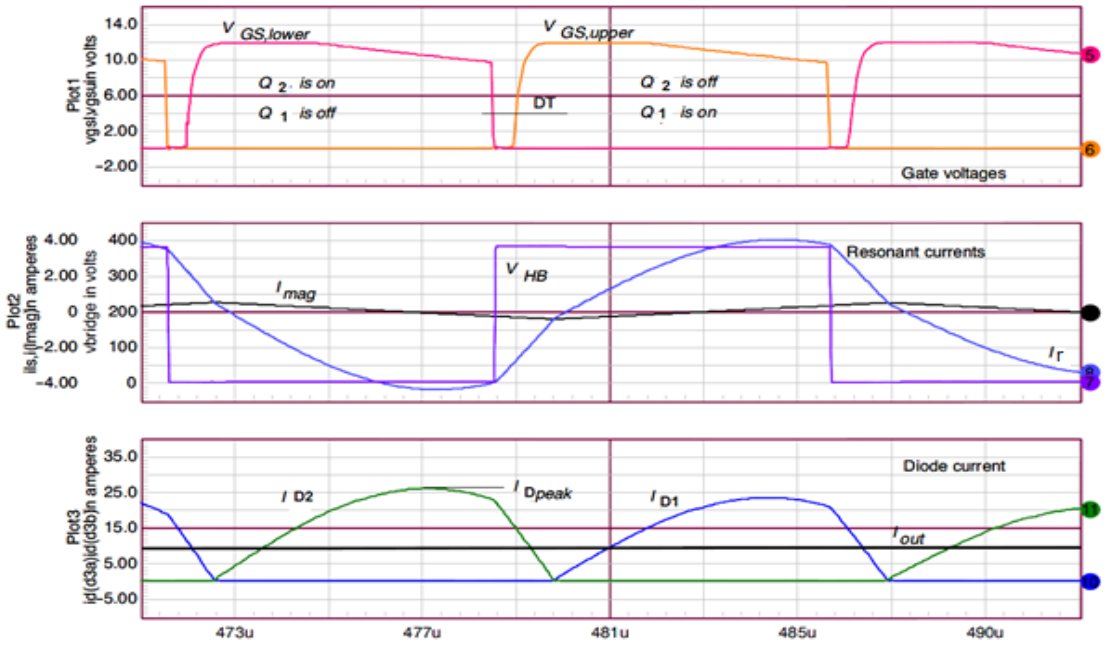

Q1 inYellow: Top MOSFET gate-source voltage, Q2 in Red: Bottom MOSFET gate-source voltage, Imag in Gray: magnetizing current, V_{HB} in Purple: Half bridge node switching voltage, I_r in Blue: Resonant current, I_{D1} in dark Blue: Output diode D1 current, I_{D2} in Green: Output diode D2 current, Io in Black: Output current.

Figure 2-25: ZVS operation waveforms (for fs>fr1) [19].

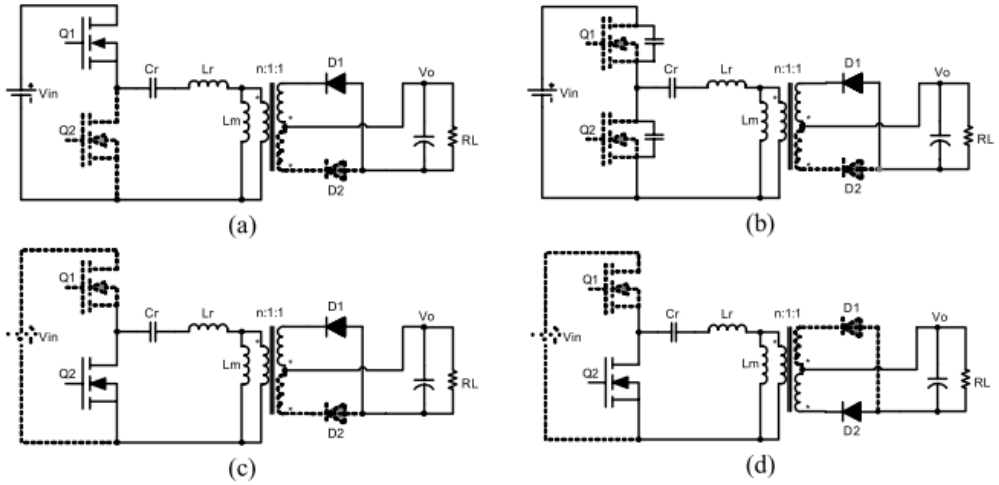

Figure 2-26: Equivalent circuit forfs>fr1.(a): Q1 and D1are conducting, (b): D1 only is conducting, (c): Q2 and D1 are conducting, (d): Q2 and D2 are conducting [20].

Observing Figure 2-26 it can be seen that at time interval (a), Q1 is conducting and the resonant tank is transferring energy to the load through D1. At time interval (b), both Q1 and Q2 are off, the bridge voltage V_{HB} (as shown in Figure 2-25) drops to zero (clamped by the body diode of Q2), but the output diode D1 is still conducting. This is because as the switching frequency is above fr1, the resonant current I_r is bigger than the magnetizing current I_{mag}. When Q1 is off, there is still some current flowing in the primary side of the transformer. The bridge voltage V_{HB} now starts charging up the Q2 and discharging the Q1 drain-source parasitic capacitor, therefore Q2 turns on with ZVS at time interval (c). Since Q2 is conducting, the resonant current I_r decreases quickly. At time interval (d), when I_r reaches the same value as I_{mag}, diode D1 turns off and D2 turns on to transfer energy to the load.

Furthermore, the magnetizing inductor Lm is always clamped by the reflected output voltage as one secondary diode is always conducting [9]. In other words, only a single resonance occurs in this mode which is defined by Lr and Cr.

2.4.2 Operation at the resonant frequency fr1

This mode occurs at the transition between region 1 and region 2 as shown in Figure 2-24, as the LLC resonant converter switching frequency is same as the resonant frequency fr1. Figure 2-27 shows the ZVS operation waveform at fs=fr1. Figure 2-28 shows the equivalent circuit operation at fs=fr1.

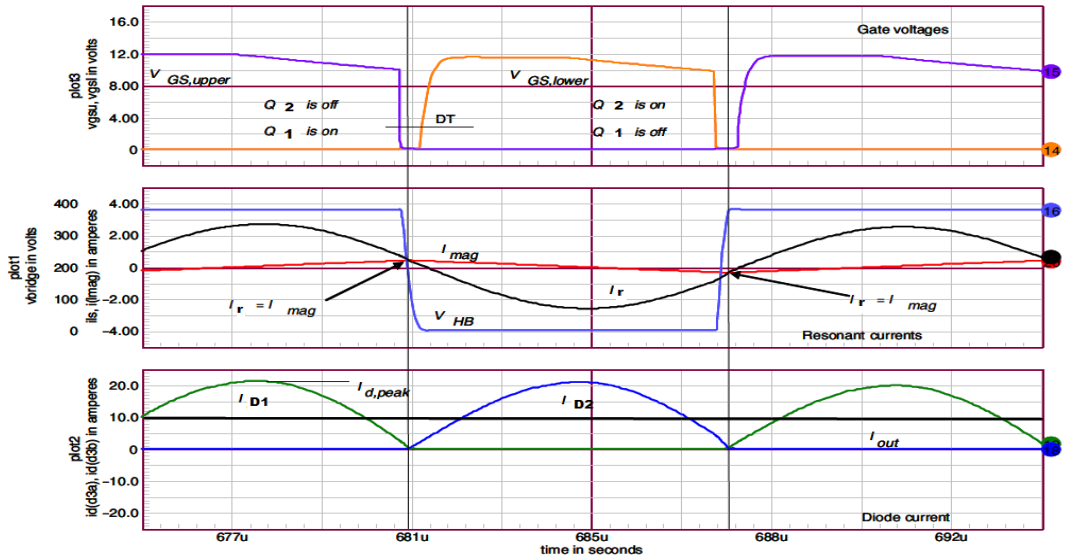

Q1 inYellow: TopMOSFET gate-source voltage, Q2 in Red: Bottom MOSFET gate-source voltage, Imag in Gray: magnetizing current, V_{HB} in Purple: Half bridge node switching voltage, I_r in Blue: Resonant current, I_{D1} in dark Blue: Output diode D1 current, I_{D2} in Green: Output diode D2 current, Io in Black: Output current.

Figure 2-27: ZVS operation waveform (at fs=fr1) [19].

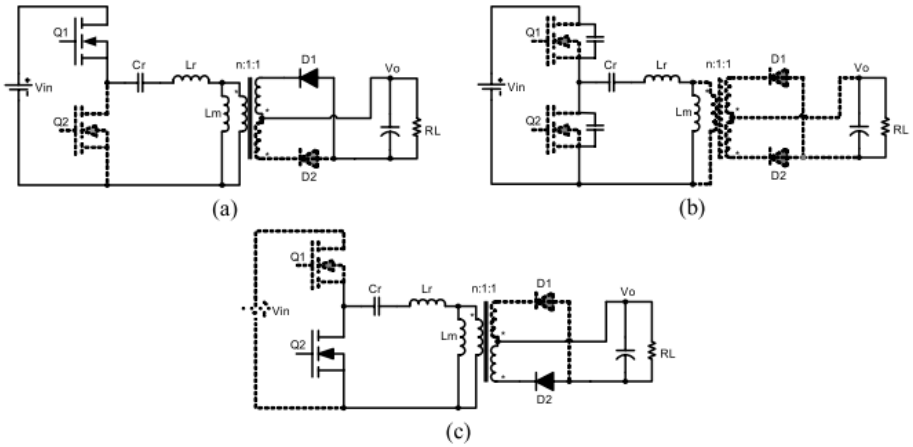

Figure 2-28:Equivalent circuit at fs=fr1. (a): Q1 and D1are conducting; (b): Q1,Q2, D1,D2 are off; (c): Q2 and D2 are conducting [20].

Observing Figure 2-28 it can be seen that at time interval (a), the resonant current I_r is bigger than the magnetizing inductor current I_{mag}, Q1 is conducting and the resonant tank is transferring energy to the load. According to the polarity of the transformer, output

diode D1 is conducting. Because the voltage on the transformer magnetizing inductor is clamped by the output voltage, the magnetizing inductor current I_{mag} increases linearly. During this period, the difference between the input and output voltage is applied to the resonant tank, so the resonant current I_r is a sinusoidal waveform. At time interval (b), I_r reaches the same value as the I_{mag}, and Q1 turns off. Output diode D1 turns off as well. This is because I_r is equal to I_{mag} and there is no current transferring to the load. The drain-source parasitic capacitance of Q1 and Q2 can help discharging the magnetizing current, therefore ZVS can be achieved. At time interval (c), Q2 turns on with ZVS, I_r is bigger than I_{mag}, and the resonant tank is transferring energy to the load through D2.

At fs=fr1, the resonant tank impedance is at a minimum. From Figure 2-24 it can be seen that the voltage gain at this frequency is equal to 1 and all curves intersect at this point. When the LLC resonant converter is operating at this point, the input and output voltages are virtually connected together, and the resonant network transfer function becomes insensitive to the load variations [19]. It is considered best practice to design the LLC resonant converter to operate at the fs=fr1 point at full load and nominal input voltage conditions [20].

2.4.3 Operation below the resonant frequency fr1

Operation of the LLC converter in region 2 is very complex, as the lower resonant frequency fr2 varies with load changes. Therefore, the boundary of region 2 and region 3 tracks with the peak gain of the load as shown by the red dotted line in Figure 2-24.

Furthermore, the complex operation can be divided into two time intervals. In the first time interval, Lr only resonates with Cr, while Lm is clamped by the output voltage. When the current in Lm reaches the same level of current in Lr, the resonance between Lr and Cr is stopped. Therefore, Lm starts to participate in the resonance and starts the second time interval. During this time, Lr and Cr are in series with Lm forming the resonant network. As a result of this special feature, the LLC resonant converter varies the switching frequency at different time intervals due to different operating conditions.

Figure 2-29 shows the ZVS operation waveforms for fs<fr1. Figure 2-30 shows the equivalent circuit operation for fs<fr1.

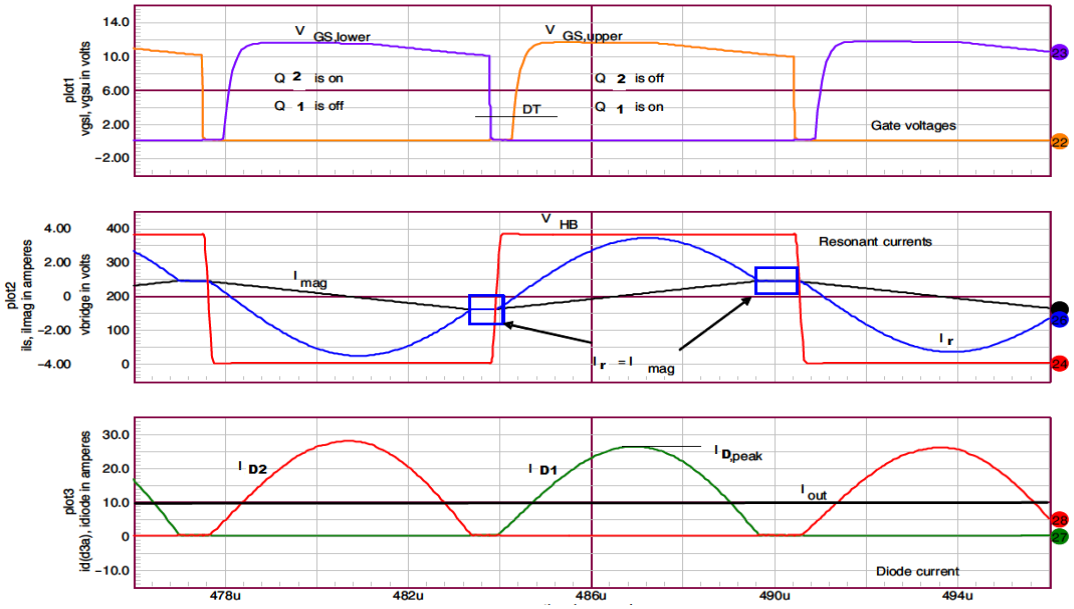

Q1 inYellow: Top MOSFET gate-source voltage, Q2 in Red: Bottom MOSFET gate-source voltage, Imag in Gray: magnetizing current, V_{HB} in Purple: Half bridge node switching voltage, I_r in Blue: Resonant current, I_{D1} in dark Blue: Output diode D1 current, I_{D2} in Green: Output diode D2 current, Io in Black: Output current.

Figure 2-29: Region 2 ZVS operation waveform (fs<fr1)[19].

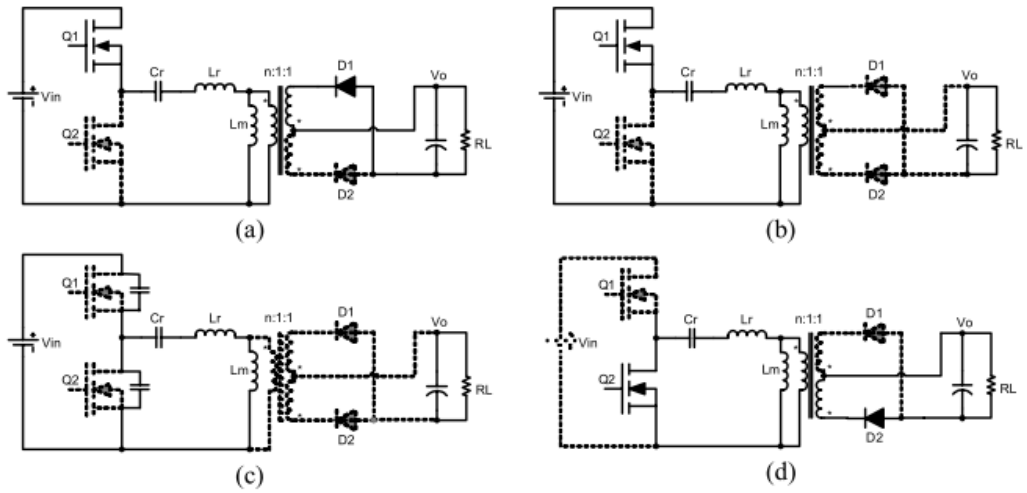

Figure 2-30: Equivalent circuit for fs<fr1 [20]. (a): Q1 and D1are conducting; (b): Q1 is conducting; (c): Q1, Q2, D1, D2 are off; (d): Q2 and D2 are conducting.

Observing Figure 2-30 it can be seen that at time interval (a), Q1 and output diode D1 are conducting, the resonant tank is transferring energy to the load, and resonant current I_r is bigger than I_{mag}. At this period, I_{mag} is increasing linearly and I_r is resonating as a sinusoidal waveform. At time interval (b), Q1 is still conducting, and I_r resonates back and equals I_{mag}. Therefore, the magnetizing inductor begins to participate in the resonant network and the switching frequency changes to the minimum frequency, with Lm in series with Lr and resonant with Cr. Since the resonant current is equal to the magnetizing inductor current, diode D1 is turned off, and resonant energy is stopped from transferring to the load. At time interval (c), Q1 turns off, both D1 and D2 are off, I_r is still circulating in the same direction, and the bottom MOSFETs Q2's drain-source parasitic capacitance start to discharge the energy. At time interval (d), Q2 turns on with ZVS at the end of the plateau where I_r no longer equals I_{mag}. The resonant tank is transferring energy to the load through D2. Therefore, the magnetizing inductor stops participating in the resonant network and the switching frequency changes to the resonant frequency fr1.

From the previous analysis, it can be seen that the LLC resonant converter is able to achieve a voltage gain larger, smaller, or equal to one. When the switching frequency operates at fr1, the converter voltage gain is equal to one, and the circuit operates optimally. ZVS can be achieved with the magnetizing current, which is not related to load current. Thus ZVS can be achieved even with no-load. Since this magnetizing current is also the turn off current of the power MOSFETs, the switching losses can be reduced.

2.5 DC Analysis Of The LLC Resonant Converter

DC characteristic analysis is the most important tool that is used for the LLC resonant converter design [18]. The major parameter values can be chosen by analysis of the DC characteristic curve. Design trade off decisions can also be made. The DC characteristic

curve reflects the true relationship between the voltage gain and switching frequency under different load and input conditions.

The switching frequency operation of the LLC resonant converter depends on the load conditions. At lower power consumption, the switching frequency is higher and further away from the resonant frequency fr1. At high power, the switching frequency is reduced to close to fr1 to deliver enough power to the load. The principle of the LLC converter operation assumes that the resonant network operates close to fr1, thus essentially only a sinusoidal current waveform occurs as the fundamental element inside the resonant network to transfer energy to the output load.

With this assumption, all harmonics can be considered as removed due to the resonant network LC filter for the square wave voltage excitation, and only the sinusoidal fundamental component passes through. As such, the First Harmonic Approximation (FHA) [10] method can be used again. The simplified circuit network is shown in Figure 2-31.

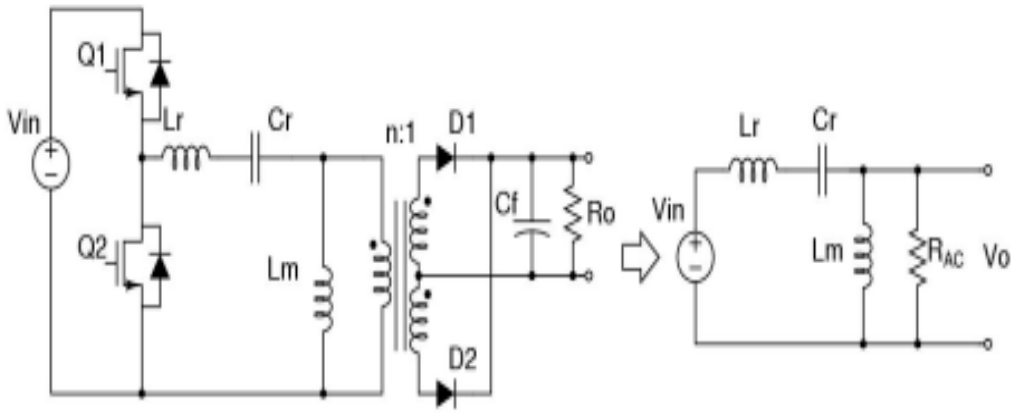

(a) (b)

Figure 2-31: Simplified network circuit with FHA [10]. (a) : LLC resonant circuit; (b) : FHA simplified LLC circuit.

Based on the FHA assumption, the nonlinear elements in the network like the MOSFETs and diodes can be replaced with linear components. This simplified circuit can be used to

derive the DC characteristic curve in a very simple way. This can be further demonstrated by SPICE model circuit simulation results.

A frequency-domain simulation circuit model is built with SPICE-based software (MicroSim Student Version 8.0) to derive an accurate DC characteristic curve according to Figure 2-31. In the simulation, by changing the output load conditions and the switching frequency, an output voltage can be plotted for each point. By stepping the load and sweeping the frequency, an accurate DC characteristic curve can be achieved. The SPICE-based simulation circuit is shown in Figure 2-32, including the transformer circuit. The simulation results are shown in Figure 2-33.

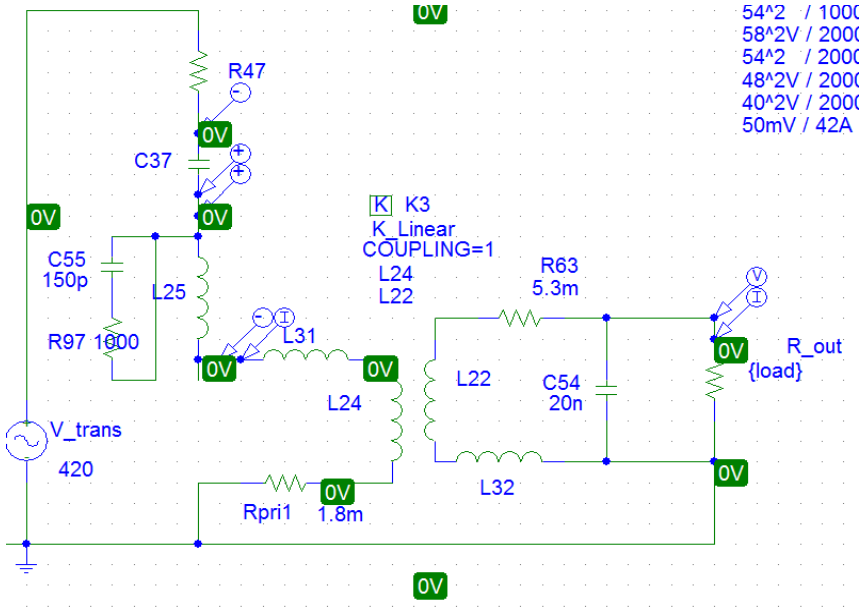

Figure 2-32: SPICE AC-domain LLC simulation circuit.

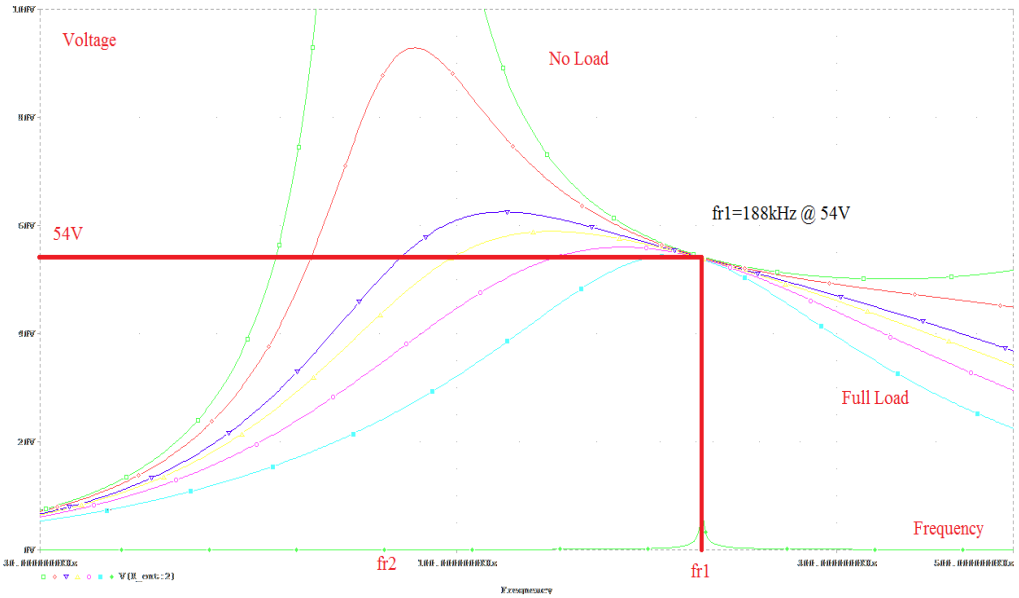

Upper green trace: No load; Red trace: 10A load; Blue trace: 15A load; Yellow trace: 20 A load; Purple trace: 30A load; Light blue trace: Full load; Lower green trace: fr1 indication.

Figure 2-33: SPICE AC-domain simulation DC characteristic curve.

The SPICE simulation circuit shown in Figure 2-32 was constructed to show the AC frequency sweep output DC characteristic of the 48VLLC DC-DC converter topology for the current Eaton APR48-3G. It defines the DC output characteristics under different input voltage or load conditions, such as no load, light load, and full load conditions.

The two resonant frequencies are calculated as shown by Eqn 2-26 and Eqn 2-27:

$$f_{r1}=\frac{1}{2\pi\sqrt{L_rC_r}}=\frac{1}{2\pi\sqrt{8*10^{-6}*72*10^{-9}}}=209.81\text{kHz} \qquad \text{Eqn 2-26}$$

$$f_{r2}=\frac{1}{2\pi\sqrt{(L_m+L_r)C_r}}=\frac{1}{2\pi\sqrt{(8*10^{-6}+26*10^{-6})*72*10^{-9}}}=101.7\text{kHz} \qquad \text{Eqn 2-27}$$

Observation of this LLC converter DC characteristic in Figure 2-33 shows that the two different resonant frequencies are located at 189.659 kHz and 101.7 kHz. The calculated

two resonant frequencies (based on Eqn 2-26 and Eqn 2-27) are 209.81 kHz and 100.25kHz. The output of this simulation work returned favorable results as the simulation results are very close to the theoretical results. The SPICE AC-domain simulation creates an initial LLC converter circuit approximation design, which can help the designer to better understand the LLC resonant circuit behavior. The differences between the calculated and SPICE simulated frequencies are within 10% which is acceptable. Simulation inaccuracies are caused by the simplified process based on the FHA theory, and the transformer SPICE model is assumed to have a perfect coupling between the primary side and the secondary side.

In order to compare the SPICE simulation performance with the actual 48VDC LLC converter hardware circuit performance, new bench experiment testing was required to collect different frequency points under different operating conditions such as no load, light load and full load. This bench testing was set up and carried out at Eaton. A close comparison has been made and the results have been summarized in Table2-1. This testing was carried out with the Eaton APR48-3G. Equipment used to generate these results are: Yokogawa WT230 AC power meter, DC meter Agilent 34970A, Agilent scope 3000 series. The input voltage is at 230Vac. The bench-test results have an error value of ±5% based on the measurement equipment errors.

	Bench Testing Frequency Measurement Results				**SPICE Simulation Frequency Measurement Results**			
Load Current	Output Voltage				Output Voltage			
	43V	48V	54V	58V	43V	48V	54V	58V
0A	500kHz	279kHz	208kHz	186kHz	465kHz	263kHz	204kHz	186kHz
10A	424kHz	272kHz	207kHz	185kHz	39d7kHz	258kHz	203kHz	185kHz
20A	336kHz	258kHz	205kHz	185kHz	321kHz	250kHz	202kHz	184kHz
30A	-------	247kHz	204kHz	184kHz	-------	243kHz	201kHz	183kHz
35A	-------	242kHz	-------	-------	-------	239kHz	-------	-------

Table2-1 : Performance comparison between simulation and actual hardware results.

Table2-1 shows that the output of the AC-domain simulations returned favorable results as they are very close (within 10%) to the experimental results. Based on the SPICE AC-domain simulation approximation circuit shown in Figure 2-32, a transient time-domain SPICE simulation approximation circuit has been created as shown in Figure 2-34.

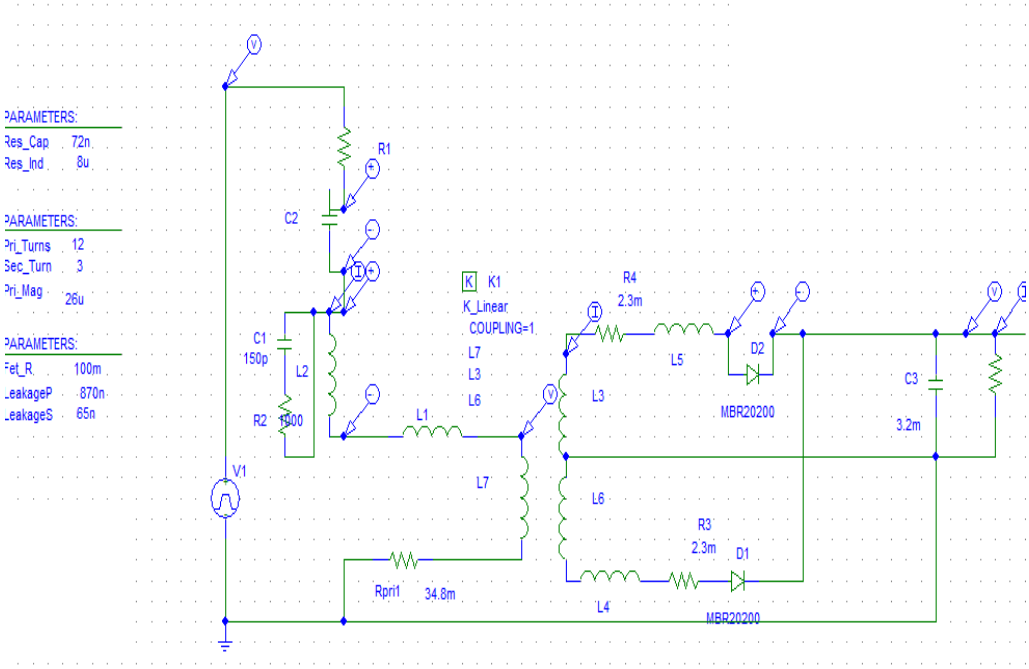

Figure 2-34: SPICE transient time-domain LLC converter simulation circuit.

A SPICE time-domain based transient analysis can calculate the LLC circuit voltage and current as a function of time when a large signal is applied [11]. This transient model approximation circuit includes the LLC converter circuit's non-linear components of two output diodes (MBR20200CT). The LLC resonant network circuit has the same values as the AC-domain simulation circuit. The secondary stage of the main transformer has two split windings in the transient model circuit to improve the SPICE simulation accuracy.

The two MBR20200CT diodes SPICE model was downloaded from the manufacturer supplier website. This part is specially designed for high voltage (200V) and high current (20A) power electronic applications. The MBR20200CT diode SPICE model has significantly improved the accuracy of the simulation outcomes.

The main transformer model has been carefully designed in order to improve the simulation accuracy. The actual main transformer electrical parameter values have been measured with an AgilentLCR-4284A (Inductor-Capacitor-Resistor) meter.

Both short circuit and open circuit tests have been done in order to measure the detailed primary and secondary parameter values. As a result, the transformer parameter values used to create the SPICE transient model are: primary leakage inductance 870nH, secondary leakage inductance 65nH, primary winding resistance 46.8mΩ, and secondary winding resistance 4.6mΩ, transformer turns ratio 4:1.

The SPICE transient simulation outputs have been obtained after inserting values of resonant inductance Lr (8μH), magnetic inductance Lm(26μH), resonant capacitor Cr(72nF), transformer turns ratio(12:3), MOSFET resistance (100mΩ) and load resistance(200Ω for no load, and 1.37Ω for full load) into the SPICE model circuit. Figure 2-35 shows the bench experimental testing results at 48VDC no load and full load. Figure 2-36 shows the SPICE time-domain transient simulation results at 48VDC no load and full load.

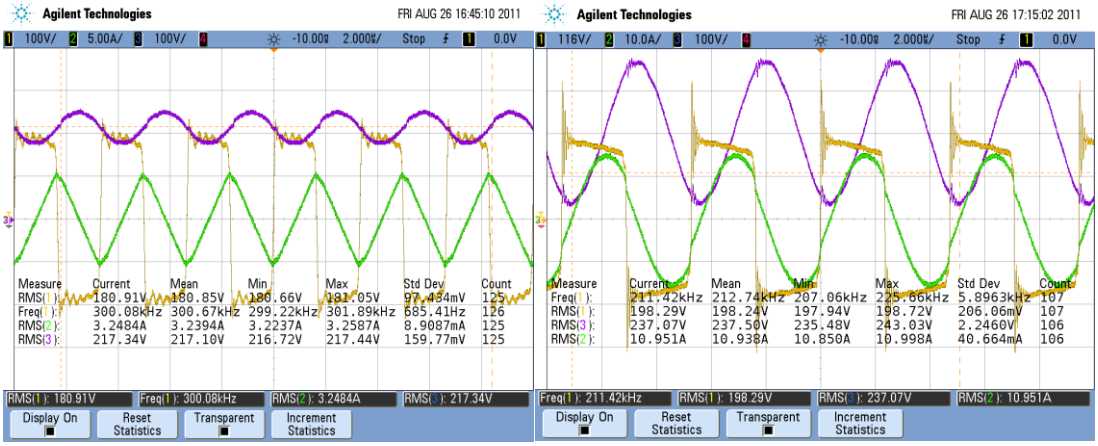

(a) No Load （b） Full Load

Figure 2-35 : Bench testing results at 48VDC no load and full load. Ch1_Yellow trace: Transformer primary voltage; Ch2_Green trace: Resonant current I_r ; Ch3_Purple trace: Resonant voltage.

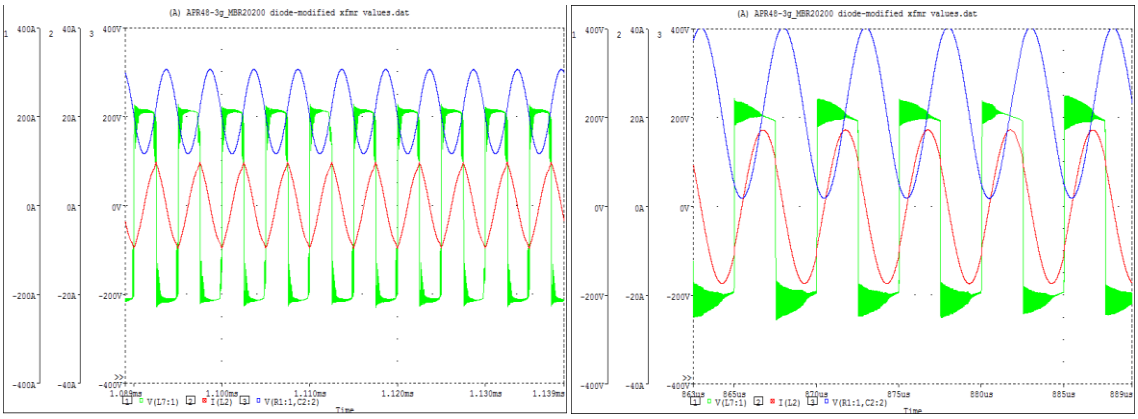

(a) No Load　　（b） Full Load

Figure 2-36：SPICE time-domain transient simulation results at 48VDC no load and full load. Ch1_Green trace: Transformer primary voltage; Ch2_Red trace: Resonant current I_r ; Ch3_Blue trace: Resonant voltage.

Observing Figure 2-35 and Figure 2-36, we can see that given the same operating conditions like: input voltage, output voltage, switching frequency, and load condition, the time-domain transient simulation provided very close results compared to the bench testing results in terms of the waveforms shape and amplitude. Both triangular shape resonant current at no load and sinusoidal shape resonant current at full load are correctly demonstrated in Figure 2-36, as this is very important aspect to define the LLC converter resonant tank switching behavior.

In Figure 2-36, at full load condition the transformer primary voltage parasitic oscillation frequency is higher than Figure 2-35. This is because the SPICE simulation circuit presented in Figure 2-34 has an approximated transformer model with a limited ability to simulate the transformer primary and secondary leakage inductance in the real world.

2.6 Summary

This chapter reviewed and compared the LLC resonant converter topology with conventional resonant topologies (SRC, PRC, and LCC). The LLC resonant converter has many additional benefits over the other three resonant converters. It can regulate the output voltage over wide input voltage range and load variations with a relatively small variation of the switching frequency, while still maintaining an excellent efficiency level. It can also achieve ZVS for turn on over the entire operating range. Therefore, using the LLC resonant configuration in an isolated half-bridge topology becomes a popular solution for modern telecommunication power rectifier design.

The traditional way to model LLC resonant converter circuits involves large mathematical equations and calculations to solve the transfer function of the circuit [18]. The FHA approximation method provides additional merit whereby a simulation model circuit can be constructed. A 48V LLC resonant converter SPICE model circuit was constructed and simulated with respect to the FHA method. The simulation output results were validated with new bench testing data. A table with captured frequency measurement results was successfully used to demonstrate the accuracy of this SPICE model based simulation result. Compared to conventional methods such as state-space average modeling, the SPICE model based simulation can offer a quick and acceptable solution with a reasonably good accuracy.

Chapter 3

Current Doubler Rectifier Converter

This chapter presents an alternative secondary side rectification topology which is called the current doubler-rectifier (CDR) converter. The CDR converter topology was invented and published in the early 1950s as a topology for a secondary rectifier [21]. It can be used as an alternative solution for low voltage, high current applications, and has reduced transformer winding loss and the ability to include magnetic component integration [22]. In this chapter, one of the biggest advantages of the CDR associated with magnetic component integration is described which could benefit the LLC resonant converter design and development. At the end of this chapter a novel LLC resonant current doubler topology solution is proposed.

3.1 Current Doubler Rectifier Converter Topology& Operation

In telecom DC/DC converters, the CDR converter topology is a favorable solution for low output voltage and high output current applications. The current doubler rectifier converter implies a single-ended transformer configuration design rather than the conventional centre-tapped design. It also consists of two identical output inductors and two output diodes [23]. Figure 3-1 shows the fundamental CDR converter topology.

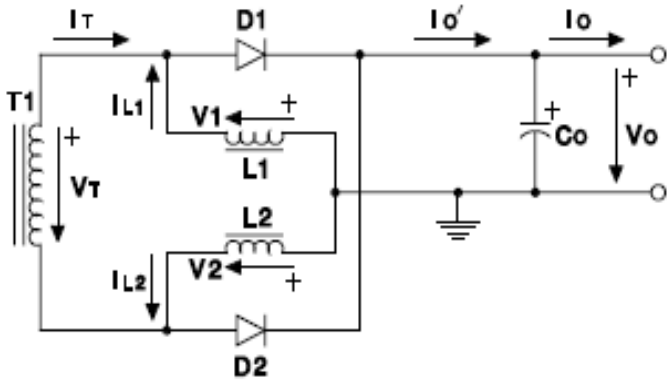

Figure 3-1: Current doubler rectifier converter topology [23].

The operation of the CDR converter on the secondary side is different to the LLC resonant converter since it has two output inductors. The detailed operational waveforms are shown in Figure 3-2 [22]. ΔI is the output current ripple.

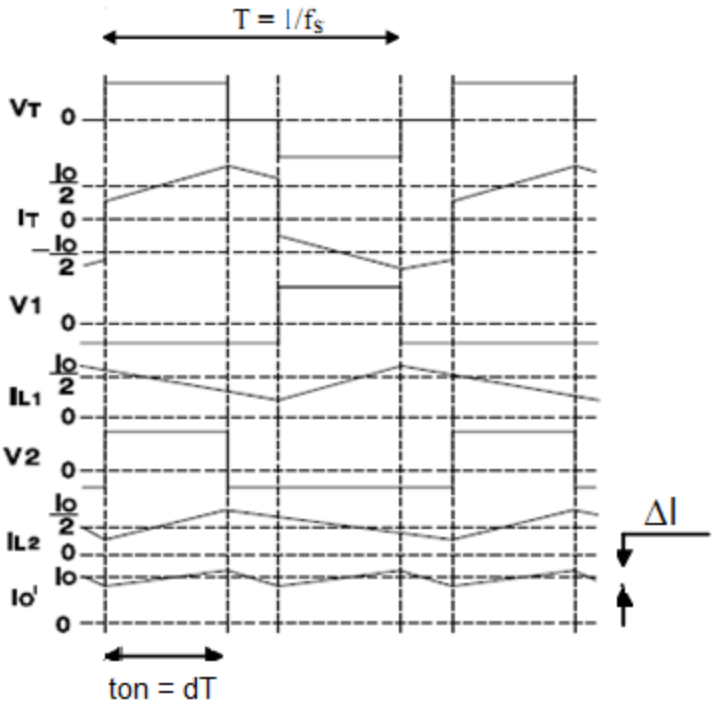

Figure 3-2: CDR converter waveforms [22].

When the secondary side transformer voltage V_T is positive, current flows in a positive direction from the transformer winding and through the inductor L2. The voltage across

L1 is negative, so the current through L1 is supported by its stored energy and as such is decreasing. During this period, D1 is forward biased and provides pathway for the current, D2 is in reverse biased condition. The current through D1 and Co ($I_{O'}$) is therefore the sum of the transformer winding current and the L1 current (the voltage across Co is assumed to be constant, and the load is assumed to be purely resistive). The current flowing in L2 is then equal to the return current flowing in the transformer winding. Since the voltage across L2 is positive, the current is ramping up and L2 is storing energy. This active period is followed by a free-wheeling period. In this period, V_T is zero, and the inductor voltage across L2 becomes negative in order to maintain current flow, and as such its current begins to decrease. The voltage across L1 stays the same, and its current continues to decrease.

When the secondary side transformer voltage V_T is negative, D1 turns off and D2 turns on. The current of L2 now flows through D2 and keeps decreasing. During this period, there is a positive voltage across L1 and the current starts to increase such that L1 now begins to store energy again. The full operating cycle is completed by another free-wheeling period.

The CDR topology has several advantages over the traditional centre-tapped secondary side topology which is mainly adopted for the half-bridge resonant LLC converter as described in Chapter 2. It simplifies the transformer design from being centre-tapped to single-ended, which makes it much easier to build and exhibits lower conduction losses [22]. In the CDR topology, the inductor current and transformer secondary current is half that of the centre-tapped half-bridge topology under the same output voltage and output current conditions. More importantly, the two output inductors equally share the total output load current which is shown in Figure 3-2.

Therefore, the CDR converter provides a simplified solution to halve the output voltage but double the output current compared to the centre-tapped topology. As a result of this, it is a favorable solution that EATON can apply this topology to their existing

48VDC/30A telecom rectifier product and transform it into a 24VDC/50A telecom rectifier.

3.2 Comparison With The Centre-Tapped Secondary Side Topology

The centre-tapped secondary side topology is commonly used in push-pull, half-bridge, and full-bridge conventional high frequency switching telecom converters [23]. This topology is used in the current high efficiency Eaton APR48-3G 48VDC/30A telecommunications rectifier product. The centre-tapped secondary side topology consists of one output inductor, two output diodes, and operates at double the primary switching frequency (it allows both half-cycles of the AC waveform to contribute to the rectified DC waveform). It tends to be used for low and medium current applications [21]. Figure 3-3 shows the centre-tapped secondary converter topology.

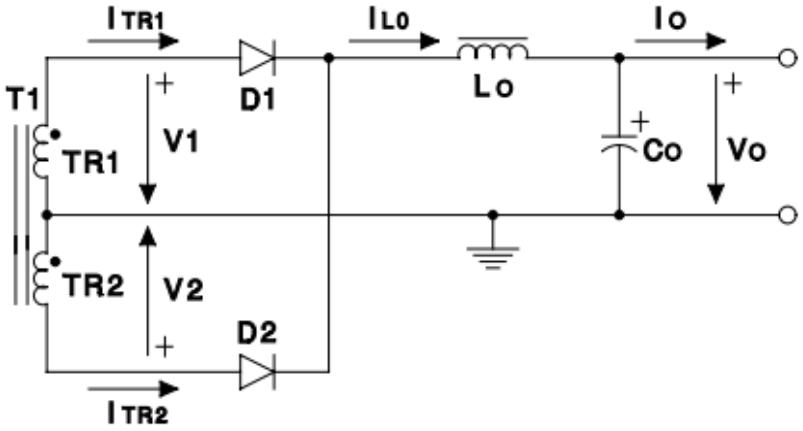

Figure 3-3: A centre-tapped converter topology [23].

Like the current doubler circuit, a centre-tapped converter circuit produces an output voltage and current which is purely DC. In a centre-tapped converter circuit two diodes are used, one for each half of the cycle. The transformer secondary winding splits equally into two halves with a centre tapped connection. This configuration results in each transformer secondary winding and diode conducting in a half cycle, so that the converter can produce an output during both half-cycles. The operational waveforms are shown in Figure 3-4.

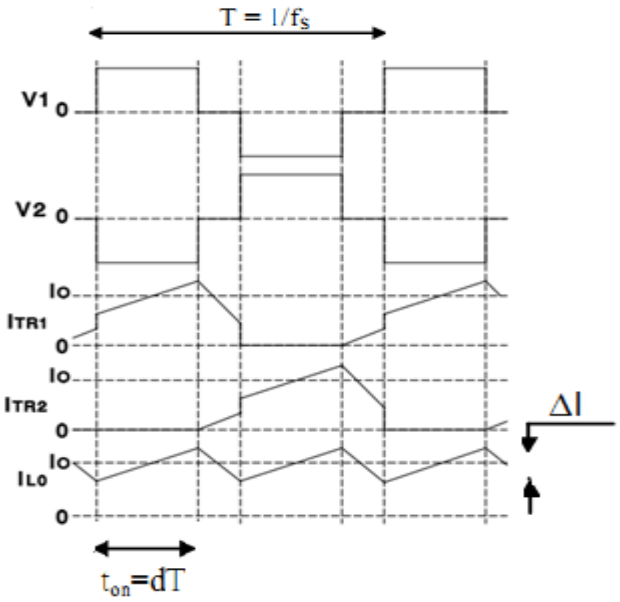

Figure 3- 4: Centre-tapped converter waveforms [23].

Figure 3-4 shows that when the voltage across the transformer secondary winding TR1 is positive, D1 is forward biased while the negative voltage across the secondary winding TR2 keeps D2 reverse biased. The output current is forced to flow through TR1, D1, and Lo to the load while TR2 carries no current. During the free-wheeling period, the voltages across TR1 and TR2 become zero and both D1 and D2 are forward biased [22]. In the next interval, V2 is positive, in which case transformer winding TR2 and D2 carry all the output current while D1 is reverse biased. Transformer winding TR1 now has no current through it. In the next free-wheeling period V1 and V2 are zero again.

In theory the output load current should be evenly distributed among the two secondary windings. However, in practice, because of the transformer secondary leakage inductance associated with the windings, the output current is not shared evenly [24]. One transformer winding always conducts more of the output current than other winding. The current slowly builds up in one of the transformer secondary windings depending on the value of the leakage inductance and the available voltage across it. This will cause a current unbalance issue and may cause unbalanced power dissipation. Additionally, this imbalance may saturate the transformer core [22].

Comparison of the centre-tapped converter topology and CDR converter topology has been done and the result is shown in Table 3-1 [25].

	No of inductors	Inductance value	Current ripple at each inductor	RMS inductor current
Centre Tapped Rectifier	1	$\frac{V_o*(1-2*d)}{2*fs*\Delta I}$	ΔI	$\sqrt{I_0^2+\frac{\Delta I^2}{12}}$
Current Doubler Rectifier	2	$\frac{V_o*(1-2*d)}{fs*\Delta I}$	$\Delta I*\frac{1-d}{1-2*d}$	$\sqrt{(\frac{I_0}{2})^2+\frac{\Delta I^2}{12}*(\frac{1-d}{1-2*d})^2}$

Table 3-1: Comparison results for centre-tapped and current doubler rectifier circuits [25]. V_o:Output Voltage; d: duty cycle; ΔI: ripple current; I_o: Output Current;f_s:switching frequency.

In some research articles [21, 23], it is claimed that the CDR converter has the substantial advantage of reduced total output current ripple level. This is due to the two output inductors operating with a180^0 phase shift, providing a ripple cancellation effect. However, in the LLC resonant converter design, because the primary main power MOSFETs are operating with zero voltage soft switching, the output current ripple is already quite low. So there is not a huge benefit in using a CDR converter to reduce the ripple level in an LLC resonant converter design.

Owing to the limited benefit of the CDR converter ripple cancellation effect, one of the main remaining advantages is the simple transformer structure design and manufacture. This is because the CDR converter only requires one secondary winding, which can substantially reduce the secondary conduction losses by having half the number of secondary windings and has no current balancing issue compared to the centre-tapped circuit. The DC component of the magnetizing current is also lower or equal to the

centre-tapped circuit which makes the transformer core size smaller. The second main advantage is that the output current is shared by the two output inductors. Additionally, the two identical output inductors can be coupled together and integrated into one magnetic core. As a result, the CDR converter is a highly recommended solution for high output current applications [24].

3.3 Improved Current Doubler Rectifier With Integrated Magnetics

One disadvantage of the conventional CDR converter is that the magnetic coupling losses are relatively high because it includes three separate magnetic components: one transformer and two individual output inductors. Besides the component size and cost concerns, the high magnetic coupling loss has a great impact for telecom high current applications with increased power losses. In order to solve this problem and improve performance, several magnetic component integration solutions have been presented in [25] to combine the transformer and two output inductors onto a single magnetic core. Figure 3-5 shows different integration configurations that have been proposed for the CDR converter.

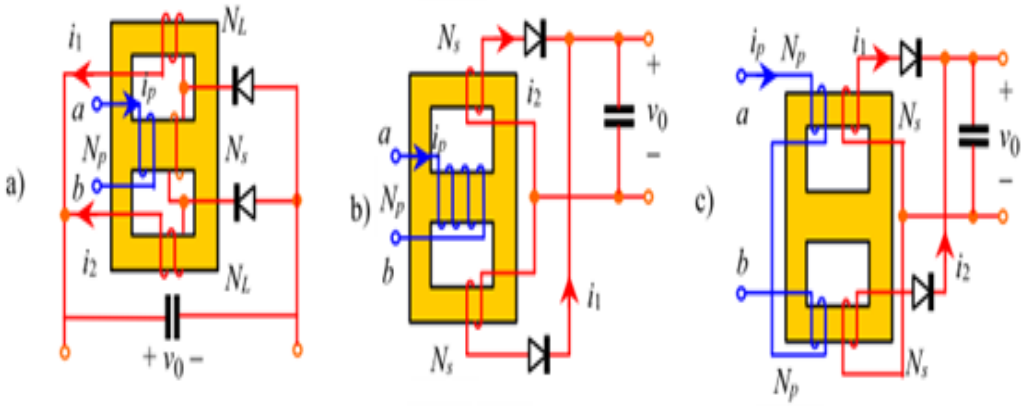

Figure 3-5: Integrated magnetic configurations for a CDR converter [25]. (a) Separate transformer and inductor windings, (b) Split inductor windings, (c) Split transformer windings.

The configuration shown in Figure 3-5(a) uses separate transformer and inductor windings integrated onto one magnetic core. Figure 3-5 (b) and (c) show how both the output inductors in these two structures can be integrated with the transformer secondary windings. Both of the configurations in Figure 3-5 (b) and (c) have the additional advantage of low leakage inductance between the primary and secondary windings, due to its compact design and good magnetic coupling [25].

Magnetic integration has already been widely used in LLC resonant converter designs to utilize the transformer primary magnetizing inductance as one resonant inductor inside the LLC resonant network [26]. To reduce the eddy current loss, the primary and secondary windings are constructed with interleaving structure as shown in Figure 3-6 [27]. The transformer outer most and inner most windings are the primary side windings, the interleaved secondary side windings are placed in between the primary side windings.

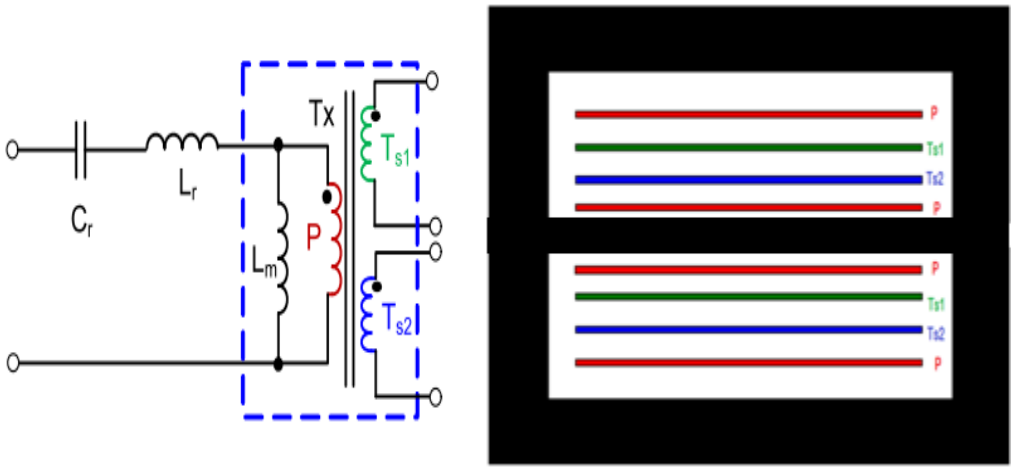

(a) (b)

Figure 3-6: (a) LLC integrated magnetic circuit; (b) Transformer with an interleaved winding structure [27]. P: primary winding; Ts1:1st secondary winding; Ts2: 2nd secondary winding.

The main scope for design is to focus on the secondary side component integration as EATON already had a well designed and performing LLC converter transformer primary winding with integrated magnetizing inductor. Based on the literature research identified

earlier on the coupled inductor integration configurations, a new integrated output inductor design was considered for this project with two output inductors coupled and integrated together on a single magnetic core as shown in Figure 3-7.

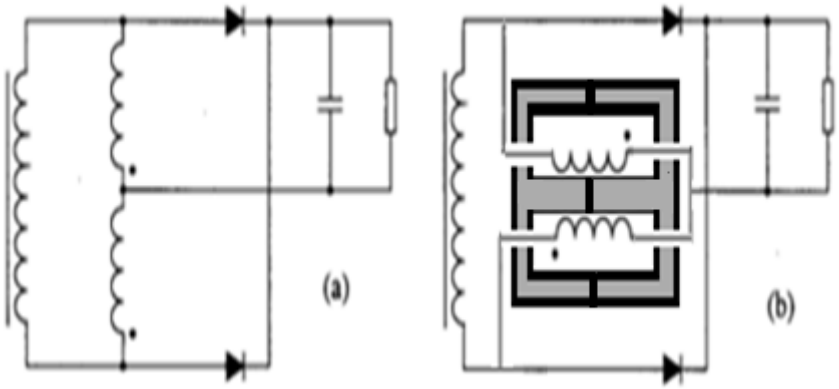

Figure 3-7: Current doubler rectifier converter with two coupled integrated inductors. (a): CDR converter with two uncoupled output inductors. (b): Proposed CDR Converter with two coupled integrated inductors.

Figure 3-7 shows the proposed new integrated coupled output inductor solution for a CDR converter. Both inductor windings are placed on the centre pole of the magnetic core (Figure 3-7 (b)). This will greatly reduce the magnetic coupling losses between the two windings. This integrated magnetic element adopts a bifilar winding structure, as shown in Figure 3-8, to provide good magnetic coupling and current carrying capability. It is also observed that the newly formed integrated coupled inductors are operating in a very similar manner to an auto transformer.

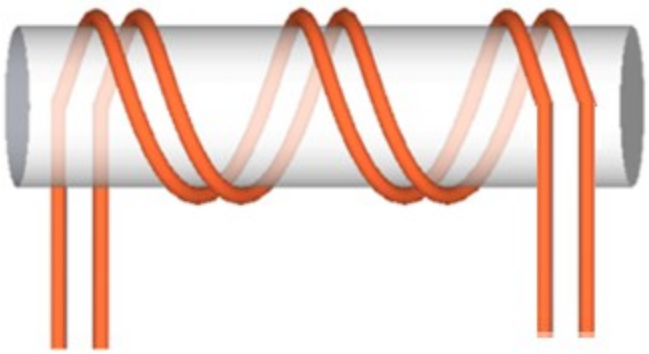

Figure 3-8 : Bifilar winding structure [27].

The primary and secondary windings of a two winding transformer have induced emf in them due to a common mutual flux and hence are in phase as shown in Figure 3-9. The currents drawn by these two windings are out of phase by 180◦.

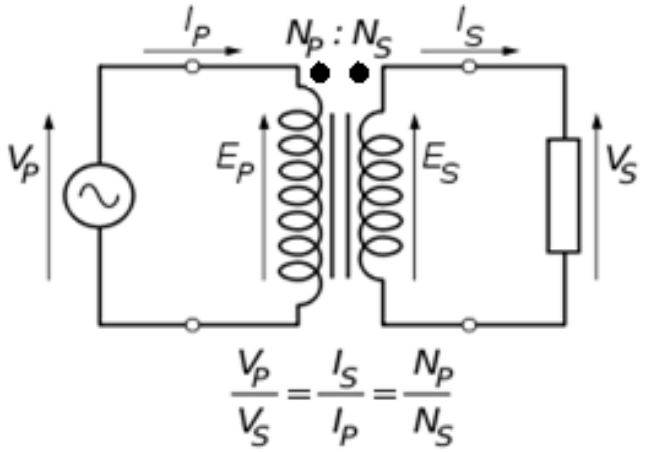

Figure 3-9: Transformer with two windings [28].

An auto transformer has a single winding with two end terminals, and an intermediate tap point (as shown in Figure 3-10 (a) for a step-down function). The end terminals act as the primary winding connections. One end terminal and the intermediate tap point act as the secondary winding connections. The primary voltage V1 is applied across the two end terminals, labeled C and A with primary turns T1, and the secondary voltage V2 taken from the two terminals B and A with secondary turns T2. There is always one terminal of the secondary in common with the primary. The primary T1 and secondary T2 circuits therefore have a number of winding turns in common.

Because in both the primary and secondary windings the volts-per-turn is the same, each winding develops a voltage in proportion to its number of turns [28]. In an auto transformer the primary input current I1 flows between C and B. The output load current I2 is subtracted from I1, leaving the current between terminals B and A of (I2-I1). One end of the winding (A) is usually connected in common to both the input and the output. The other end of the source and load are connected to the winding end terminal (C) and intermediate tap (B) respectively. Different tap points on the winding correspond to different secondary voltages, measured from the common end.

Auto transformers can be used to step up or step down voltages [29]. Only the step-down configuration has been shown as this is the function performed in the telecommunications rectifier application of interest.

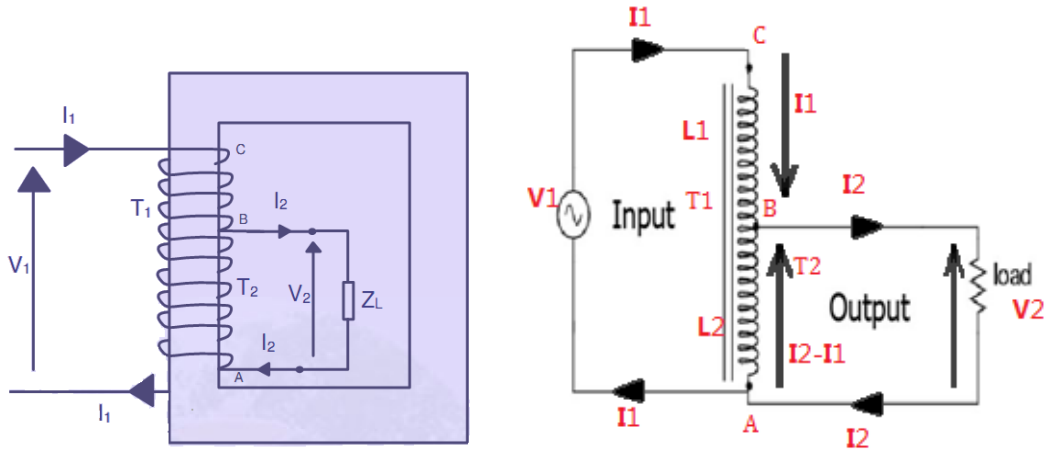

(a) (b)

Figure 3-10: (a) Auto transformer circuit (step-down function) [29]; (b) Auto transformer equivalent circuit.

From the equivalent circuit in Figure 3-10 (b), as the volts per turn is proportional to the flux in the autotransformer, which is the same for the whole winding, the auto transformer primary and secondary voltage relationship with respect to turns ratio and current ratio is $\frac{V_1}{V_2}=\frac{T_1}{T_2}=\frac{I_2}{I_1}$. Assuming the primary voltage V_1 is twice the secondary voltage V_2, so that the turns ratio T1:T2 is 2:1, the load current I_2 will be double the primary input current I_1.

As a result of this, the newly formed integrated coupled output inductors in Figure 3-7 (b) acts as a step down auto transformer, with a turns ratio equivalent to 2:1, giving double the output current and half the output voltage. Therefore, it appears that this would be a very good configuration to improve the CDR converter topology design.

Another important aspect of auto transformers is that both primary and secondary windings are very well coupled due to their common mutual flux structure as shown in

Figure 3-10 [29]. Therefore, it can be integrated into a single compact magnetic component.

This analysis suggests a feasible solution to reduce the total amount of magnetic components that are used to form the conventional CDR converter, but also can meet the high output current requirements. With an integrated magnetic solution with interleaved bifilar windings, the interconnection coupling losses can be greatly reduced compared to the conventional integrated solution. This makes it a very attractive topology especially for high output current telecom converter applications.

3.4 Proposed New LLC Resonant Current Doubler Rectifier Converter with Coupled Output Inductors

Based on the literature research and circuit investigation above, it has been determined that the CDR converter is a very popular topology used in high output current applications. The unique characteristic of two output inductors can be redesigned so that they are coupled and integrated onto a single magnetic core. In addition, it has been shown that this integrated structure performs similarly to an auto transformer configured such that, as required, the output current is doubled and output voltage is halved. Moreover, a novel topology is proposed here to apply the CDR converter as the secondary side output stage for the half-bridge LLC resonant converter for high output current telecom applications. Figure 3-11 shows the proposed novel LLC resonant current doubler rectifier (LLC-CDR) converter circuit.

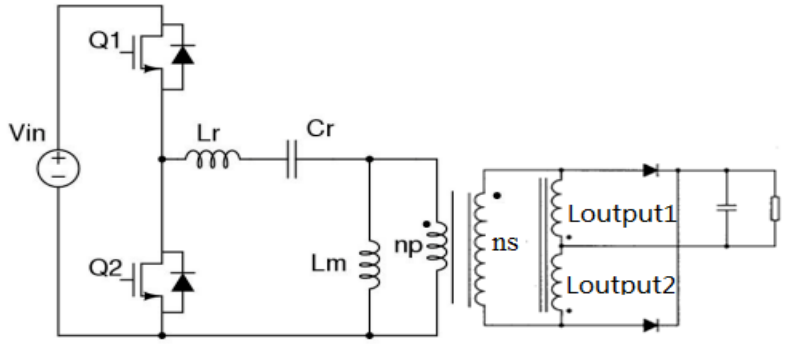

Figure 3-11: Proposed half-bridge LLC resonant CDR converter.

The primary side of this topology operates in the same way as the normal half bridge LLC resonant converter. The secondary side of this topology operates in the same way as the traditional CDR converter, but contains an integrated coupled output inductor component. In high frequency switching operation, the two coupled inductances cancel out and behave like an auto transformer. Therefore the output inductance of the proposed topology should have negligible effect on the primary side resonant tank switching. This assumption needs to be verified by SPICE based simulations and bench experimental results, and this verification is detailed in the following chapters. To be practical, the primary side bridge MOSFETs should still operate under ZVS mode, and the original resonant switching frequency fr1 should not be substantially affected. Furthermore, the size of the main transformer should be able to be reduced due to its single winding configuration, the current unbalancing issue for the centre-tapped configuration is improved, and the traditional current doubler's poor coupling and high magnetic coupling losses can be reduced.

Chapter 4

LLC Resonant Current Doubler Converter Simulation and Testing with Two Uncoupled Inductors

In this chapter, the physical hardware implementation of a novel half-bridge LLC-CDR converter is shown in the traditional method which includes two identical output inductors in the uncoupled configuration as shown in Figure 3-1. Two SPICE based simulation modeling circuits are presented for both time-domain transient simulation and frequency-domain AC simulation. Based on these simulation results, a hardware prototype circuit was built and tested, the performance of this proposed circuit is then discussed.

4.1 Transient Simulation

In order to gain a better understanding of the behavior of the novel LLC resonant current doubler circuit topology, and to show this circuit can provide required performance with acceptable design results, a time-domain transient simulation circuit model was constructed in SPICE-based software as shown in Figure 4-1, according to the circuit diagram proposed in Figure 3-11.Both the transformer and the output inductor coupling coefficient factors (K3 and K11 respectively) are shown in Figure 4-1. Here K11 is equal to 0 which indicates the output inductors are magnetically uncoupled.

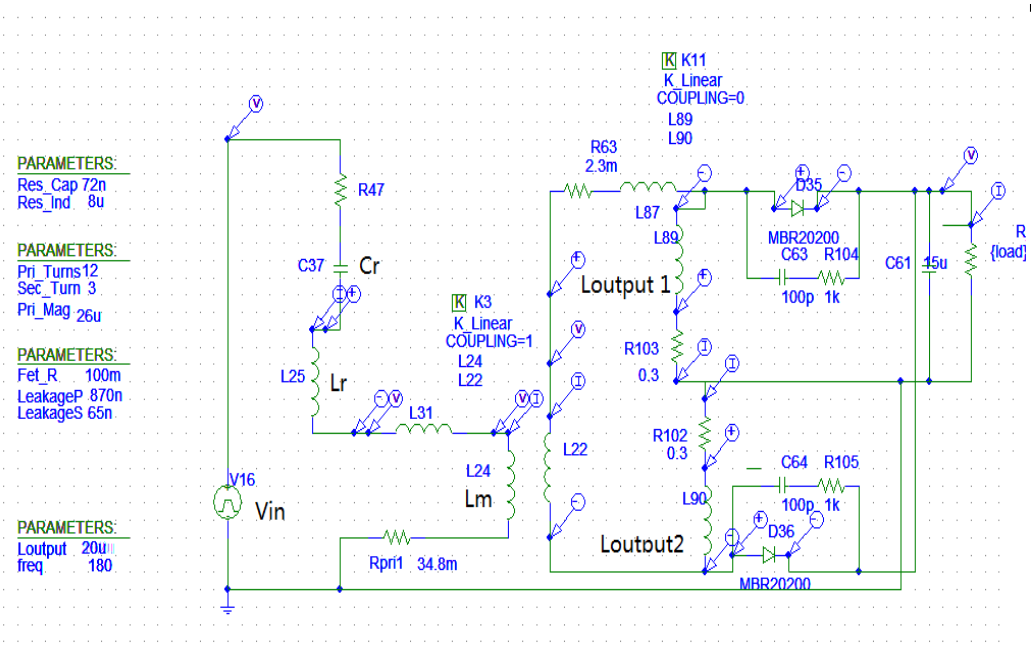

Figure 4-1: SPICE time-domain transient simulation circuit.

This simulation circuit as shown in Figure 4-1 is designed to transform a 48VDC converter into a 24VDC converter by using the same LLC resonant network circuit on the primary side. This converter was supplied by a 420VDC input voltage with a PWM switching waveform and selectable switching frequency to simulate the actual circuit operating voltage.

As can be seen from the proposed simulation circuit, the primary side LLC resonant stage is very similar to the SPICE simulation circuit that was presented in Figure 2-19 from Section 2.3. As a result, the primary component parameter values are selected from the same LLC resonant network circuit. In addition, MOSFET turn on resistance, and transformer leakage inductance and resistance have been added to the simulation circuit.

The transformer model is redesigned to use a single-ended configuration instead of the centre-tapped configuration, which means it has only one secondary winding.
As a result, the secondary can be wound with parallel-connected conductors (bifilar) to reduce conduction losses and improve the magnetic coupling between the primary side and secondary side of the transformer. In addition, it also simplifies the manufacturing of

the transformer. Another important advantage is that the RMS current in the secondary winding is smaller since only half the output current is circulating through it. This is very important for high output current applications [7]. The stated transformer 4:1 turns ratio (as shown in Figure 2-34) is used in the EATON APR48-3G and the other LLC circuit parameters can keep the same values as used in Chapter 2. This is because the secondary stage CDR converter offers the unique solution of halving the output voltage from 48VDC to 24VDC without changing the transformer turns ratio as shown in Section 3.3.

Two individual and identical output inductors are operating in parallel and carry half of the output current each. In the SPICE simulation, the coupling coefficient for these two output inductors was set to 0 to correspond with the design circuit in Figure 4-1. This means they are two individual and magnetically uncoupled components. The two output inductors are both designed to pass high DC current, consequently both inductor cores require to be gapped. The inductor value was calculated as 20μH by Eqn 4-1 [9].

$$L = V\frac{d_t}{d_i} = \frac{V_o * D/f}{\Delta i} = \frac{24*0.057/210000}{0.3} = 20\mu H \qquad \text{Eqn 4-1}$$

Design details will be shown in the following sections. The simulation output waveforms shown in Figure 4-2 to Figure 4-4 clearly show that the two output inductors are sharing the total load current and the output voltage has been halved to 24VDC. Figure 4-2, Figure 4-3, and Figure 4-4, show the simulation waveforms under no load, light load (30A), and full load (50A) operation.

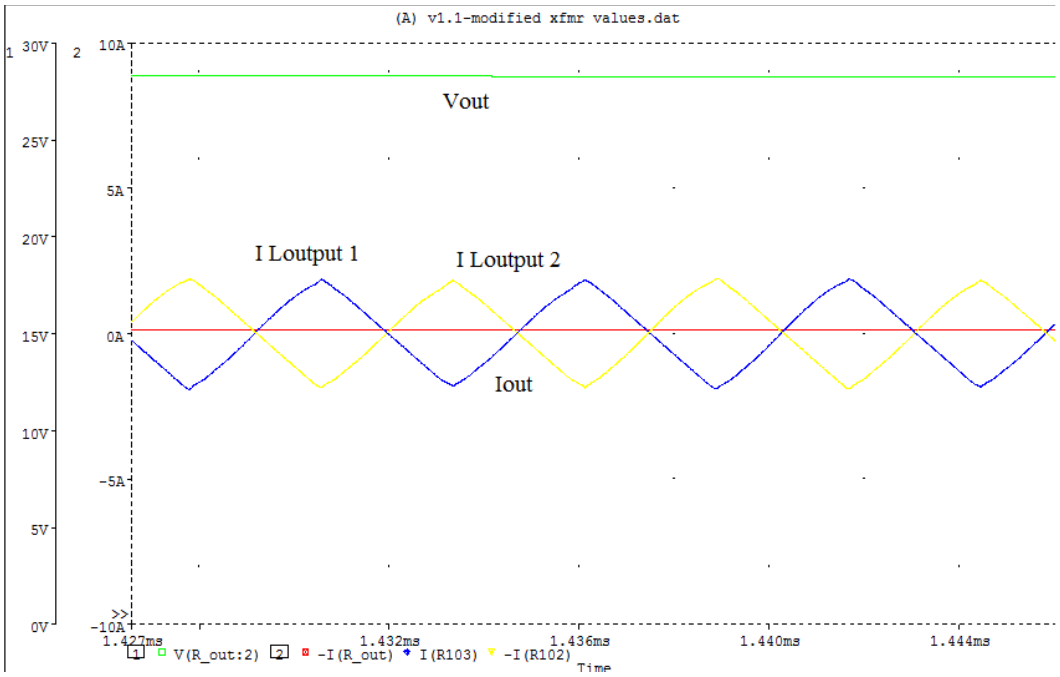

Figure 4-2: Transient simulation output waveforms at no load. Green trace: Vout, Blue trace: Current in Loutput1, Yellow trace: Loutput2 current, Red trace: Total output current Iout.

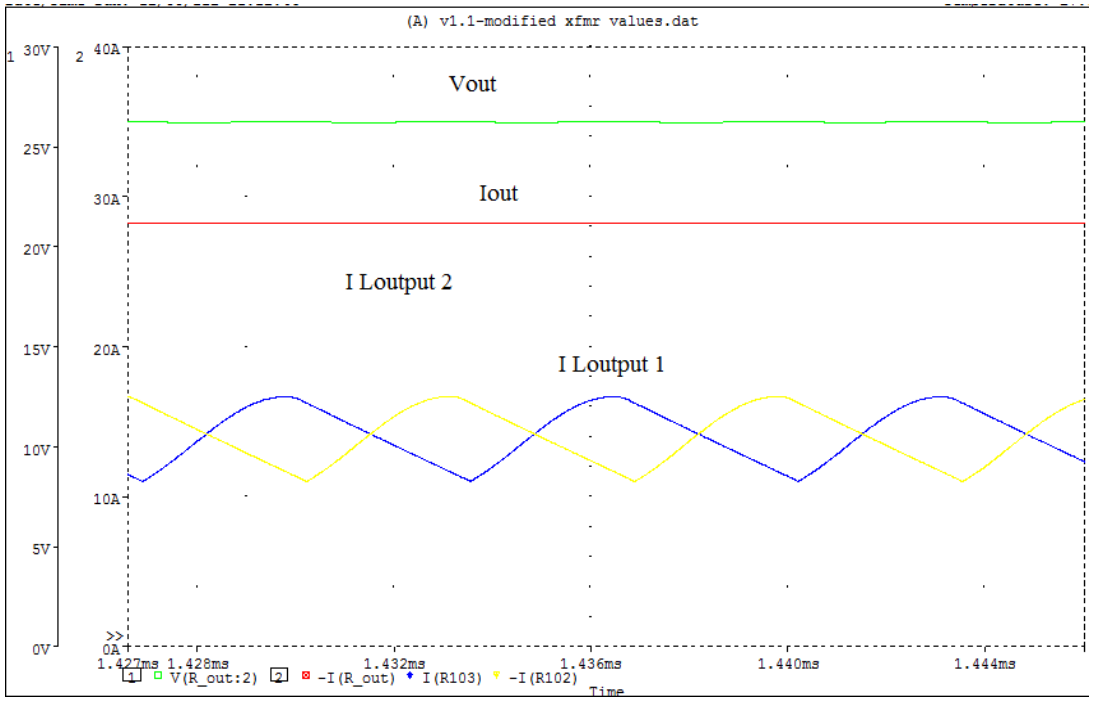

Figure 4-3: SPICE transient simulation output waveforms at light load 30A. Green trace: Vout, Blue trace: Current in Loutput1, Yellow trace: Loutput2 current, Red trace: Total output current Iout.

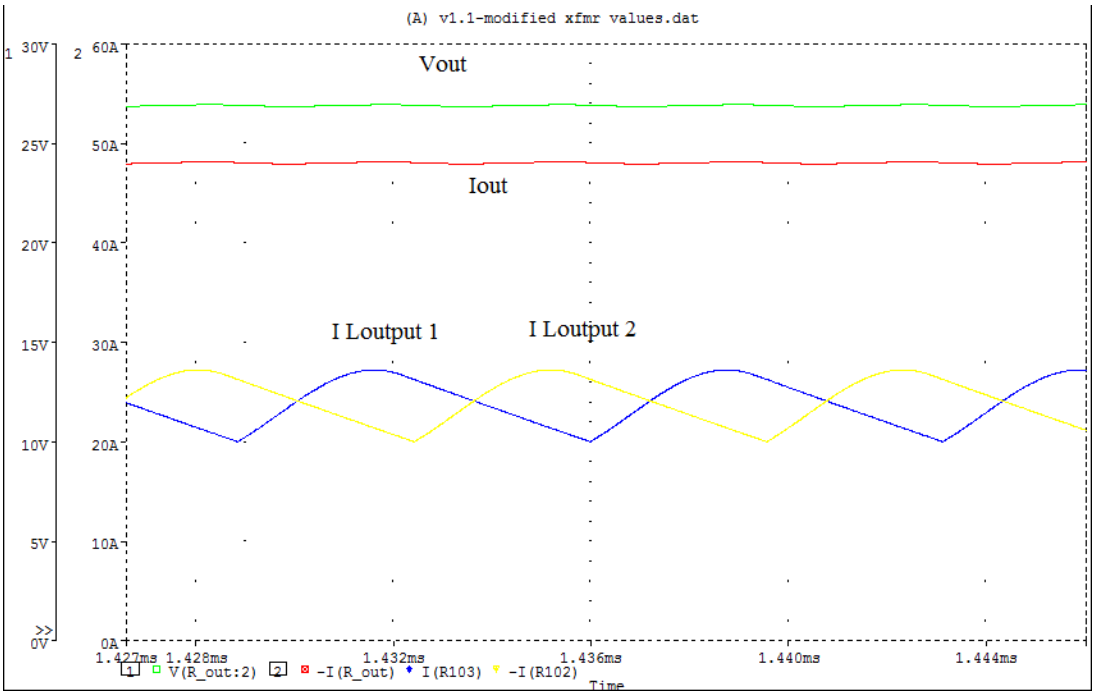

Figure 4-4: Transient simulation output waveforms at full load 50A. Green trace: Vout, Blue trace: Current in Loutput1, Yellow trace: Loutput2 current, Red trace: Total output current Iout.

The output waveforms observed in Figure 4-2 to Figure 4-4 are very similar to the general topology waveforms observed in Figure 3-2, especially for the output inductors. It can be observed that each output inductor is carrying half of the total load current and it also shows the correct waveform shape for the CDR inductor. It also can be observed that by using the same LLC resonant converter transformer turns ratio (4:1) setting, the output voltage can meet the desired 27VDC (actual DC voltage for a fully-charged lead-acid battery bank - nominal 24V) design requirement (based on the SPICE simulation result). Therefore, by applying the theory proposed in Section 3.4, the 48VDC output voltage in a LLC resonant converter can be halved to 24VDC by using two output inductors in a current doubler configuration. The performance of the simulation results suggest a valid transient circuit model was designed corresponding to the proposed LLC resonant current doubler circuit shown in Figure 3-11. It also suggests that based on this transient simulation circuit model, it should be possible to create a frequency-domain simulation

circuit that can be used to evaluate the AC frequency response performance. Further comparison should be made with actual bench testing results.

4.2 AC Frequency Response Simulation

The transient simulation provides expected results on the secondary side output stage by applying the CDR to the LLC resonant converter at a particular frequency point. However, the primary side resonant tank switching performance is still unknown, and any effects caused by the two 20µH output inductors need to be simulated over a relevant frequency range. The frequency-domain simulation circuit is constructed in SPICE as shown in Figure 4-5, which corresponds to the circuit shown in Figure 4-1.

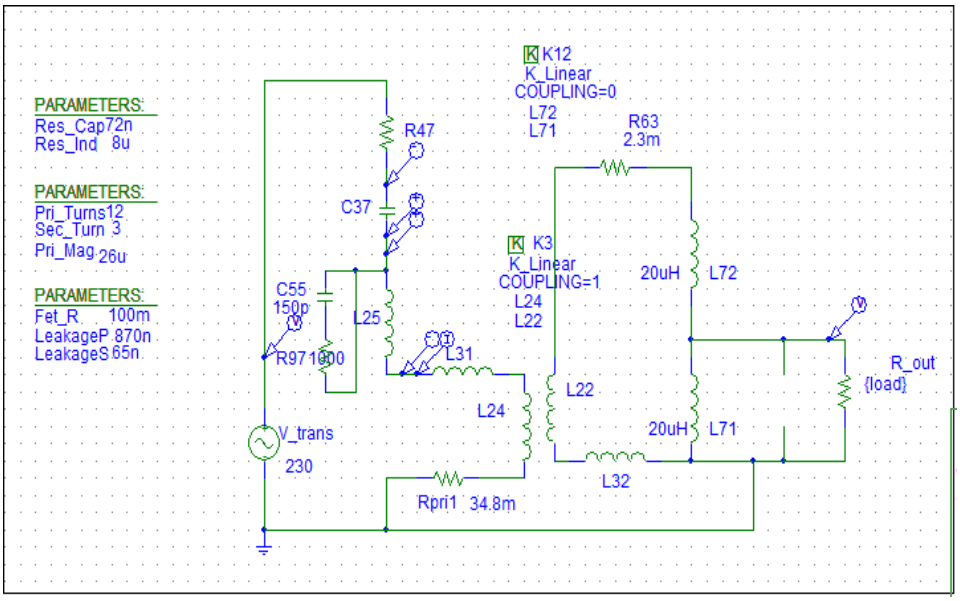

Figure 4-5 : Frequency-domain AC simulation circuit.

In this AC simulation circuit, the input voltage is 230VAC with a 50 Hz sinusoidal waveform which follows the FHA approximation theory explained in Section 2.4. The output inductors coupling coefficient factor K is set to 0 which is same as the circuit shown in Figure 4-1. The circuit is simulated with respect to the frequency range of 40kHz to 400kHz. The AC simulation result is shown in Figure 4-6.

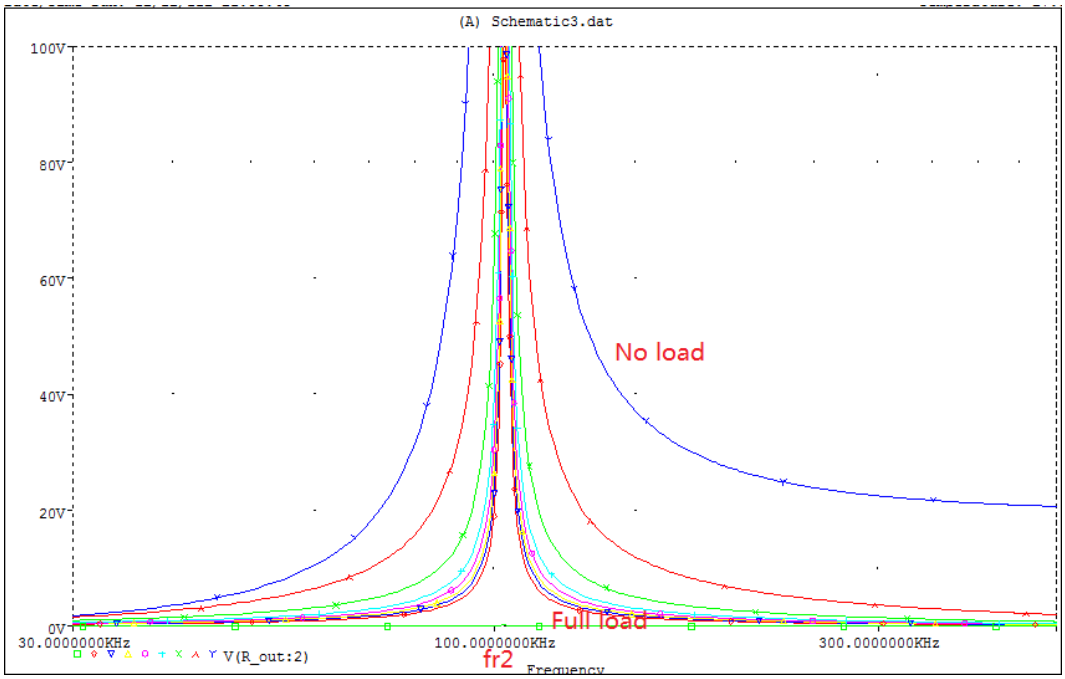

Figure 4-6 : Frequency-domain AC simulation result.

The AC simulation result is unexpected and several important aspects are observed from Figure 4-6. First of all, this output AC frequency curve looks different to the previous LLC resonant converter AC frequency simulation curve as shown in Figure 2-33. From the curve shown in Figure 4-6, it only indicates one resonant frequency fr2 located at around 103 kHz. The other resonant frequency fr1 is not shown on the plot. This could suggest that either this AC modeling method is not performed correctly or the proposed LLC resonant current doubler converter topology is invalid from the AC simulation viewpoint. The unexpected AC simulation result may suggest that the LLC stage resonant switching performance is greatly affected by the additional uncoupled output inductors, therefore it failed to maintain its resonant frequency fr1 and could cause high switching losses. ZVS could still be achieved as Figure 4-6 shows a similar plot as the SRC characteristic plot. It is still unknown what the actual circuit performance is, therefore a hardware prototype is constructed in order to further investigate the transient and AC frequency simulation results.

4.3 Main Transformer and Output Inductor Design

An existing transformer that was originally constructed for the LLC resonant converter circuit was available and was used in the new LLC resonant current doubler circuit. Some required modifications were made on the transformer secondary windings. The transformer turns ratio (58VDC maximum output voltage for a nominal 48VDC telecom rectifier product) can be calculated according to Eqn 4-2 [22].

$$N=\frac{Vin/2}{Vout}=\frac{420/2}{58(V_{max})}\approx 4 \qquad \text{Eqn 4-2}$$

Results shown in Section 4.1 proved that the same transformer turns ratio used in the 48VDC LLC resonant circuit can be used to achieve the desired 24VDC output voltage through using the current doubler topology, where the secondary winding structure needs to be changed from a centre-tapped configuration to a single-ended configuration. Because the current transformer developed by EATON has the ability to handle 30A on each output winding, it provides the ability to connect both windings in parallel to comfortably handle 50A under full load operation. Figure 4-7 shows the circuit schematic of the transformer winding structure.

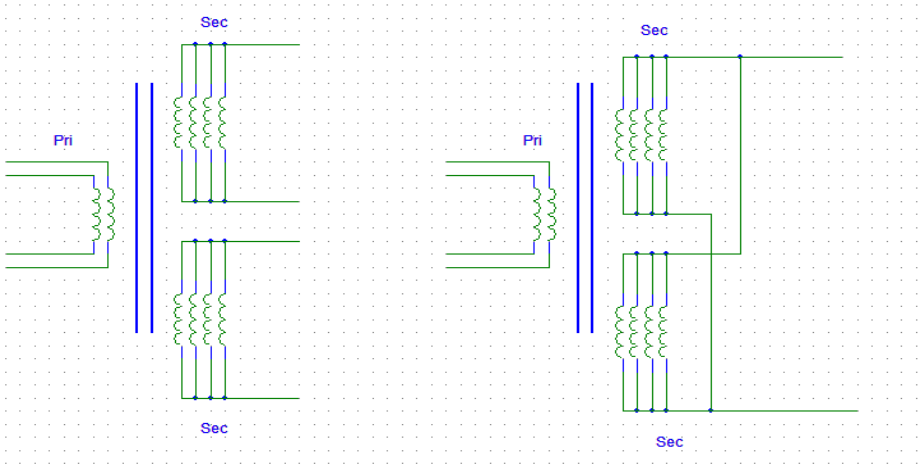

(a) (b)

Figure 4-7 : (a) LLC resonant converter transformer; (b) Modified LLC resonant current doubler transformer.

In order to build and evaluate the hardware prototype, two new output inductors were designed and constructed. The output inductors were designed and constructed on a RM12 magnetic core. Because these two output inductors have to operate with high DC current, Ferroxcube 3F3 type material is chosen to be used with a gapped core. The RM12 core parameters are shown in the Table 4-1[20].

Effective core parameters

SYMBOL	PARAMETER	VALUE	UNIT
$\Sigma(l/A)$	core factor (C1)	0.388	mm^{-1}
V_e	effective volume	8340	mm^3
l_e	effective length	56.6	mm
A_e	effective area	146	mm^2
A_{min}	minimum area	125	mm^2
m	mass of set	= 46	g

Table 4-1: Ferroxcube RM12 core parameters [20].

As we already know the inductance value from the simulation result was 20μH, and given the Bmax=250mT and Ac = 146 mm^2 from the information given by the supplier data sheet in Table 4-1, we can calculate the number of turns from Eqn 4-3 [22].

$$N=\frac{LI_{max}}{B_{max}A_c}=\frac{20*10^{-6}*30}{0.25*146*10^{-6}}=16.4 \qquad \text{Eqn 4-3}$$

To prevent core saturation, the maximum flux density was designed for Bmax=250mT. According to the RM12 data sheet [20] the product of I^2L is a measure of the energy that is stored in the core. Using the data sheet graph given in Figure 4-8, the inductor air gap can be quickly selected at 2.5mm with I^2L value calculated at 0.018J.

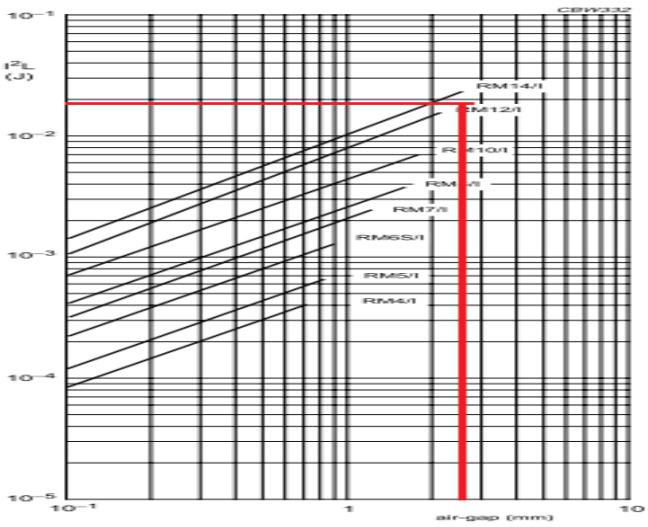

Figure 4-8: Inductor air gap selection [20].

The air gap length also can be calculated based on the formula as shown in Eqn 4-4 [21]. Both the calculated and estimated values are very close.

$$\text{Airgap}=\frac{\mu_0 L I^2}{B_{max^2} A_c}=\frac{4\pi*10^{-7}*20*10^{-6}*30^2}{0.25^2*146*10^{-6}}=2.5\text{mm} \qquad \text{Eqn 4-4}$$

Finally, Litz wire is used to construct the inductor with 825/AWG44 wire rating and formed by the parallel-connected conductor winding method. The transformer and two inductors for the LLC current doubler converter are shown in Figure 4-9.

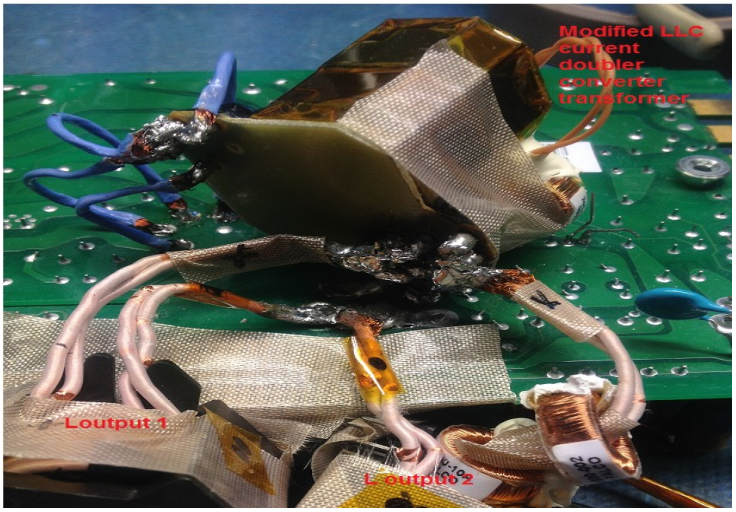

Figure 4-9 : Magnetic prototype of the transformer and two uncoupled inductors.

The proposed transformer with improved winding structure has some significant merits. Firstly, the modified transformer can still achieve its interleaved winding structure. Secondly, the transformer modification is very simple and can be done through PCB layout changes. This means there is no extra cost for the new transformer since no new transformer component is created.

4.4 Experimental Test Results Comparison

In this section, a LLC resonant current doubler converter hardware prototype was built and tested to verify the converter performance. Bench testing results were collected in order to compare with the simulation results presented in sections 4.1 and 4.2. Comparison work was mainly focused on 24V at no load, half load (30A) and close to full load (40A). However, more test results under different operating conditions can be found in Appendix A.

In these tests, the output diode voltage (especially dv/dt) was closely monitored on the oscilloscope to prevent any component damage caused by unacceptably large magnitude and speed switching voltage. The primary side resonant current was observed to determine the LLC resonant tank switching characteristic. The primary side half bridge switching voltage was observed to obtain the converter actual switching frequency under different switching modes and load conditions.

Figure 4-10 and Figure 4-11 show the hardware prototype bench testing results and time-domain transient simulation result at 24V with no load.

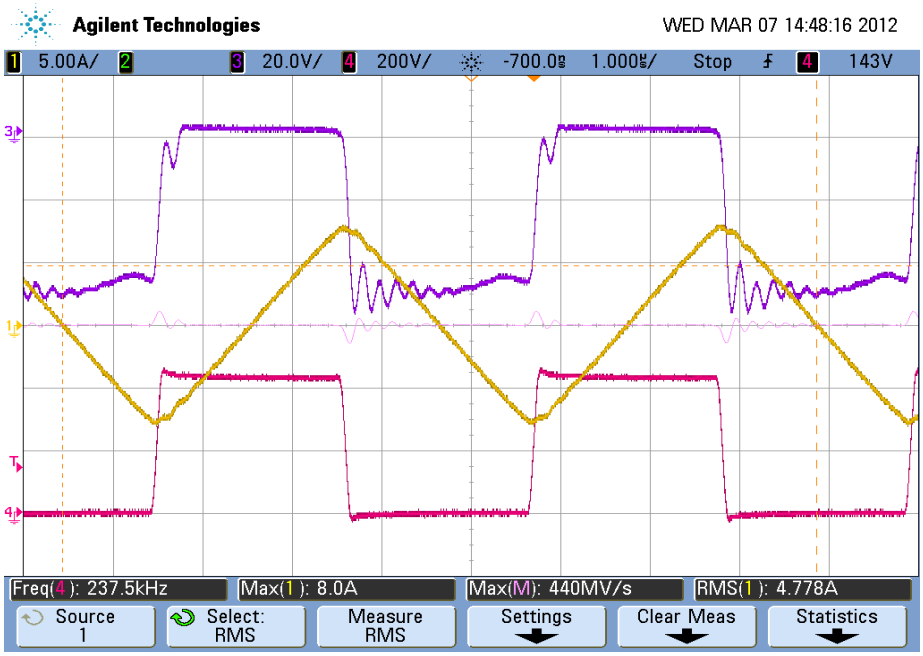

Figure 4-10: Bench testing result at 24V with no load. Ch1_Yellow trace: Resonant current; Ch3_Blue trace: Resonant voltage; Ch4_Red trace: Transformer primary voltage.

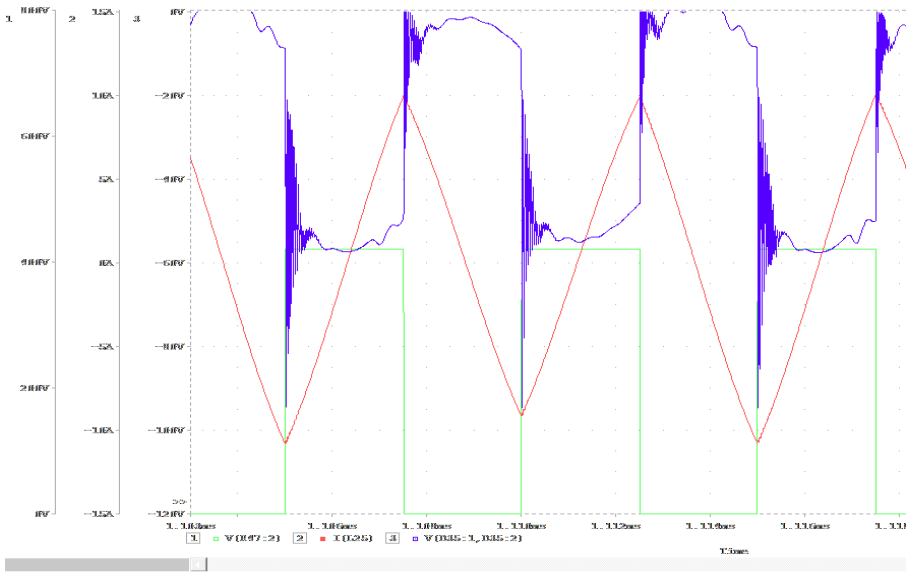

Figure 4-11 : Transient simulation result at 24V with no load. Ch1_Green trace: Transformer primary voltage; Ch2_Red trace: Resonant current ; Ch3_Blue trace: Resonant voltage.

Figure 4-12 and Figure 4-13 show the hardware prototype bench testing result and time-domain transient simulation result at 24V with 30 A load.

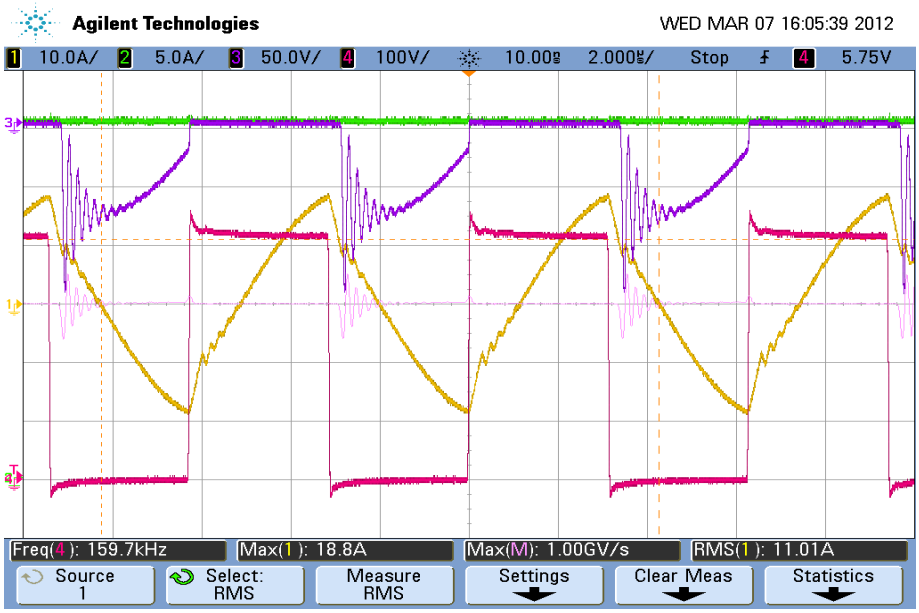

Figure 4-12: Bench testing result at 24V with 30A load. Ch1_Yellow trace: Resonant current; Ch2_Green trace: Output current ; Ch3_Blue trace: Resonant voltage; Ch4_Red trace: Transformer primary voltage.

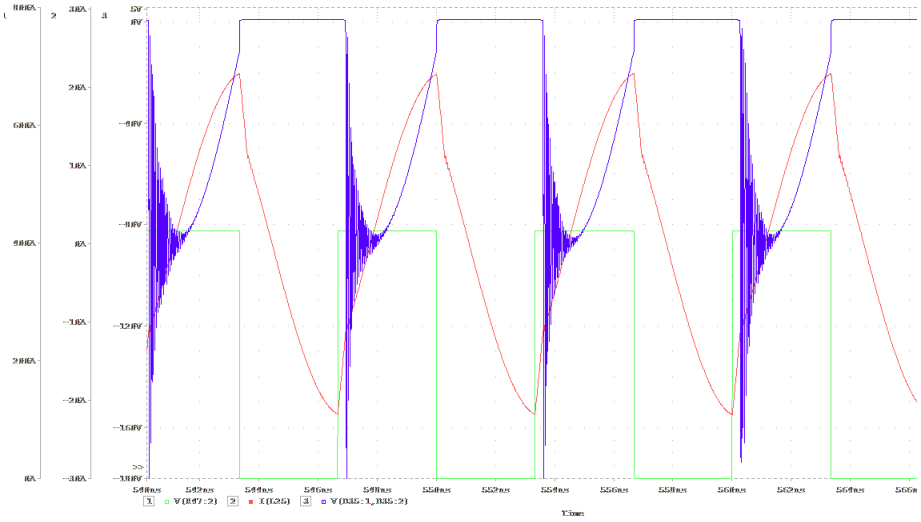

Figure 4-13 : Transient simulation result at 24V with30A load. Ch1_Green trace: Transformer primary voltage; Ch2_Red trace: Resonant current; Ch3_Blue trace: Resonant voltage;

Figure 4-14 and Figure 4-15 show the hardware prototype bench testing result and time-domain transient simulation result at 24V with full load.

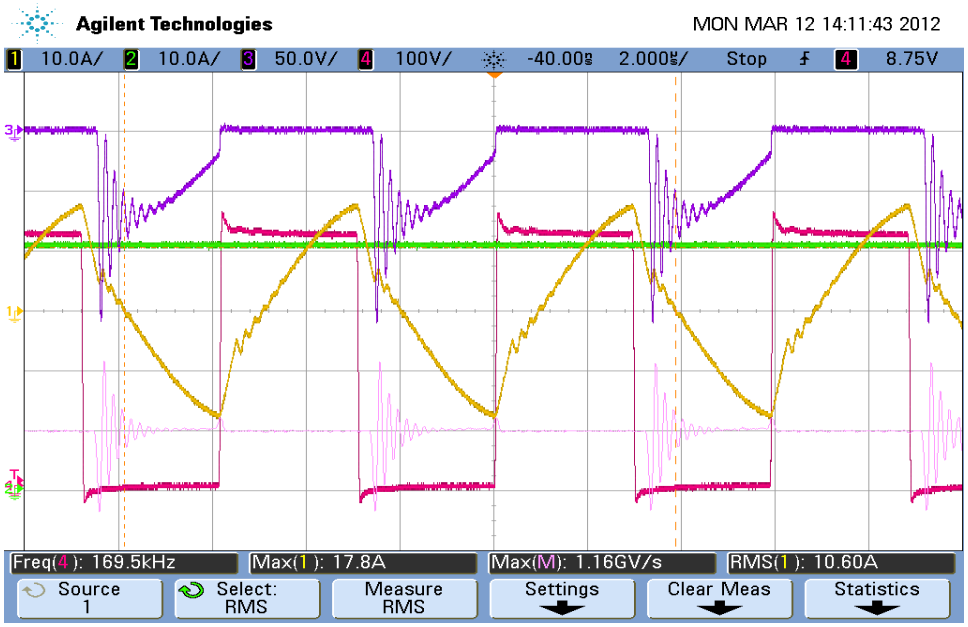

Figure 4-14: Bench testing result at 24V with 40A load. Ch1_Yellow trace: Resonant current; Ch2_Green trace: Output current; Ch3_Blue trace: Resonant voltage; Ch4_Red trace: Transformer primary voltage.

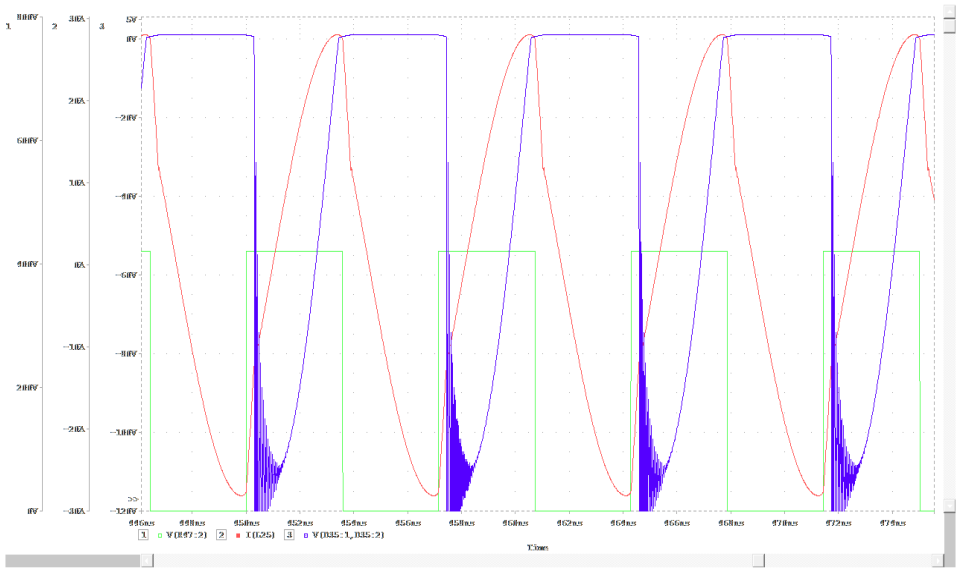

Figure 4-15 : Transient simulation result at 24V with 40A load. Ch1_Green trace: Transformer primary voltage; Ch2_Red trace: Resonant current; Ch3_Blue trace: Resonant voltage.

The results obtained from the bench testing were compared and evaluated with the SPICE

transient simulation performance. It can be clearly seen that given the same operating conditions like: input voltage, output voltage, switching frequency, and load condition, the time-domain transient simulation provided very close simulation results to the hardware results in terms of the waveform shape and magnitude. It can be seen that at no load, the hardware prototype has a triangular resonant current switching waveform similar to that shown in Figure 2-35, but at full load instead of showing the sinusoidal shape resonant current waveform, it is still a triangular waveform with a high peak. These outputs may suggest that the two uncoupled output inductors adopted in the hardware prototype resulted in a bad LLC resonant switching characteristic under near full load condition. Because the performance can not meet the design criteria, the bench testing was not carried above 40A.

In order to verify the hardware prototype circuit AC frequency performance, the second main task is to compare the actual switching frequency measurements with the AC simulation frequency measurements. This is because the frequency measurement is a key design methodology that is used to control the LLC converter switching characteristic. Table 4-2 shows the bench frequency measurement results and the AC frequency simulation measurement results. This bench frequency measurement was set up and carried out at 230 Vac input voltage (420Vdc appears on the input of the LLC resonant converter).

	Bench Experimental Results			**AC Frequency Simulation Results**		
Load Condition	Output Voltage			Output Voltage		
	22V	24V	27V	22V	24V	27V
0A	361kHz	237.5kHz	191.2kHz	1MHz	341kHz	268kHz
10A	215.5kHz	189kHz	167.2kHz	831kHz	338kHz	267kHz
20A	200.8kHz	185.9kHz	166.1kHz	586kHz	334kHz	266.5kHz
30A	197kHz	175.4kHz	159.7kHz	491kHz	328kHz	265.9kHz
40A	183.2kHz	169.5kHz	157kHz	440kHz	321kHz	265 kHz

Table 4-2: Hardware prototype switching frequency measurement results.

The bench-test results have an error value of ±5% - based on the measurement equipment errors. The actual switching frequency was measured on the LLC half bridge switching voltage using an Agilent 3000 series oscilloscope under the different operating conditions.

From Table 4-2 it can be seen that the actual bench frequency measurement results are substantially different to the results obtained from the AC simulation (although the general trends versus output voltage and current are similar). The difference of these measurement results suggest that the proposed LLC resonant current doubler converter with uncoupled output inductors configuration AC simulation circuit in Figure 4-5 could not accurately represent the real circuit. The AC frequency results in the simulation are higher than the bench measurement results which suggest the LLC resonant circuit seen a different load. One of the most important performance metrics for the LLC resonant current doubler converter is the efficiency measurement. This measurement was performed on the test bench circuit with calibrated test equipment. Equipment used to generate these results are: Yokogawa WT230 AC power meter, DC meter Agilent 34970A, Agilent scope 3000 series. The input voltage is at 230Vac, the bench-test results have an error value of ±5% of the nominal value (not ±5% efficiency) - based on the measurement equipment errors. To better demonstrate the advantage of this novel topology, the prototype efficiency was compared with the current EATON 24VDC product (APR24-3G). The APR24-3G was measured up to its rated output full current at 50A. The prototype circuit was only measured up to 40A load current for this test. Figure 4-16 shows the efficiency comparison plot with an error of ±5% of the nominal value. The efficiency plot suggests that this prototype circuit did not rival the conventional LLC resonant converter topology utilized in the current EATON 24VDC product.

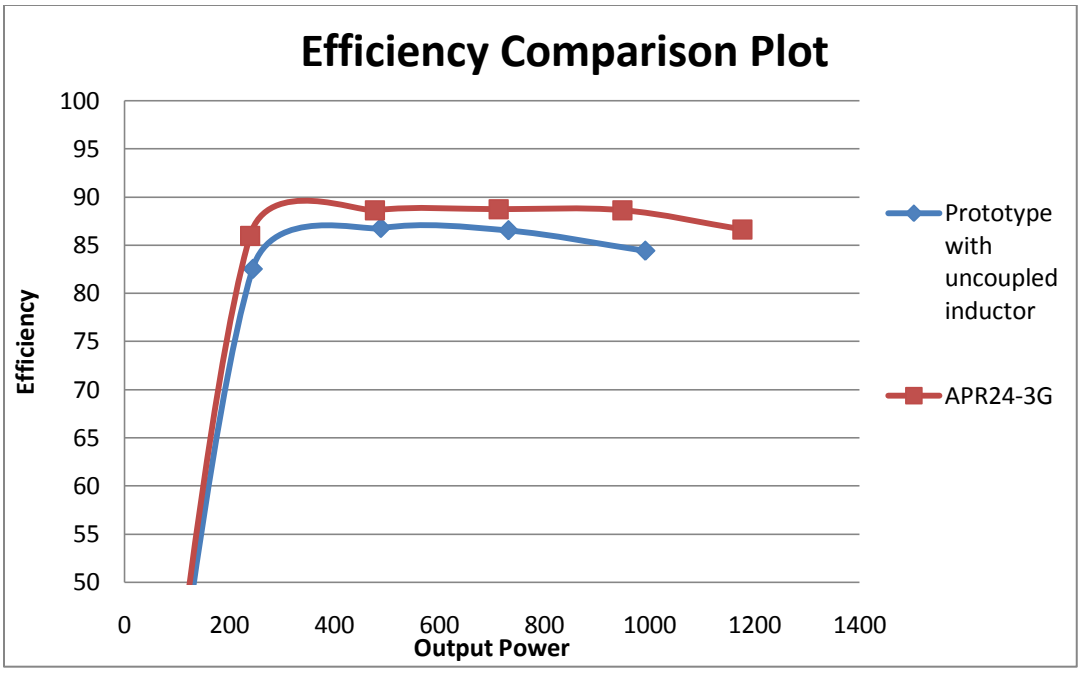

Figure 4-16: Efficiency comparison plot with uncoupled inductors prototype and the EATON 24VDC product (APR24-3G).

4.5 Conclusion

A hardware prototype for the half-bridge LLC resonant current doubler converter with two uncoupled output inductors was constructed and tested as proposed in Chapter 3. Both a time-domain based transient simulation circuit model and a frequency-domain domain based AC simulation circuit model were designed and simulated. A more desirable approach to show the modification of the main transformer design from a centre-tapped configuration to a single-ended configuration for the proposed topology was presented in Figure 4-7 this chapter. The proposed hardware prototype was operated up to 1kW power level. Correct circuit operation waveforms with two output inductors sharing the total load current for the current doubler converter topology were observed both from the time-domain based transient simulation results and prototype bench testing results under the same operating conditions.

However, the results shown in the 40A load bench prototype testing, AC frequency and transient simulation highlighted that it is not a desirable solution to use two uncoupled output inductors in the proposed novel LLC current doubler converter topology. The hardware results may suggest that this uncoupled output inductors topology may not operate well with the LLC resonant converter in the primary side because it has greatly changed the LLC resonant tank switching characteristic as shown in Figure 4-6. The findings in this Chapter demonstrate that the current doubler topology can be used to develop a novel LLC resonant converter for low output voltage and high output current application, however the two uncoupled output inductors configuration can not provide an overall higher efficiency performance compared to the current APR24-3G product.

Chapter 5

LLC Resonant Current Doubler Converter Simulation and Testing With Two Coupled Inductors

A 1kW novel half-bridge LLC resonant current doubler converter prototype with two output inductors in the uncoupled configuration was evaluated in Chapter 4. However, a major difference in the frequency measurement was highlighted with respect to AC simulation results and the efficiency of this proposed converter did not rival that of the EATON APR24-3G best efficiency. Moreover, the research of an integrated coupled inductor application identified in Chapter 3.3 suggests that an overall advantage may be obtained through the refinement of the current doubler topology. Simulation models and a new hardware prototype circuit were developed to find out whether coupled output inductors could offer a significant performance improvement.

5.1 Transient Simulation

A new time-domain transient simulation circuit model was designed for coupled output inductor simulation modeling purposes, based on a similar structure as shown in Figure 4-1. In order to meet the desired performance targets, a number of design changes were made to the CDR converter. For modeling, the two output inductor values were recalculated to meet the new design requirements for the integrated magnetic components. The coupling coefficient factor K11 was now set to 1 to reflect the output inductors close magnetic coupling condition. Figure 5-1 shows the new transient simulation circuit with two output coupled inductors.

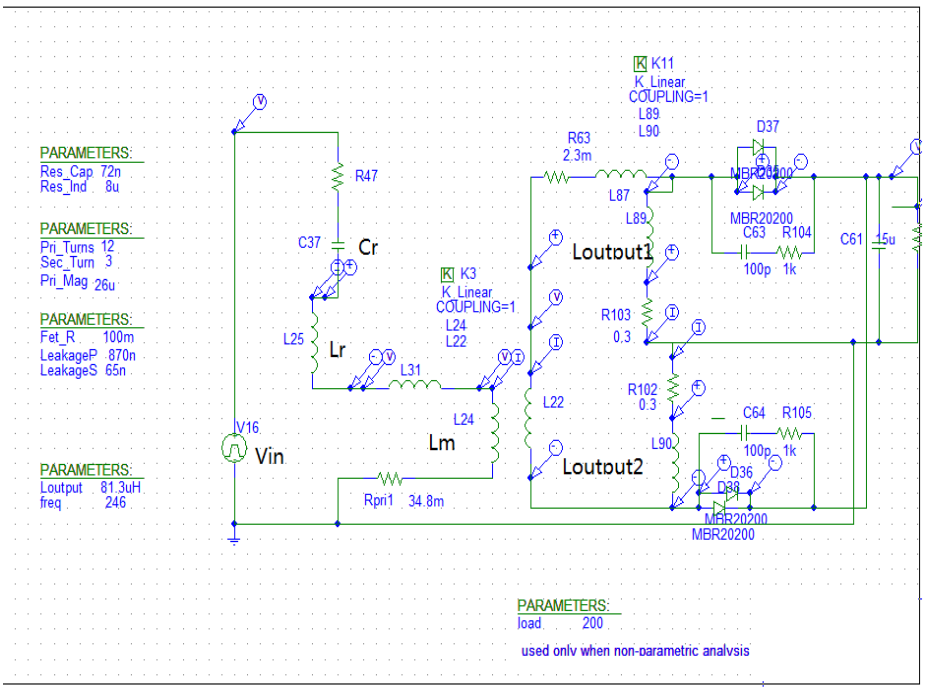

Figure 5-1: Time-domain transient simulation circuit with coupled inductors.

The design of the two output coupled inductors based on the auto transformer theory that was presented in Section 3.4. Therefore, in this simulation circuit, both output inductors are no longer behaving like the conventional current doubler output inductors. The two magnetically coupled output inductors are operating as a step down auto transformer.

The simulation output waveforms shown in Figure 5-2 clearly identify that the two output inductors are sharing the total load current and have halved the output voltage to 27VDC (actual DC voltage for a fully-charged lead-acid battery bank - nominal 24V). Figure 5-2, Figure 5-3, and Figure 5-4 show the simulation waveforms under no load, light load (30A), and full load (50A) operation.

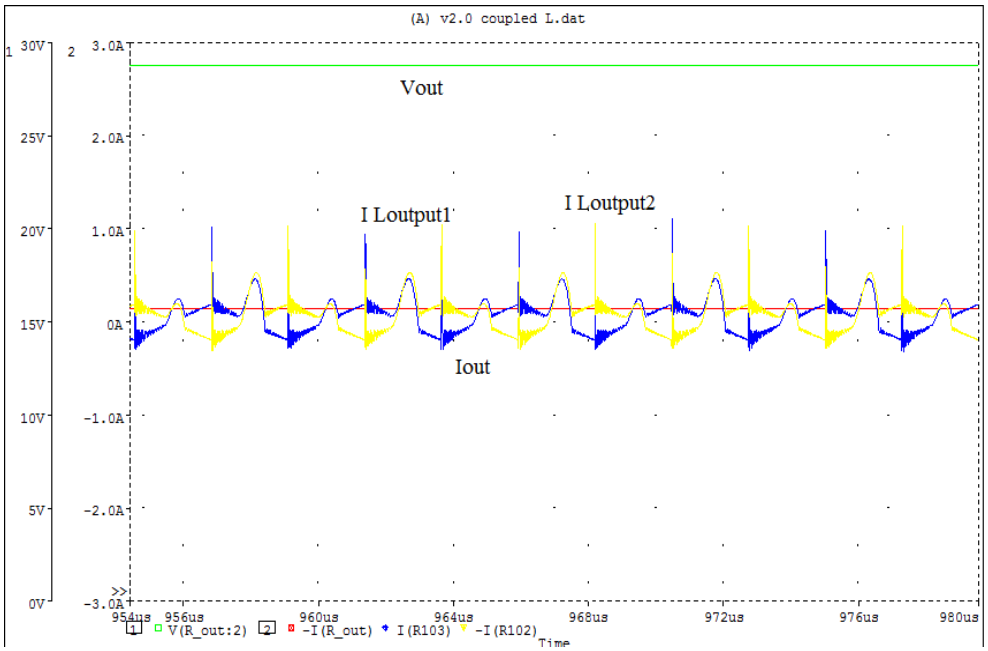

Figure 5-2 : Transient simulation waveform at no load with new design. Green trace: Vout, Blue trace: Loutput1current, Yellow trace: Loutput2 current, Red trace: Total output current Iout.

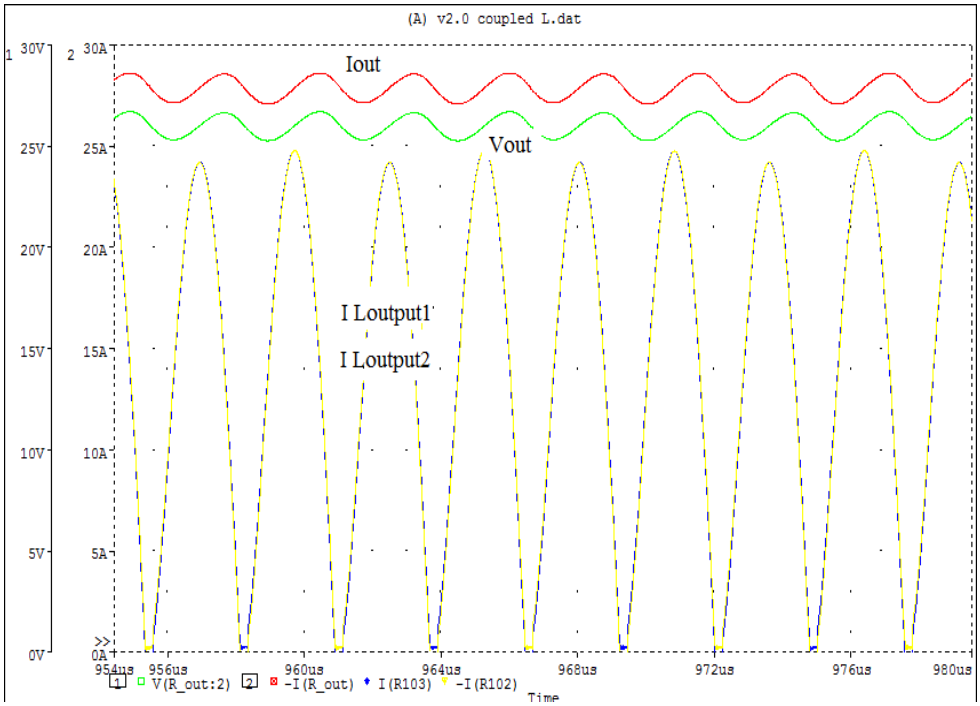

Figure 5-3 : Transient simulation waveform at 30A load with new design. Green trace: Vout, Blue trace: Loutput1current (superimposed), Yellow trace: Loutput2 current (superimposed), Red trace: Total output current Iout.

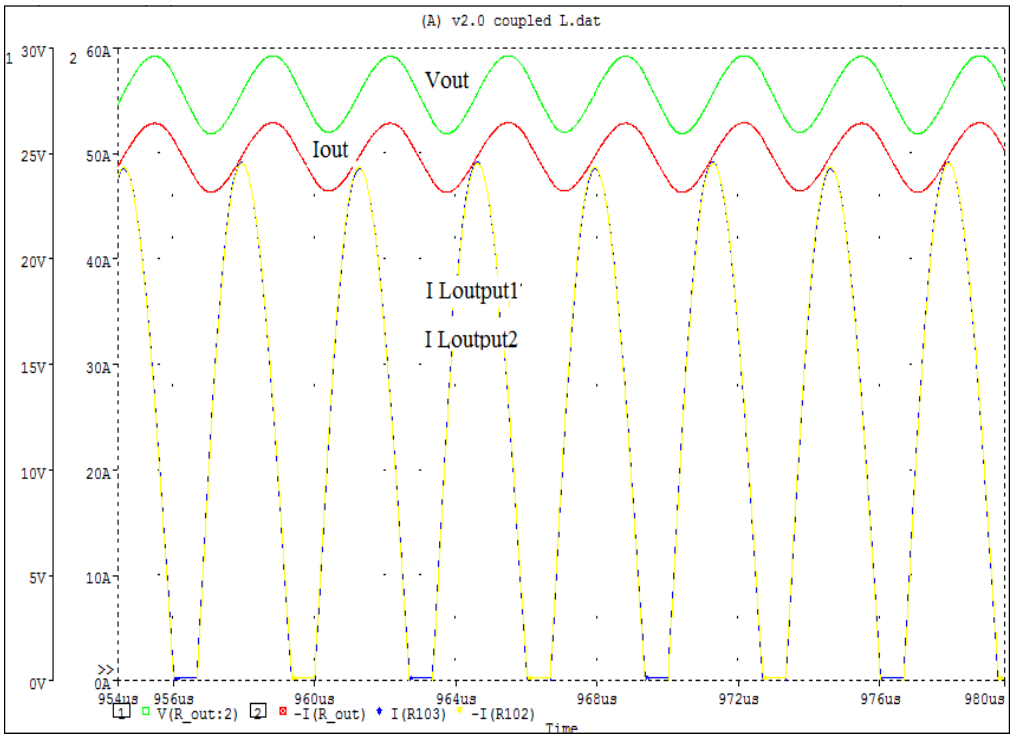

Figure 5-4 : SPICE transient simulation waveform at full load with new design. Green trace: Vout, Blue trace: Loutput1current (superimposed), Yellow trace: Loutput2 current (superimposed), Red trace: Total output current Iout.

The transient simulation tests shown demonstrate that the new coupled output inductors arrangement for this novel LLC resonant current doubler converter application could potentially work in practice. Correct operation waveforms, output voltage and output current results are observed from the Figure 5-4 in terms of the waveform shape and magnitude. Two identical and superimposed output inductor currents are also observed which indicates that the two magnetically coupled output inductors are operating in a similar manner as an auto transformer, as shown in Figure 3-10 (b). One important finding is that the output inductor current waveforms are both identical and superimposed as shown in Figure 5-3, and Figure 5-4 under light load and full load condition. They are different to the conventional current waveforms observed in Figure 4-2, Figure 4-3, and Figure 4-4. This is because the new configuration is operating in close agreement with the auto transformer theory. This finding is important for constructing the new hardware

prototype. It also suggests that the expected transient simulation results observed from the coupled output inductors may also result in an improved AC simulation performance.

5.2 AC Frequency Simulation

The transient simulation detailed in Section 5.1 suggests that an overall advantage has been obtained through the application of the auto transformer technique applied to the current doubler converter topology. The output voltage and output current results were very similar to the design proposed in Chapter 4. However, the AC frequency simulation in Chapter 4 was observed with a notable difference compared to the LLC characteristic plot which showed only one resonant frequency fr2. In order to find out whether the new coupled inductor circuit could offer a significant performance improvement for AC simulation under different load conditions, a new AC simulation circuit model was constructed as shown in Figure 5-5 based on the transient simulation circuit from Section 5.1.

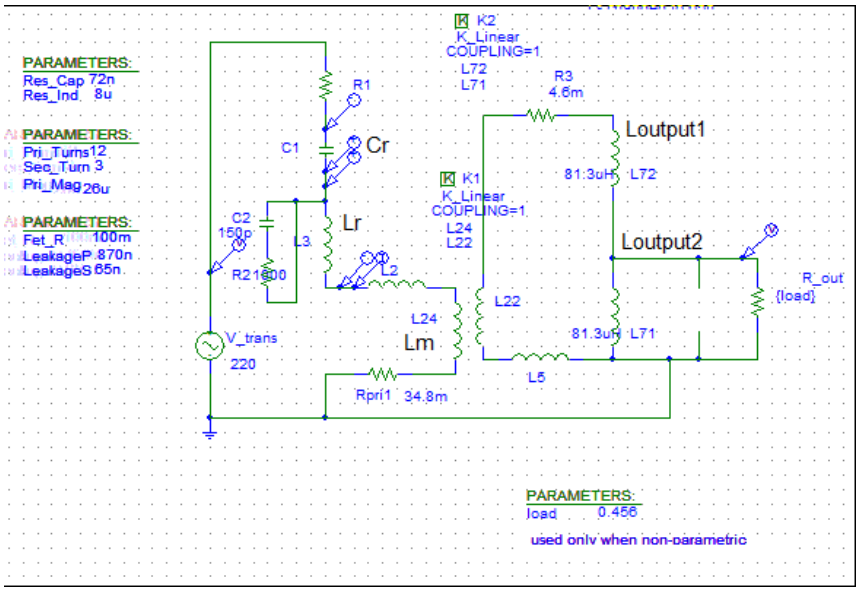

Figure 5-5： AC frequency-domain simulation circuit with coupled inductors.

The AC frequency simulation was carried out with the same input and output conditions as shown in Figure 4-5. The output inductors coupling coefficient factor K2 was set to 1 as in the transient circuit. The circuit was simulated with respect to the frequency range of 30kHz to 500kHz. The AC simulation results are shown in Figure 5-6.

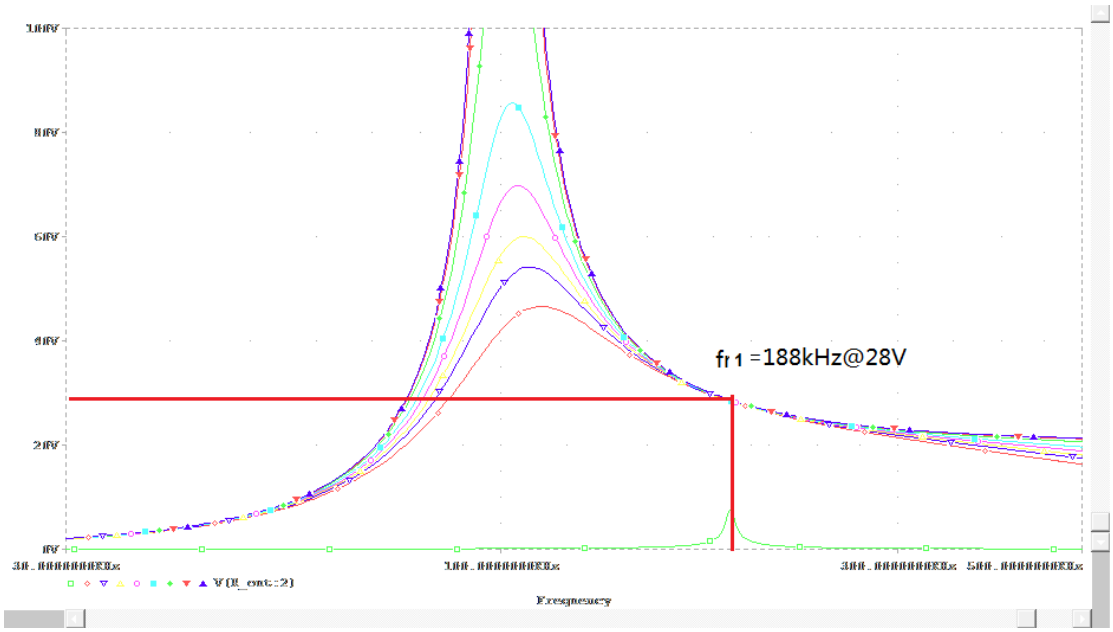

Figure 5-6: AC frequency simulation result with coupled inductors. Upper red trace: No load; Green trace: 10A load; Light blue trace: 20A load; Pink trace: 30 A load; Purple trace: 40A load; Red trace 50A full load; Lower green trace: fr1 indication.

Figure 5-6 illustrates that the AC frequency simulation with coupled inductors has significantly improved the AC frequency performance compared to the old design shown in Figure 4-5. The resonant frequency fr1 was measured at 188kHz as shown in Figure 5-6 with the output voltage at 28V where all traces (different load conditions) intersect at this resonant point. These results have demonstrated that the design goal has been achieved since the AC frequency simulation obtained as shown in Figure 5-6 is very similar to the standard LLC resonant converter characteristic plot as shown in Figure 2-22. This new model also demonstrates the likely validity of this concept for a new LLC resonant current doubler topology utilizing coupled output inductors.

The performance of the new LLC resonant current doubler converter with coupled inductors in AC frequency simulation was also compared to the AC frequency simulation of the APR24-3G (24VDC) and the APR48-3G (48VDC) LLC resonant converter. Figure 5-7 shows the AC simulation circuit for the APR24-3G and Figure 5-8 shows the simulation result.

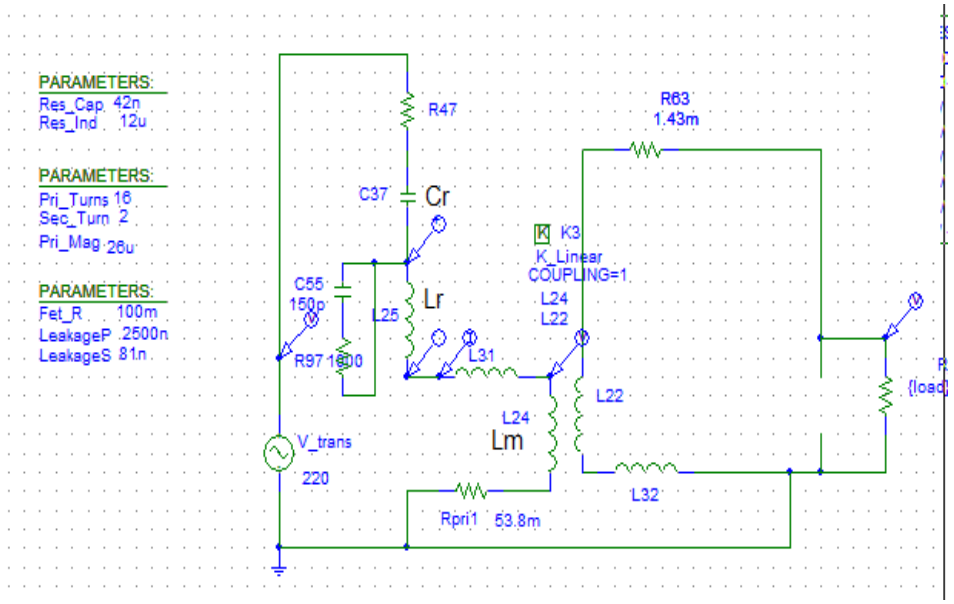

Figure 5-7: AC frequency simulation circuit of the current 24VDC product.

The simulation circuit key component parameters such as the resonant tank network, transformer turns ratio, and transformer parameter values were modified to accommodate the actual circuit design.

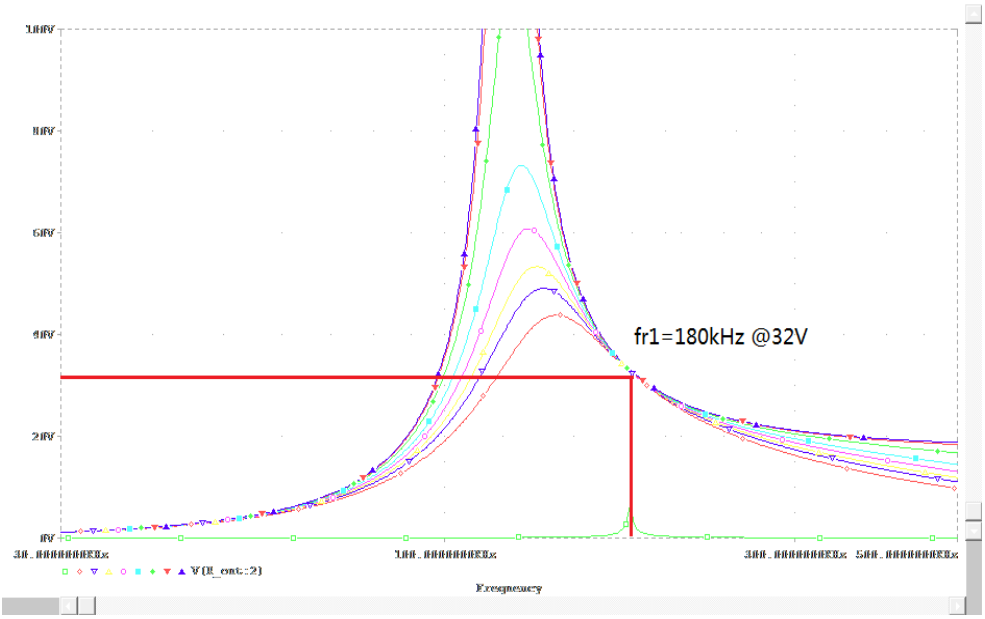

Figure 5-8: AC frequency simulation result of the current 24VDC product.

The resonant frequency fr1 observed in Figure 5-8 was at 180 kHz with an output voltage of 32V which is very close to the result observed in Figure 5-6. Figure 5-6 and Figure 5-8

demonstrate that the new LLC resonant current doubler converter with coupled inductors allows a similar AC frequency performance to be achieved compared to the current APR24-3G (24VDC) product.

Compared to the APR48-3G (48VDC) product, the resonant frequency fr1 observed in Figure 2-33 was measured at 188kHz and the output voltage was measured at 54V (rated output voltage for APR48-3G /48VDC product). Figure 5-6 demonstrates that the new LLC resonant current doubler converter with the coupled inductors concept can still offer the same competitive advantage as the conventional current doubler topology which halves the output nominal voltage from 54V to 28V and doubles the output current, but now appears to allow the LLC resonant tank operate normally.

These results strongly indicate that the new LLC resonant current doubler converter with coupled output inductors would provide better overall performance than the old LLC resonant current doubler design demonstrated in Chapter 4.A clear improvement was observed with the coupled inductors solution compared to the uncoupled inductors solution, particularly in the AC frequency simulation performance, which would also suggest a better performance for the hardware prototype testing.

5.3 Integrated Magnetically Coupled Inductors

Bench testing was conducted to evaluate and confirm that a coupled output inductors circuit would offer better performance which was observed from the transient and AC frequency simulation results. In order to perform the testing, a new hardware prototype based on the equivalent simulation circuit was designed and built which had a similar structure to the previous prototype shown in Chapter 4. The proposed new hardware prototype circuit requires an integrated magnetic component which would be created from two coupled output inductors as shown in the simulation circuits.

The important parameters such as full load current, output current ripple level, and switching frequency were considered in the inductor design. The output inductor value can be calculated as shown in Eqn 5-1.

$$L=V\frac{d_t}{d_i}=\frac{V_o*D/f}{\Delta i}=\frac{24*0.18/180000}{0.3}=80\mu H \qquad \text{Eqn 5-1}$$

The same transformer that was modified and implemented in the design presented in Chapter 4 was used here since no changes were made on the primary side LLC resonant network circuit and the transformer. A new integrated magnetic structure with coupled inductors is proposed here and shown in Figure 5-9 in order to improve the existing uncoupled inductor performance that was demonstrated in Chapter 4.

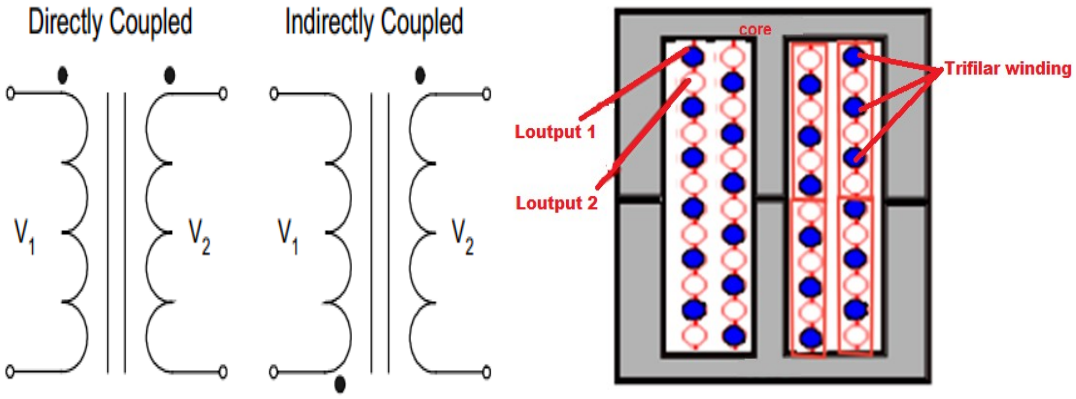

(a) (b)

Figure 5-9 : (a): Coupled inductor arrangement with direct and indirect coupling method [21]. (b) Proposed new integrated coupled inductor magnetic structure.

The magnetically integrated inductors can be coupled in two ways as shown in Figure 5-9 (a). Direct coupling means all inductors are wound with the same polarity, and indirect coupling has the two inductors wound in the opposite polarity with flux cancellation advantage [21]. Indirect coupling is better suited for pairs of inductors due to flux cancellation in the mutual inductance path and can be used to reduce the converter current ripple as the coupling coefficient is increased [22]. The hardware prototype presented in this Chapter uses indirect coupling on the coupled inductors, and has the winding structure as shown in Figure 5-9 (b). Furthermore, the magnetically coupled

inductors could offer additional benefit to improve the overall EMC performance by reducing the output noise. This noise reduction would occur because the coupled inductors could also be used as part of the coupled output inductor filter [23]. With equal numbers of turns on the two windings, the ideal auto transformer (formed for the new integrated coupled inductor structure) has a 1:1 turns ratio. The gapping configuration and gap lengths affect the values of inductance. Because in this coupled inductor application the inductors are ungapped, the inductance's energy storage is negligible. Therefore, the values of the leakage inductances are equal to the values of the uncoupled inductors [22].

It also can be seen from Figure 5-9 (b) that the two inductor windings are wound in a trifilar format, which is a common technique for multiple windings to reduce the winding losses [16]. The word trifilar describes a winding that is made of three filaments or strands. As shown in Figure 5-9 (b), two inductor windings are constructed with an interleaving termination scheme. Therefore lower conduction loss can be attained through the evenly distributed current among the termination pins. The physical component of the integrated coupled inductors is shown in Figure 5-10.

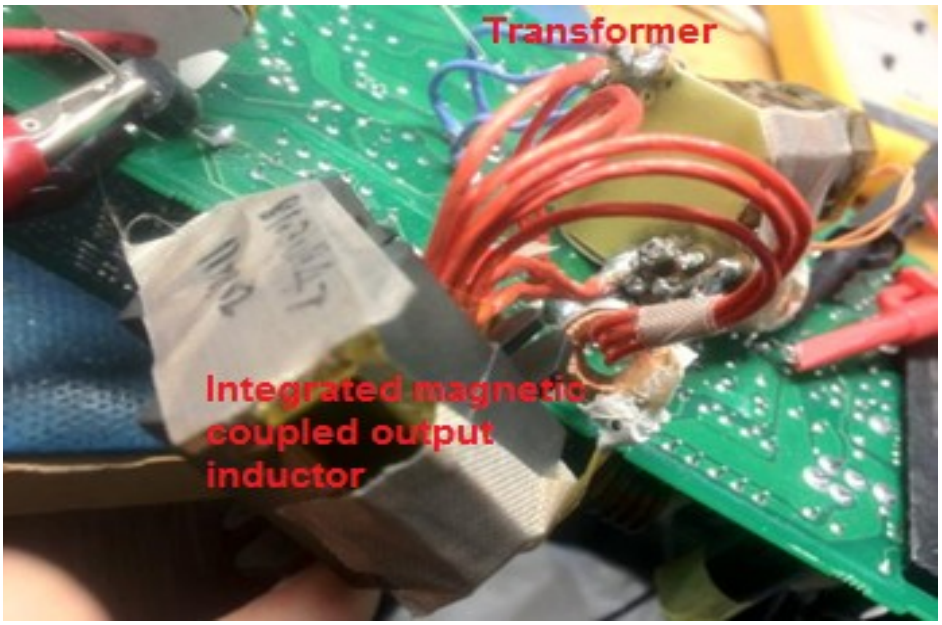

Figure 5-10: Integrated magnetically coupled output inductors.

In Figure 5-10, each of the coupled inductor is wound with 3 strands of 825*44 AWG type litz wire with 4 turns in order to meet the designed inductor value. The 3F3 RM12 magnetic core is used with the inductance factor A_L (no gap) equals to 5050 nH [20]. The turns ratio can be calculated using Eqn 5-2 [20] below.

$$N=\sqrt{\frac{L}{A_L}}=\sqrt{\frac{80*10^{-3}}{5.05*10^{-6}}}=3.9\approx 4 \qquad \text{Eqn 5-2}$$

The inductor performance was designed to meet the same performance as the APR48-3G main transformer. Both of their windings need to deliver same amount of current (25A maximum) by using the same type of litz wire. A coupled inductor where a single core is shared by the multiple inductors instead of using multiple discrete inductors offers a potential approach to reducing parts count, cost, volume, and weight. Coupled inductor topologies can also provide additional advantages such as reduced core and winding loss as well as improved input and inductor current ripple characteristics [17]. The integrated coupled output inductors performance is evaluated by bench testing through a new hardware prototype which is detailed in Section 5.4.

5.4 Experimental Test Results and Discussion

In this section, a new LLC resonant current doubler converter hardware prototype with integrated coupled output inductors is detailed. It was built and tested to verify the converter theoretical analysis and simulation analysis results. In Figure 5-11, a 24VDC, 50A, 1.25kW prototype was built to demonstrate the advantages of the proposed new LLC resonant current doubler converter. In the real circuit, Lm =26µH (±3%), Lr =8µH (±3%), Cr =72nF (±3%), Lout =81.3µH (±3%), and the turns ratio is 12:3.

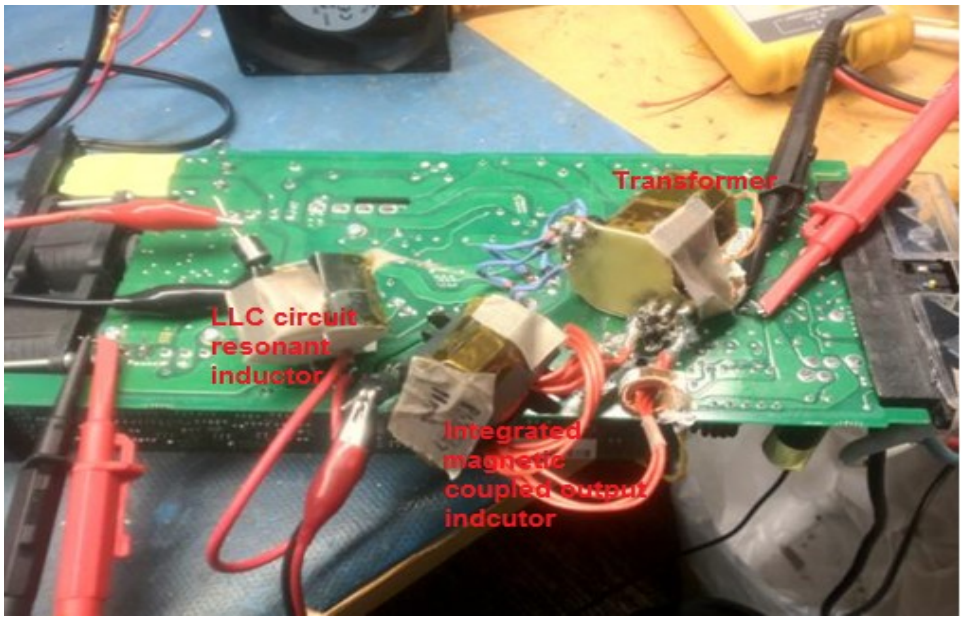

Figure 5-11：New hardware prototype with integrated output inductors.

The bench testing waveform results were collected in order to compare with the transient simulation results presented in sections 5.1 and 5.2. Comparison work was mainly focused on the operation conditions of 24VDC at no load, 30A load and 50A load. However, more test results under different operating conditions can be found in Appendix B.

In preparation for testing the prototype, the output diode voltage and dv/dt was closely monitored to prevent component damage caused by unacceptably large magnitude and speed switching voltage. The primary side resonant current was observed to demonstrate the maintained LLC resonant tank switching characteristic. The primary side half bridge switching voltage was observed to obtain the converter actual switching frequency under different switching modes and load conditions. The output inductor current was observed to demonstrate the integrated coupled inductors performance. Only one inductor output current is shown in the following set of figures because both the output inductor currents are measured as being identical. Figure 5-12 and Figure 5-13 show the hardware prototype bench testing waveforms and SPICE transient simulation result at 24V with no load.

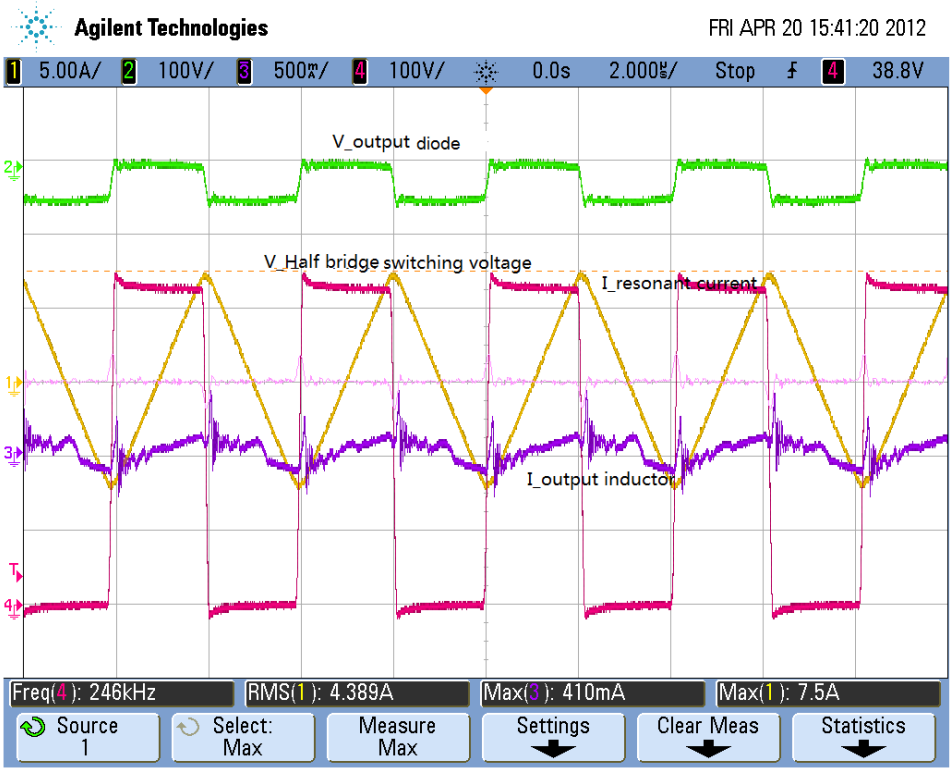

Figure 5-12: Bench testing waveforms at 24V with no load. Yellow trace: Resonant current, Green trace: Output diode voltage, Blue trace: Current in Loutput1, Red trace: Half bridge voltage,

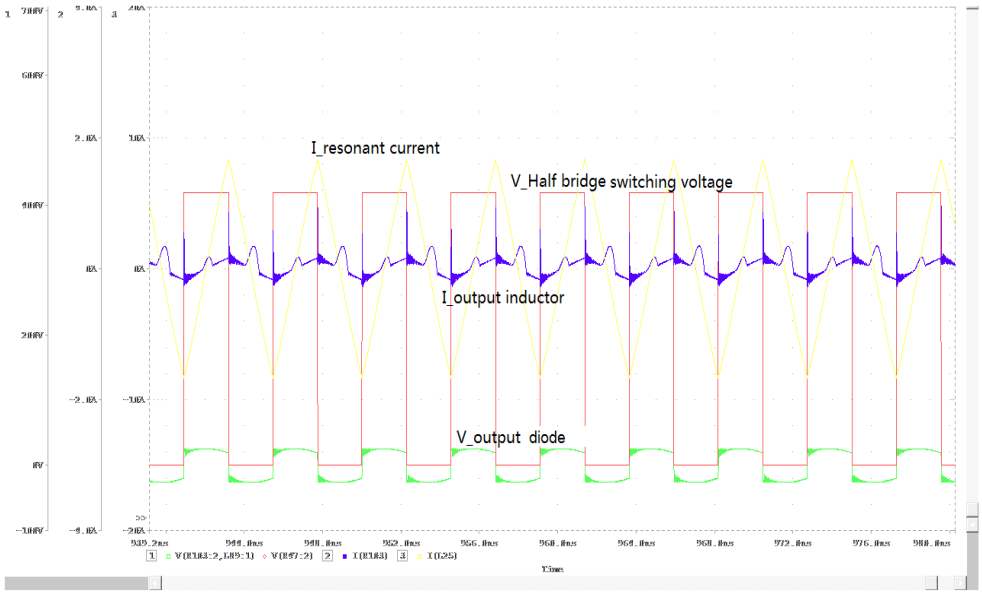

Figure 5-13 : Transient simulation results at 24V with no load. Yellow trace: Resonant current, Green trace: Output diode voltage, Blue trace: Current in Loutput1, Red trace: Half bridge voltage.

Figure 5-14 and Figure 5-15 show the hardware prototype bench testing waveforms and transient simulation results at 24V with a 30 A load.

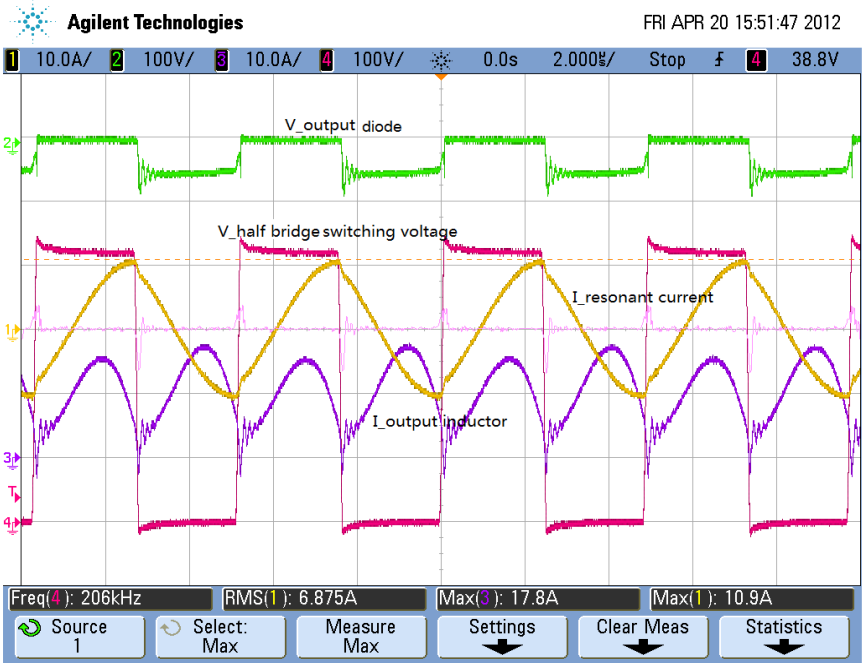

Figure 5-14: Bench testing waveforms at 24V with 30A load. Yellow trace: Resonant current, Green trace: Output diode voltage, Blue trace: Current in Loutput1, Red trace: Half bridge voltage,

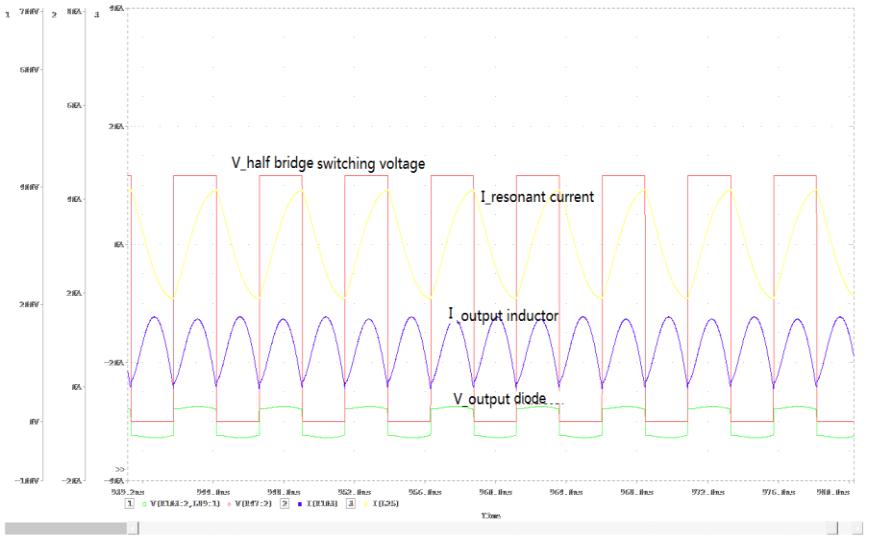

Figure 5-15: Transient simulation results at 24V with 30A load. Yellow trace: Resonant current, Green trace: Output diode voltage, Blue trace: Current in Loutput1, Red trace: Half bridge voltage,

Figure 5-16 and Figure 5-17 show the hardware prototype bench testing waveforms and SPICE transient simulation results at 24V with 50 A load.

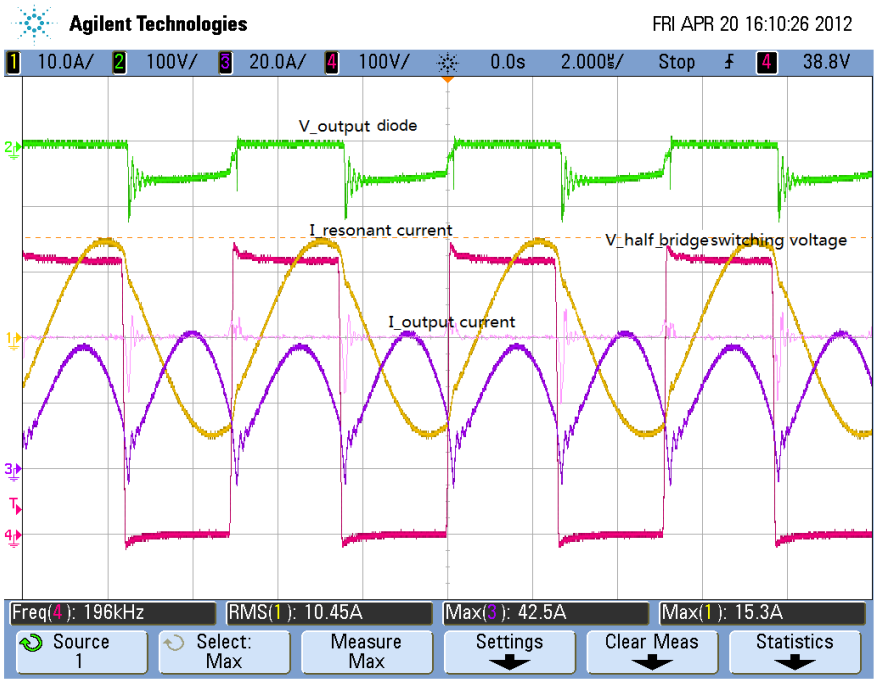

Figure 5-16: Bench testing waveforms at 24V with 50A load. Yellow trace: Resonant current, Green trace: Output diode voltage, Blue trace: Current in Loutput1, Red trace: Half bridge voltage.

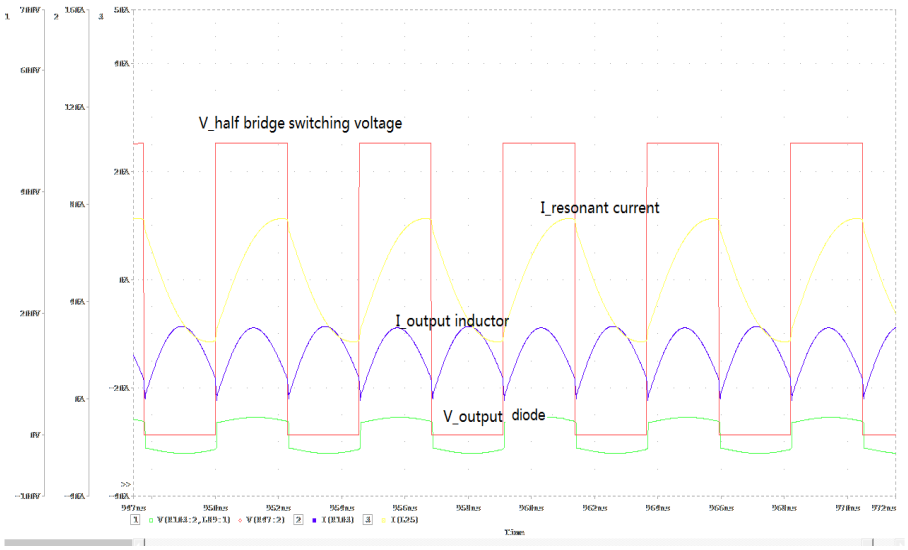

Figure 5-17 : Transient simulation results at 24V with 50A load. Yellow trace: Resonant current, Green trace: Output diode voltage, Blue trace: Current in Loutput1, Red trace: Half bridge voltage.

The operational waveforms obtained from the bench testing were compared and evaluated with the transient simulation results. It can be clearly seen that the bench measurements provide close agreement with the transient simulation results in terms of the shape of the waveform and the magnitude given the same operating conditions like: input voltage, output voltage, switching frequency, load condition. It can be seen that at no load, the new hardware prototype provides a triangular resonant current switching waveform as shown in Figure 5-12. This current waveform is very similar to that shown in Figure 2-35 (a) and the uncoupled prototype in Figure 4-10. At light load, instead of showing the triangular waveform with a high peak as shown in Figure 4-12 for uncoupled inductors, Figure 5-14 shows a triangular resonant current waveform is obtained with a small peak. At full load, compared to the uncoupled inductor hardware which shows a high peak triangular resonant current waveform in Figure 4-14, the new hardware prototype resonant current waveform shown in Figure 5-16 is very similar to the sinusoidal resonant current waveform as shown in Figure 2-35 (b). It also can be observed that the parasitic oscillation in the simulation results are lower in magnitude and higher in frequency than the bench testing results. This indicates that the hardware prototype circuit parasitic leakage inductance is much larger than the simulation circuit.

The bench testing also confirms that the new LLC resonant current doubler prototype with integrated coupled output inductors exhibits better performance than the old prototype circuit, particularly with respect to the resonant current switching waveform. The peak of the resonant current was lower and the overall component stress was reduced compared to the uncoupled inductors configuration. These results strongly suggest that the integrated coupled inductors configuration offers the advantage of good magnetic coupling between the two output inductors so that any effects on the primary resonant network circuit is limited and negligible.

The performance of the AC frequency simulation was also compared with the new hardware prototype to find out whether the integrated coupled inductors would offer any benefit to improve the frequency simulation results demonstrated in Section 4.4. The bench switching frequency measurement was conducted and the result was observed by

using an oscilloscope under the different operating conditions. The results are summarized in Table 5-1.

	Bench Experimental Results			**AC Frequency Simulation Results**		
Load Condition	Output Voltage			Output Voltage		
	22V	24V	27V	22V	24V	27V
0A	309 kHz	246 kHz	201 kHz	300.8 kHz	212 kHz	180 kHz
10A	253 kHz	215 kHz	183.8 kHz	250 kHz	211.4 kHz	179 kHz
20A	234 kHz	206 kHz	182.5 kHz	249kHz	210 kHz	178.4 kHz
30A	224 kHz	201 kHz	177.3 kHz	246kHz	209 kHz	177 kHz
40A	219 kHz	195 kHz	180.5 kHz	243 kHz	208 kHz	176 kHz
50A	210 kHz	196 kHz	183.2 kHz	239 kHz	207 kHz	175 kHz

Table 5-1 : New prototype circuit frequency measurement results.

This bench frequency measurement was set up and carried out at 230 Vac input voltage (420Vdc appears on the input of the LLC resonant converter). The summarized results in Table 5-1 strongly indicate that a significant simulation accuracy improvement was observed compared to the results in Table 4-2. The natural implication of this is that the model of the uncoupled inductor configuration is not an accurate representation of the actual circuit. Table 5-1 also suggests that the integrated coupled inductors AC simulation model provides better converter operation with respect to frequency characteristics than the uncoupled inductor solution as shown in Table 4-2. The implementation of the new integrated coupled inductor has been proved to successfully minimize the difference between the actual circuit frequency and the simulated frequency. Considering the simulation tool is only used for the purpose of circuit operation estimation, the tolerance is acceptable, and the small difference can be improved by adjusting the integrated magnetic parameter values in the model.

One of the most important performance metrics for the LLC resonant current doubler converter is the efficiency measurement. This measurement was performed on the prototype circuit with calibrated test equipment. Equipment used to generate these results are: Yokogawa WT230 AC power meter, DC meter Agilent 34970A, Agilent scope 3000 series. The input voltage is at 230Vac, the bench test results have an error value of ±5% - based on the measurement equipment errors. To better demonstrate the advantage of this novel topology, the efficiency of the new prototype was also then compared with the current standard LLC converter APR24-3G. Both the APR24-3G and the new prototype were measured up to the rated full output current at 50A. Figure 5-18 shows the efficiency comparison plot.

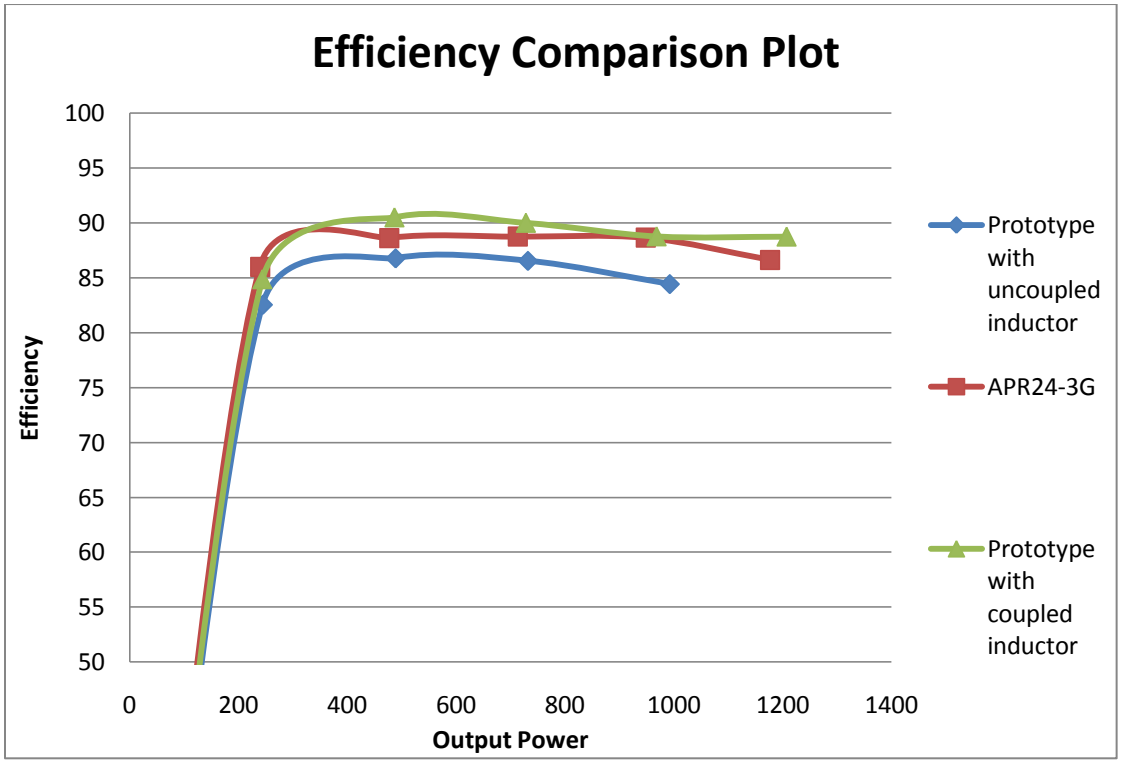

Figure 5-18: Efficiency comparison plot

The efficiency plot shows a significant improvement has been achieved by using the integrated coupled inductors topology compared to the topology with uncoupled inductors, but only a little improvement compared to the APR24-3G (24VDC). The efficiency of the integrated coupled inductor topology was above the APR24-3G

efficiency. This is because the proposed LLC resonant current doubler topology with integrated coupled inductors better utilizes the APR48-3G transformer with modified output windings which reduced the power losses. It also shows that the proposed new topology would offer a competitive advantage in low output voltage, high output current applications for telecom rectifiers.

5.5 Conclusion

Testing of the prototype LLC resonant current doubler converter with two uncoupled output inductors revealed unexpected AC frequency characteristics and excessive resonant current problems (as detailed in Chapter 4). A new hardware prototype with integrated coupled output inductors was considered and successfully demonstrated in this Chapter with improved AC frequency characteristics, and alleviated the excessive resonant current.

The results of the simulation and bench testing confirmed the suitability of an integrated coupled winding configuration for the novel LLC resonant current doubler converter application. In addition, these results illustrate that the converter topology using integrated coupled inductors in general could offer an overall benefit in terms of reduction of magnetic component size, cost and weight compare to the uncoupled inductor topology.

Inductor flux coupling can be realized using either direct or indirect winding configurations. For the purposes of our study and potential applications of interest, indirect inductor coupling was selected for the integrated output inductor winding configuration with an interleaved structure rated for carrying the full load current. For the indirect coupling configuration, the flux generated by the two windings will cancel rather than sum within the core. As a result, the output inductors current waveforms are no longer similar to the uncoupled inductor waveforms as shown in Chapter 4. The secondary side magnetic inductance is not large enough to cause any significant

interference to the primary LLC resonant switching network. Therefore, the use of the integrated indirect coupled inductors improved the primary resonant current switching waveform significantly, particularly at high output current conditions.

Furthermore, the efficiency of the two hardware prototypes were plotted in comparison to the current EATON 24VDC product with the primary LLC resonant converter topology. The result suggests that this prototype circuit can achieve slightly better efficiency performance.

Chapter 6

Summary and Future Work

6.1 Summary

The half-bridge LLC resonant converter is the most attractive topology to design telecom power converters. The increasing popularity of the LLC resonant converter is due to its high efficiency, high power density and low switching noise. The current doubler converter topology was evaluated as a complementary solution with its unique characteristic to improve the LLC resonant converter performance, especially for the low output voltage and high output current applications.

A novel half-bridge LLC-CDR converter is proposed in this thesis which can offer several performance benefits compared to the conventional design. A commercial single phase telecom power converter was modified to verify the operation of this novel topology which utilized both the topologies from the LLC resonant converter and the current doubler converter. The unique auto transformer characteristics based on the current doubler converter topology with integrated coupled inductors were discovered that had not previously been presented in the literature. The implication of the new integrated coupled output inductor design exhibited better performance than the old uncoupled approach. This unique characteristic that was described in this thesis, contributes valuable knowledge in the redesign of the LLC resonant converter for EATON's new product development, especially for the low voltage, high current applications.

The hardware prototype of the LLC-CDR successfully operated at both no load and full load condition with the output voltage halved from 48VDC to 24VDC, and doubled the output current to match the same power density. The efficiency of this novel converter was also compared with the EATON APR24-3G 24VDC LLC resonant converter. It strongly indicates that this novel half-bridge LLC resonant current doubler converter achieved slightly better performance which had also fulfilled the research goals.

SPICE-based software was used to simulate the operation of this novel LLC-CDR converter circuit design. Both the time-domain based transient analysis simulation method and the frequency-domain based AC analysis method are applied to both the half-bridge LLC resonant converter topology with and without output inductors in the magnetically coupled mode. Some undesirable simulation results were observed during the AC frequency-domain simulation analysis with the uncoupled output inductors design as indicated in Table 4-2. However, these undesirable simulation results were not observed for the novel and more effective coupled inductors design, and simulated results compared well with bench-test results as summarized in Table 5-1. The results in this table contributed valuable insights to analyze and compare the converter hardware prototype LLC network resonant switching performance with the simulated switching performance.

Compared to the uncoupled output inductors design, the coupled inductor design performed very well together with the LLC resonant converter. Therefore, the novel LLC-CDR can achieve similar AC frequency switching characteristics as the APR24-3G (24VDC) as shown in Figure 5-8, and the APR48-3G (48VDC) as shown in Figure 2-33 without changing the primary side LLC resonant network components including the main transformer design. These results confirmed the suitability of an integrated coupled winding configuration for the novel LLC resonant current doubler converter application. In addition, these results illustrated the potential benefit of the converter topology using integrated coupled inductors in general could offer an overall benefit in terms of

reduction of magnetic component size, cost and weight compare to the uncoupled inductor topology.

Finally, several efficiency plots were presented in Figure 5-18 in order to compare to EATON APR24-3G (24VDC) LLC resonant converter topology and the LLC-CDR with coupled inductors topology. It was shown that the improvement achieved in the integrated magnetic coupled inductors design enabled this novel LLC resonant current doubler converter topology to obtain slightly better efficiency performance. The finding in this thesis demonstrated a viable alternative solution to simply transform the current 48VDC EATON product into a 24VDC product with no need to make any design changes for the LLC resonant network components and the main transformer.

6.2 Future Work

Although in this thesis both the simulation analysis and the prototype hardware testing results successfully illustrated that a current doubler with integrated magnetic coupled inductors can provide an alternative solution to redesigning the LLC resonant converter, further investigation is still needed to improve the overall performance in terms of the output power rating and the efficiency.

The Electromagnetic Interference (*EMI*) Compliance comparison between the APR24-3G and the proposed novel LLC resonant current doubler converter circuit presented in Chapter 5 should be further investigated. The existing LLC resonant converter exhibits good EMI performance in the APR24-3G product. Although in this thesis it was proved that the integrated magnetic coupled output inductors had minimum effect on the primary side LLC resonant network switching characteristic, to make the proposed LLC-CDR converter a promising topology for telecom power rectifiers, it must be able to meet EMI compliance standards.

Synchronous rectification has been widely used to improve converter efficiency. Also, the integrated coupled inductors solution was proven to achieve better efficiency than the

uncoupled topology. Adopting synchronous rectification into this novel LLC-CDR converter could bring a benefit to further increase the overall efficiency.

Finally, the summarized frequency measurement results presented in Table 5-1 demonstrated a reasonably performing simulation model circuit. However, there were still some differences between the bench testing results and the simulation measurement results. A close investigation of the transformer SPICE model primary and secondary parameter values is likely to improve the accuracy of the simulation measurement.

Chapter 7 References

[1] Antonia V. Herzog, Timothy E. Lipman, Daniel M. Kammen. *Renewable Energy Sources.* Published in the Encyclopedia of Life Support Systems (EOLSS) Forerunner Volume "Perspectives and Overview of Life Support Systems and Sustainable Development," 2010.

[2] Eaton Corporation *.APR48-ES Energy Saver Rectifier*.2009

[3] Majlesi. *An Overview of Single Phase Telecommunication Converter Topologies: A Comparative* Study*,* Journal of Electrical Engineering. 2002.

[4] Bhaumik, S. *Energy-efficient design and optimization of wireline access networks*. In INFOCOM, 2011 Proceedings IEEE. 2011.

[5] Bo Yang, *Topology Investigation for Front End DC/DCPower Conversion for Distributed Power System.*Phd thesis submitted to Virginia Polytechnic Institute and State University, 2003.

[6] P. Alou, J. A. Oliver, O. García, R. Prieto, J. A. Cobos. *Comparson of current doubler rectifier and centre tapped rectifier for low voltage applications*. In Applied Power Electronics Conference and Exposition, 2006. APEC '06. Twenty-First Annual IEEE. 2006.

[7] M. Bildgen, *Resonant Converter Topologies*, Application Note AN658/1194, STMicroelectronics, 1999.

[8] Bill Andreycak, *Zero Voltage Switching Resonant Power Conversion*, Application Note U-138,Texas Instruments, 1999.

[9] Mohan, N., T.M. Undeland, and W.P. Robbins, *Power electronics : converters, applications, and design*. 3rd ed. 2003, Hoboken, NJ: John Wiley & Sons. xvii, 802.

[10] Prof. Bob Erickson, *Resonant Power Conversion*, Colorado Power Electronics Center, University of Colorado, Boulder. 21 Oct 2010.

[11] Dianbo Fu, *Topology Investigation and System Optimization of Resonant Converters*, Phd thesis submitted to Virginia Polytechnic Institute and State University, 2010.

[12] Kimball, Arthur Lalanne (1917). *A College Text-book of Physics*, 2nd Ed.. New York: Henry Hold and Co. pp. 516–517.

[13] Prof.Bob Erickson*, Resonant Power Conversion*, Colorado Power Electronics Center, University of Colorado, Boulder. 21 Oct 2010.

[14] P. Chandrasekhar1, S. Rama Reddy, *Design Of Lcl Resonant Converter For Electrolyser*, University Of Galati Fascicle III, Vol.33, No.1, ISSN 1221-454X, 2010.

[15] Chin-Hsing Cheng, Yao-Chou Lee, *DC Power Supply Based on Half Bridge LCC Resonant Converter,* International Conference on Power Electronics and Drive Systems, 2009.

[16] M. Prabhakar, S. Arulmozhi, Dr. V. Kamaraj, *Selection Criteria and Analysis of LCC Resonant DC – DC Converters for Automotive Applications,* Modern Applied Science Journal, Vol 3, No 7, July 2009.

[17] Christophe Basso, *A Simple DC SPICE Model for the LLC Converter*, Application note AND8255/D, ON Semiconductor, October, 2006 − Rev. 2

[18] Hong Huang Application Engineer, *Designing an LLC Resonant Half-Bridge Power Converter*, Texas Instruments Application Note, 2009.

[19] Christophe Basso, *Understanding the LLC Structure in Resonant Applications*, Application note AND8311/D, ON Semiconductor, October, 2008 − Rev. 0.

[20] RM12/I cores and accessories soft ferrite data sheet, Ferrexcube, Sep 01, 2008.

[21] Robert W. Erickson, Dragan Maksimovic, Fundamentals of Power Electronics, 2001.

[22] Marcel Dekker, Transformer and Inductor design handbook, DC Inductor Design Using Powder Cores, 3rd edition, 2004

[23] Steve Mappus*, Current Doubler Rectifier Offers Ripple Current Cancellation*, Texas Instruments Application Note, SLUA 323, Sep 2004.

[24] P. Alou, J. A. Oliver, O. García, R. Prieto, J. A. Cobos, *Comparison of Current Doubler Rectifier and Center Tapped Rectifier for Low Voltage Applications*, APEC conference, 2006.

[25] Laszlo Balogh, *The Current-Doubler Rectifier: An Alternative Rectification Technique For Push-Pull And Bridge Converters*, Texas Instruments Application Note, SLUA 121.

[26] Laszlo Huber, Milan M. Jovanovic, *Forward Converter with Current –Double r*ectifier: Analysis, Design, and Evaluation Results. Published In Industrial Electronics and Applications, IEEE, ICIEA 2007.

[27] Jian Sun, Member, IEEE, Kenneth F. Webb, and Vivek Mehrotra, *Integrated Magnetics for Current-Doubler Rectifiers*, IEEE Transactions On Power Electronics, VOL. 19, NO. 3, MAY 2004

[28] Application note AN2644, *LLC resonant half-bridge converter design guideline,* Rev 5, ST Microelectronics, Oct 2007.

[29] DrHuaZhou, *Magnetics Design For High Current Low Voltage Dc/Dc Converter*, PhdThesis ,University of Central Florida, 2007.

[30] J Pansini. *Electrical Transformers and Power Equipment*.3rd editioin, pp. 89–91.

[31] Prof. Krishna Vasudevan, Prof. G. SridharaRao, Prof. P. SasidharaRao, *Electrical Machines I*, Indian Institute of Technology Madras. 2000.

APPENDIX A.

In this section, a LLC resonant current doubler converter with two output inductors hardware prototype was tested to verify the converter performance. Bench testing results were collected in order to compare with the simulation. Comparison work was done at three different output voltages, they are 22Vdc, 24Vdc and 28Vdc. At each output voltage, test results are collected at different load conditions: 0A, 10A, 20A, 30A, 40A. Chapter 4 already covered the test results for 24Vdc at no load, half load (30A) and full load (40A), therefore this section mainly focused on 22Vdc and 28Vdc with different load conditions.

Figure A – 1 shows the hardware prototype bench testing results at 22Vdc and 28Vdc with 0A load.

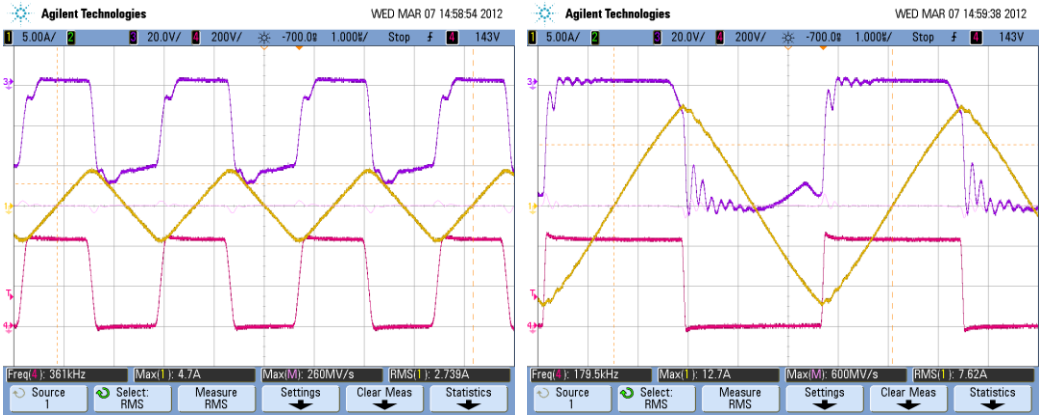

(a) (b)

Figure A - 1 : (a) 22Vdc with 0A load waveforms. (b) 28Vdc with 0A load waveforms. Ch1_Yellow trace: Resonant current; Ch3_Blue trace: Resonant voltage; Ch4_Red trace: Transformer primary voltage

Figure A – 2 shows the hardware prototype bench testing results at 22Vdc and 28Vdc with 10A load.

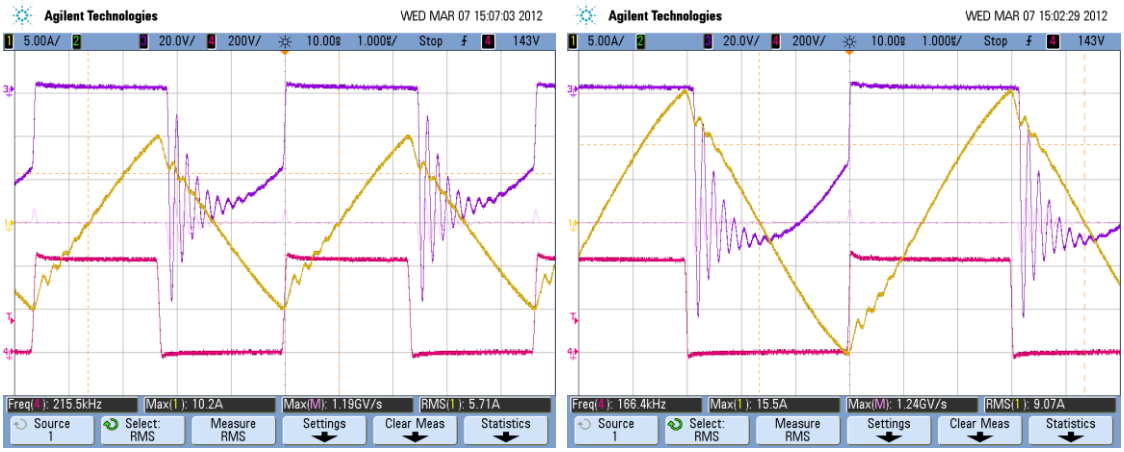

(a) (b)

Figure A - 2 : (a) 22Vdc with 10A load waveforms. (b) 28Vdc with 10A load waveforms. Ch1_Yellow trace: Resonant current; Ch3_Blue trace: Resonant voltage; Ch4_Red trace: Transformer primary voltage

Figure A – 3 shows the hardware prototype bench testing results at 22Vdc and 28Vdc with 20A load.

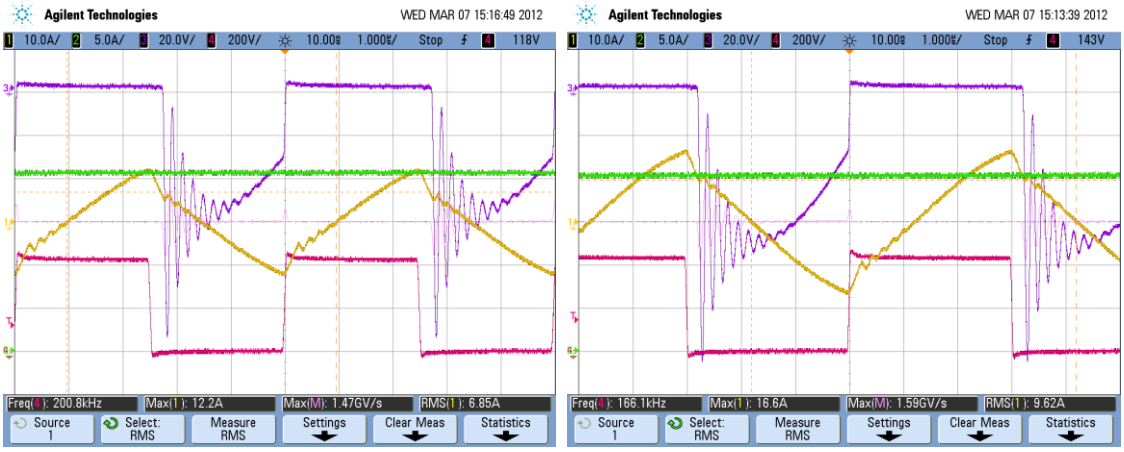

(b) (b)

Figure A - 3 : (a) 22Vdc with 20A load waveforms. (b) 28Vdc with 20A load waveforms. Ch1_Yellow trace: Resonant current; Ch2_Green trace: Output load current; Ch3_Blue trace: Resonant voltage; Ch4_Red trace: Transformer primary voltage

Figure A – 4 shows the hardware prototype bench testing results at 22Vdc and 28Vdc with 30A load.

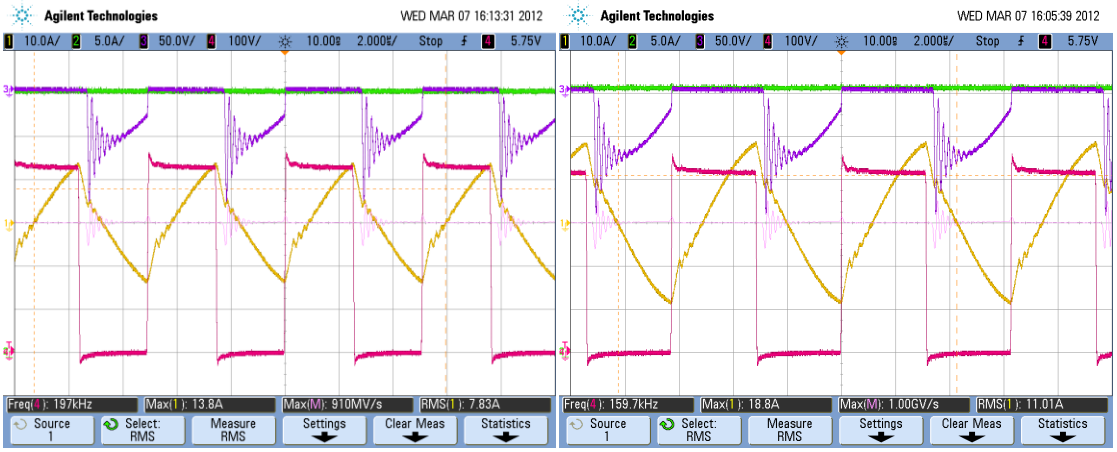

(a) (b)

Figure A - 4 : (a) 22Vdc with 30A load waveforms. (b) 28Vdc with 30A load waveforms. Ch1_Yellow trace: Resonant current; Ch2_Green trace: Output load current; Ch3_Blue trace: Resonant voltage; Ch4_Red trace: Transformer primary voltage

Figure A – 5 shows the hardware prototype bench testing results at 22Vdc and 28Vdc with 40A load.

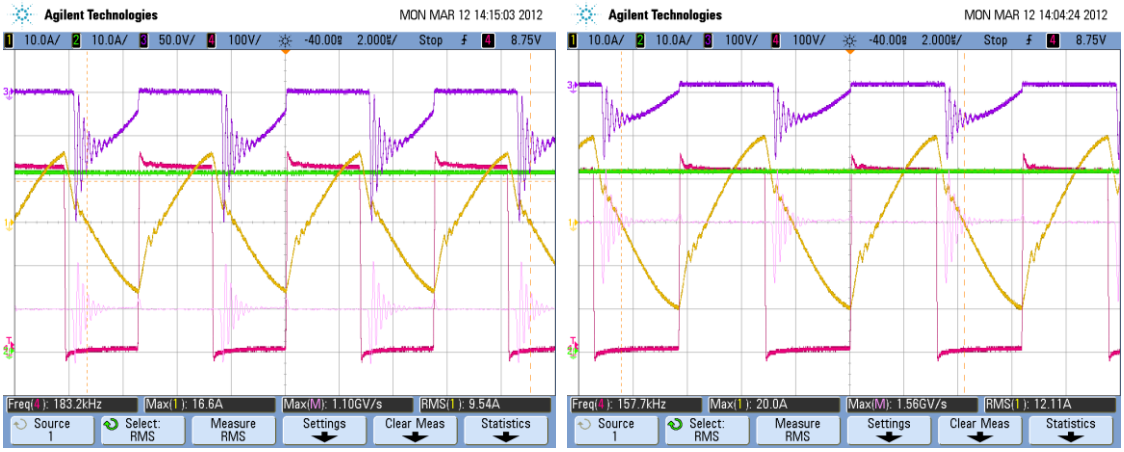

(a) (b)

Figure A - 5 : (a) 22Vdc with 40A load waveforms. (b) 28Vdc with 40A load waveforms. Ch1_Yellow trace: Resonant current; Ch2_Green trace: Output load current; Ch3_Blue trace: Resonant voltage; Ch4_Red trace: Transformer primary voltage

APPENDIX B.

In this section, a LLC resonant current doubler converter with two magnetic coupled output inductors hardware prototype was tested to verify the converter performance. Bench testing results were collected in order to compare with the simulation. Comparison work was done at three different output voltages, they are 22Vdc, 24Vdc and 28Vdc. At each output voltage, test results were collected at different load conditions: 0A, 10A, 20A, 30A, 40A,50A. Chapter 5 already covered the test results for 24Vdc at 0A, 30A, 50A, therefore this section mainly focused on 22Vdc and 28Vdc at different load conditions.

Figure B – 1 shows the hardware prototype bench testing results at 22Vdc and 28Vdc with 0A load.

(a) (b)

Figure B - 1 : (a) 22Vdc with 0A load waveforms. (b) 28Vdc with 0A load waveforms. Yellow trace: Resonant current; Green trace: Output diode voltage, Blue trace: Current in Loutput1; Red trace: Half bridge voltage,

Figure B – 2 shows the hardware prototype bench testing results at 22Vdc and 28Vdc with 10A load.

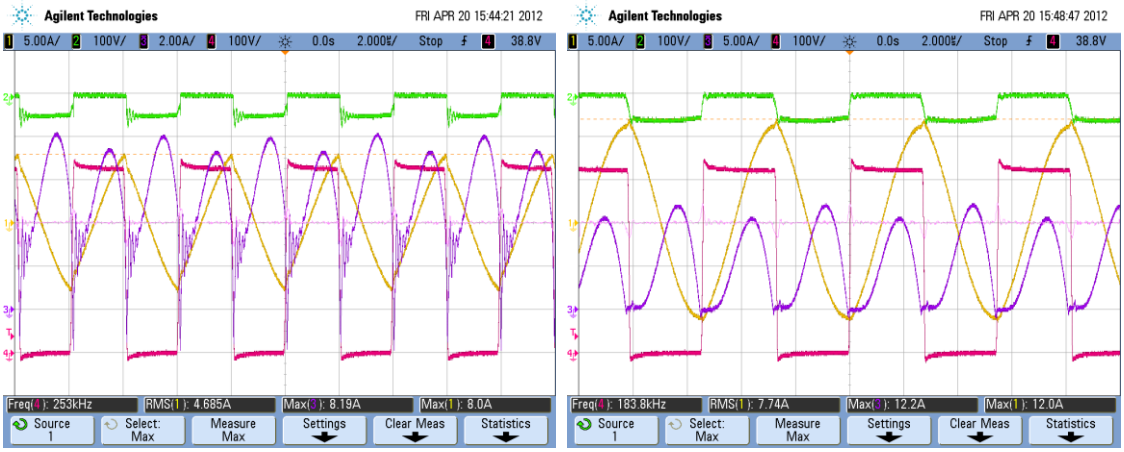

(a) (b)

Figure B - 2 : (a) 22Vdc with 10A load waveforms. (b) 28Vdc with 10A load waveforms. Yellow trace: Resonant current; Green trace: Output diode voltage, Blue trace: Current in Loutput1; Red trace: Half bridge voltage,

Figure B – 3 shows the hardware prototype bench testing results at 22Vdc and 28Vdc with 20A load.

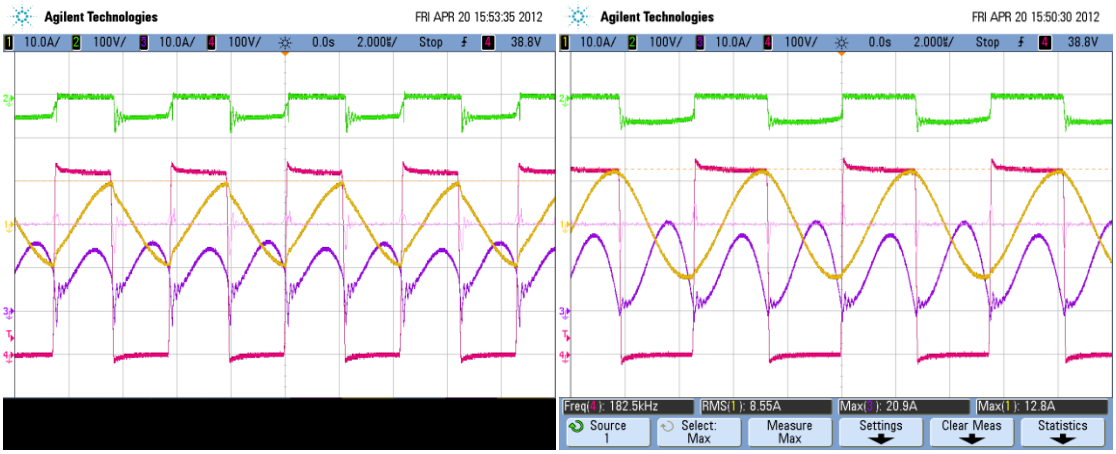

(a) (b)

Figure B - 3 : (a) 22Vdc with 20A load waveforms. (b) 28Vdc with 20A load waveforms. Yellow trace: Resonant current; Green trace: Output diode voltage, Blue trace: Current in Loutput1; Red trace: Half bridge voltage,

Figure B – 4 shows the hardware prototype bench testing results at 22Vdc and 28Vdc with 30A load.

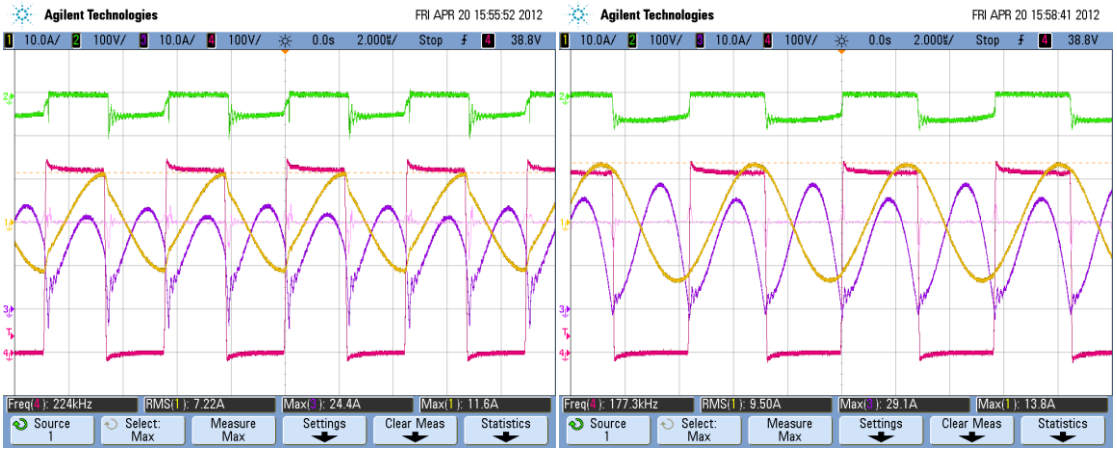

(a) (b)

Figure B - 4 : (a) 22Vdc with 30A load waveforms. (b) 28Vdc with 30A load waveforms. Yellow trace: Resonant current; Green trace: Output diode voltage,Blue trace: Current in Loutput1; Red trace: Half bridge voltage,

Figure B – 5 shows the hardware prototype bench testing results at 22Vdc and 28Vdc with 40A load.

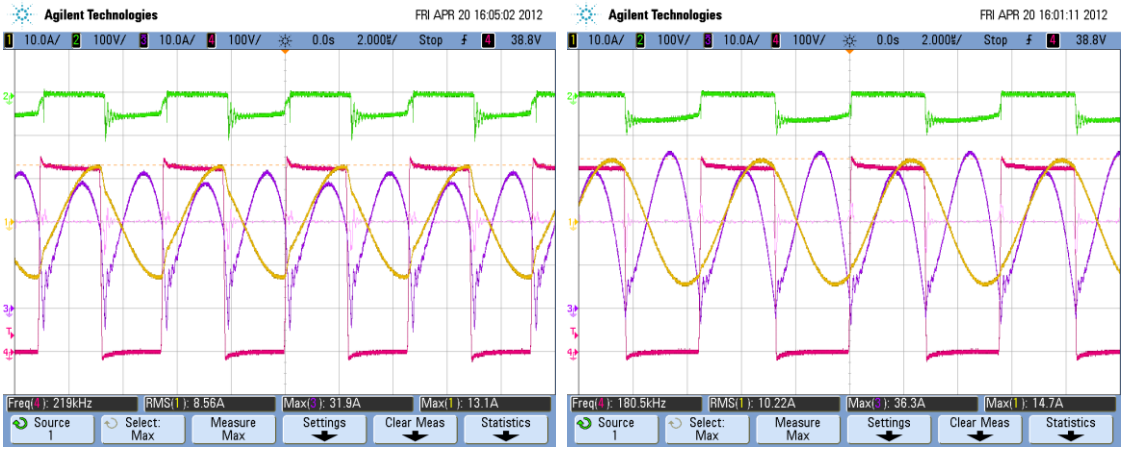

(a) (b)

Figure B - 5 : (a) 22Vdc with 40A load waveforms. (b) 28Vdc with 40A load waveforms. Yellow trace: Resonant current; Green trace: Output diode voltage, Blue trace: Current in Loutput1; Red trace: Half bridge voltage,

Figure B – 6 shows the hardware prototype bench testing results at 22Vdc and 28Vdc with 50A load.

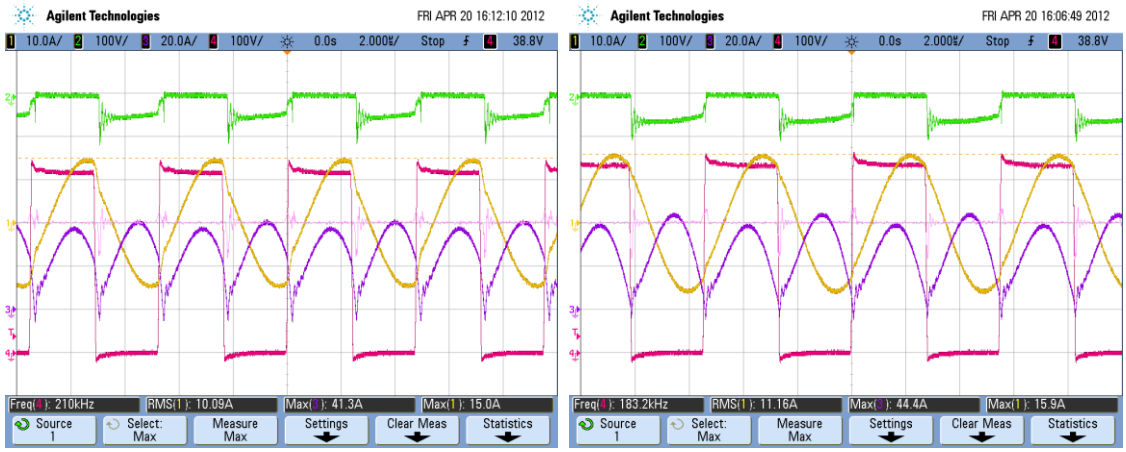

(a) (b)

Figure B - 6 : (a) 22Vdc with 50A load waveforms. (b) 28Vdc with 50A load waveforms. Yellow trace: Resonant current; Green trace: Output diode voltage, Blue trace: Current in Loutput1; Red trace: Half bridge voltage,